

12-2017

# Studies on Stable Crack Growth

Mohammed Juma Humaid Al-Ghafri

Follow this and additional works at: [https://scholarworks.uaeu.ac.ae/all\\_theses](https://scholarworks.uaeu.ac.ae/all_theses)

Part of the [Materials Science and Engineering Commons](#)

---

## Recommended Citation

Humaid Al-Ghafri, Mohammed Juma, "Studies on Stable Crack Growth" (2017). *Theses*. 507.  
[https://scholarworks.uaeu.ac.ae/all\\_theses/507](https://scholarworks.uaeu.ac.ae/all_theses/507)

This Thesis is brought to you for free and open access by the Electronic Theses and Dissertations at Scholarworks@UAEU. It has been accepted for inclusion in Theses by an authorized administrator of Scholarworks@UAEU. For more information, please contact [fadl.musa@uaeu.ac.ae](mailto:fadl.musa@uaeu.ac.ae).



U.A.E University  
Deanship of Graduate Studies  
Material Science and Engineering Program

## **STUDIES ON STABLE CRACK GROWTH**

By

Mohammed Juma Humaid Al-Ghafri

Thesis Submitted to the Deanship of Graduate Studies  
in Partial Fulfillment of the  
Requirements for the Degree of Master of Science in  
Materials Science and Engineering

Supervised By

Dr. Abdel-Hamid I. Mourad

Mechanical Engineering Department

U.A.E. University

Prof. Osama Abu Zeid

Mechanical Engineering Department

U.A.E. University

December 2002



## Thesis Supervisors

**Abdel-Hamid I. Mourad, PH.D**

Assistant Professor

U.A.E. University

College of Engineering

Mechanical Engineering Department

**Osama- Abu-zeid, PHD**

Professor

U.A.E. University

College of Engineering

Mechanical Engineering Department

UAEU Library



1000400747



مكتبة زايد المركزية  
ZAYED CENTRAL LIB.

**United Arab Emirates Univers**  
**Graduate Studies**  
**M.S.c. Program in Materials Science and Engineering**  
**THESIS EXAMINATION REPORT**

tudent ID : 200050211  
 tudent Name : Mohammed Juma Humaid Al-Ghafri

itle of The Thesis : Studies on Stable Crack Growth

he Thesis Examination as A Partial Fulfillment of M. Sc. Degree in Materilas Science and Engineering Was conducted on ..... Based on Examining the Thesis and the Students Presentation and the Subsequent Discussion, The ommittee Recommends:

- Thesis is Satisfactory as is.
- Thesis is Satisfactory After Minor Modifications.
- Thesis should be Re-Evaluated After Major Modifications.
- Thesis is Rejected.

**Examining Committee Members:**

Thesis Supervisor: Name: ..Dr. Abdel-Hamid I. Mourad	Signature: .. <i>Junad</i> ...	Date:
Thesis Co-Advisor: Name Prof...Osama...Abu Zeid	Signature: .. <i>[Signature]</i> .....	Date: 25/12/2002
Member : Name: ..Dr. Hany A. ElKadi	Signature: .. <i>[Signature]</i> .....	Date:
Name: ..Dr. Khaled El-Sawy	Signature: .. <i>[Signature]</i> .....	Date:

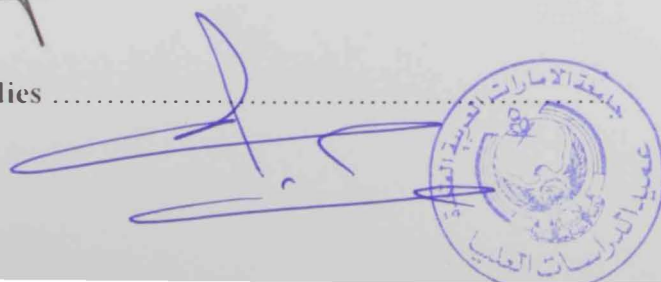
**Approval of Program Coordinator:**

Date: 30/12/2002

**APPROVAL:**

Dean of Graduate Studies .....

Date: 30/12/2002



## ACKNOWLEDGEMENT

I would like first to thank my advisor, Dr. Abdel-Hamid I. Mourad for his continuous encouragement and inspiration. His guidance, patience, imagination and insight have been a positive influence on both my professional and personal development.

My grateful thanks to my second advisor Prof. Osama abu Zaid for his guidance and help throughout this research.

I would like to take this opportunity to thank Miss Aida Al-Ryami Director General of specification and measurement for her constant encouragement and support.

I'm grateful to Dr, Khalid Al-Sawy for his help with finite element simulation and design. Without his help, I wouldn't have as much progress in finite element.

I would also like to take this opportunity to thank department of mechanical engineering for helping me in providing facilities. Special thanks to Engineer Abdul-Alstar for his help in motivation of the research.

I would like to thank the following collaborators who made it possible to perform various studies in this dissertation: Engineer Abdulstar, material lab, College of engineering workshop staff, central laboratory unit and Interplast Company at Al sharjah for their cooperation and patience.

Finally, I would like to thank my family for their immense support and constant encouragement.

## ABSTRACT

The goal of this work is to experimentally investigate the stable crack growth (SCG) fracture behavior of AISI 4340 alloy steel. A series of mode I and mixed mode SCG fracture tests were carried out on 8 mm thick compact tension (CT) specimens subjected to quasistatic loading. The wire cutting technique was used to introduce a pre-notch / pre-crack of 0.05 mm root radius to the specimen. Five different loading angles  $\psi$  between the loading axis and the crack surface were employed;  $90^\circ$  (mode I),  $75^\circ$ ,  $65^\circ$ ,  $60^\circ$  and  $50^\circ$ . Five different ratios of original crack length to specimen width  $a_0/w$  were also employed, 0.41, 0.42, 0.43, 0.44 and 0.45. Different combinations of  $\psi$  and  $a_0/w$  were used. Data concerned with direction of initial crack extension load-load line displacement (L-LLD) diagrams, initiation and maximum loads, range of stable crack growth, crack blunting, crack front geometry, fracture surfaces, and scanning electron microscope fractographs were obtained. A noticeable blunting was observed prior the crack initiation. Although the crack commences its growth from a pre-notch / pre-crack of a straight front it has a considerable tunneling at each stage of stable crack growth. In mixed mode, the crack takes place along a straight-line path initially, inclined with the main crack at an angle equal to the direction of crack extension. The loading angle  $\psi$  and the initial crack length to the specimen width  $a_0/w$  ratio affect the SCG fracture behavior significantly. The direction of initial stable crack extension was determined through an elastic finite element analysis. There was reasonably good agreement between the experimental and the predicted results.



# CONTENTS

Abstract	I
List of Tables	V
List of Figures	VI
Abbreviation	X
<b>1 INTRODUCTION</b>	<b>1</b>
1.1. MOTIVATION	1
1.2 AIMS AND OBJECTIVES	4
1.3 OUTLINE OF THE DISSERTATION.	5
<b>2 LITERATURE REVIEW</b>	<b>6</b>
2.1. INTRODUCTION	6
2.2. FRACTURE MECHANICS	6
2.3. HISTORICAL REVIEW	7
2.4. LINEAR ELASTIC FRACTURE MECHANICS (LEFM)	11
2.5. UNSTABLE PATH OF CRACK EXTENSION	14
2.6. SMALL SCALE YIELDING	15
2.7. ELASTIC-PLASTIC FRACTURE MECHANICS	18
2.8. CRACK TIP FIELD	24
2.8.1. Crack Tip Field for a Stationary Crack in Ductile Material	24
2.8.2. Crack-Tip Field for a Propagating Crack in Ductile Material	27

2.9. CRITERIA FOR CRACK GROWTH	33
2.9.1. Crack Growth Initiation	33
2.9.2. Stable Crack Growth	34
2.9.3. Finite Element Analysis of Stable Crack Growth	35
2.10. MIXED MODE STUDIES	36
2.11. EFFECT OF CRACK BLUNTING ON SUBSEQUENT CRACK GROWTH	38
2.12. CRACK FRONT TUNNELING	41
2.13. CLOSURE	42
<b>3 EXPERIMENTAL PROCEDURE</b>	
3.1. INTRODUCTION	44
3.2. MATERIAL	44
3.3. SPECIMENS PREPARATION	45
3.3.1. Tensile Specimens Preparation	45
3.3.2. Fracture Specimens Preparations	45
3.4. FIXTURE	46
3.5. TEST PROCEDURES	47
3.5.1. Tensile Test	47
3.5.2. Fracture Test	47
<b>4. MODE I STABLE CRACK GROWTH</b>	<b>55</b>
4.1. INTRODUCTION	55

4.2. EXPERIMENTAL STUDIES	55
4.3. FINITE ELEMENT ANALYSIS	59
<b>5. MIXED MODE STABLE CRACK GROWTH</b>	<b>79</b>
5.1. INTRODUCTION	79
5.2. EXPERIMENTAL STUDIES	79
5.3. FINITE ELEMENT ANALYSIS	83
<b>6. DISCUSSION AND CONCLUSIONS</b>	<b>104</b>
6.1. INTRODUCTION	104
6.2. DISCUSSION	104
6.3. CONCLUSION	106
<b>7- REFERENCE</b>	<b>108</b>
<b>8- APPENDIXES</b>	<b>120</b>

# List of Tables

Table 3.1: Chemical composition of AISI 4340 steel alloy.	49
Table 3.2: Mechanical properties of AISI 4340 steel alloy (at room temperature)	49
Table 4.1 Summary of the experimental results	61
Table 5.1 Summary of experimental and predicted results for mixed mode stable crack growth.	85

## List of Figures

Figure 2.1. Types of structural failure.	8
Figure 2.2 the basic modes of loading (crack surface displacement) that can be applied to a crack. [1]	12
Figure 2.3 Basics of Linear Elastic Fracture Mechanics.	16
Figure 2.4. Cracked tip opening displacement	19
Figure 2.5. J contour integral along arbitrary path $\Gamma$ enclosing a crack tip in non-linear elastic material.	21
Figure 2.6 Schematic of the field surrounding a growing crack	27
Figure 3.1 Tensile test specimen geometry	50
Figure 3.2 Compact tensions (CT) specimen geometry for mode I and mixed mode loading. Thickness $t = 8$ mm.	51
Figure 3.3 Photograph showing the fork-type fixture	52
Figure 3.4 Experimental setup	53
Figure 3.5 Photograph showing the clip gauge position	53
Figure 3.6 Calibration curve of the clip gauge	54
Figure 4.1 Compact tension (CT) specimen for mode I stable crack growth specimen geometry	61
Figure 4.2 Sample photographs for fractured specimens for different $a_0/w$ ratios	62
Figure 4.3 Mode I Load – Load line displacement diagram for $a_0/w = 0.41$	63
Figure 4.4 Mode I Load – Load line displacement diagram for $a_0/w = 0.42$	64
Figure 4.5 Mode I Load – Load line displacement diagram for $a_0/w = 0.43$	65

Figure 4.6 Mode I Mode I Load – Load line displacement diagram for $a_0/w = 0.44$	66
Figure 4.7 Mode I Mode I Load – Load line displacement diagram for $a_0/w = 0.45$	67
Figure 4.8 Comparison of mode I Load – Load line displacement diagrams for different $a_0/w$ ratios.	68
Figure 4.9 Variation of $P_{max}$ and $P_i$ against $a_0/w$ ratio	69
Figure 4.10 Sample photograph of crack front around initiation and maximum load for $a_0/w = 0.41$	70
Figure 4.11 Sample photograph of crack front around initiation and maximum load for $a_0/w = 0.42$	70
Figure 4.12 Sample photograph of crack front around initiation and maximum load for $a_0/w = 0.41$	70
Figure 4.13 Sample photographs of fracture surfaces	71
Figure 4.14 Scanning electron micrographs samples for mode I stable crack growth region	72
Figure 4.15 Scanning electron micrographs samples for mode I unstable crack growth region.	73
Figure 4.16 Discretisation for mode I specimen, ( $a_0/w = 0.43$ )	74
Figure 4.17 Variation of the equivalent stress ahead of crack tip at the onset of crack extension.	75
Figure 4.18 Plastic Zone in mode I at the onset of crack extension. $a_0/w = 0.41$ , $P_i = 22$ kN, (b) $a_0/w = 0.42$ , $P_i = 20$ kN, (c) $a_0/w = 0.43$ , $P_i = 18$ kN, (d) $a_0/w = 0.44$ , $P_i = 16$ kN, (e) $a_0/w = 0.45$ , $P_i = 14$ kN.	76-77

Figure 4.19 Deformed shape of ct specimen in mode I at initiation load, (a) $a_0/w = 0.42$ , and (b) $a_0/w = 0.45$	78
Figure 5.1. Compact tension (CT) specimen geometry for mixed modes stable crack growth	86
Figures 5.2 Load – Load line displacement diagram for $a_0/w = 0.42$ and loading angle $\psi = 60^\circ$ .	87
Figures 5.3 Load – Load line displacement diagram for $a_0/w = 0.42$ and loading angle $\psi = 65^\circ$ .	88
Figures 5.4 Load – Load line displacement diagram for $a_0/w = 0.42$ and loading angle $\psi = 75^\circ$ .	89
Figure 5.5 Comparison of load – load line displacement diagrams for different loading angles ( $\psi = 60^\circ, 65^\circ$ , and $75^\circ$ ) and $a_0/w = 0.42$	90
Figure 5.6 A comparison of load displacement diagrams for different loading angle ( $\psi =$ $50^\circ, 60^\circ, 65^\circ$ , and $75^\circ$ ) and $a_0/w = 0.43$	91
Figure 5.7 Effect $a_0/w$ ratios on the load-load line displacement diagrams	92
Figure 5.8 Variation of maximum load ( $P_{max}$ ) for $a_0/w = 0.42$ and $0.43$ against loading angle ( $\psi$ )	93
Figure 5.9 Variation of initial load ( $P_i$ ) for $a_0/w = 0.42$ and $0.43$ against loading angle ( $\psi$ )	94
Figures 5.10 Sample photograph of fractured specimen for $a_0/w = 0.42$ ; (a) $\psi = 60^\circ$ ; (b) $\psi = 65^\circ$ ; (c) $\psi = 75^\circ$ .	95
Figures 5.11 Sample photograph of fractured specimen for $a_0/w = 0.42$ ; (a) $\psi = 50^\circ$ ; (b) $\psi = 60^\circ$ ; (c) $\psi = 65^\circ$ ; (d) $\psi = 75^\circ$	96

Figure 5.12 Comparison between experimental and predicted mixed mode crack initiation direction $\theta^\circ$ and loading angle $\psi^\circ$	97
Figure 5.13 Sample photograph of crack front tunneling after crack initiation and maximum load in mixed mode.	98
Figure 5.14 Sample photograph of the fracture surfaces in mixed mode specimen for different loading angles.	98
Figure 5.15 Scanning electron micrographs samples for mixed mode ( $a_0/w = 0.43$ , $\psi = 50^\circ$ ) stable crack growth region.	99
Figure 5.16 Scanning electron micrographs samples for mixed mode ( $a_0/w = 0.43$ , $\psi = 50^\circ$ ) unstable crack growth region.	100
Figure 5.17 Discretisation for determining direction of initial stable crack extension; number of element = 4365, number of nodes = 13467. $a_0/w = 0.42$ , $\psi = 75^\circ$ , (b) $a_0/w = 0.43$ , $\psi = 75^\circ$ . (c) $a_0/w = 0.43$ , $\psi = 65^\circ$ . (d) $a_0/w = 0.43$ , $\psi = 60^\circ$ , (e) $a_0/w = 0.43$ , $\psi = 50^\circ$ .	101-103



## ABBREVIATION

SCG	stable crack growth
CT	Compact tension specimen
L-LLD	Load-Load load line displacement
LEFM	Linear Elastic Fracture Mechanics
MTS	Maximum tangential stress
SED	Strain energy density
MTSN	Maximum tangential strain
MTPS	Maximum tangential principal stress
EPFM	Elastic Plastic fracture Mechanics
COD	Crack Opening displacement
SIF	Stress intensity Factor
CTOD	Crack tips opening displacement
HRR	Hutchinson Rice and Rosengren singularity field
COA	Crack opening analysis
CTOA	Crack tip opening angles
SZW	Stretch zone width
TPB	Three point bend
SEM	Scanning electron microscope
FEA	Finite element analysis.

# Chapter one

## 1.1 INTRODUCTION

The first part of the book is devoted to a general introduction to the subject of the book. It is divided into two main parts: the first part deals with the general theory of the subject, and the second part deals with the special theory of the subject. The first part is divided into two main sections: the first section deals with the general theory of the subject, and the second section deals with the special theory of the subject. The second part is divided into two main sections: the first section deals with the general theory of the subject, and the second section deals with the special theory of the subject.

The second part of the book is devoted to a general introduction to the subject of the book. It is divided into two main parts: the first part deals with the general theory of the subject, and the second part deals with the special theory of the subject. The first part is divided into two main sections: the first section deals with the general theory of the subject, and the second section deals with the special theory of the subject. The second part is divided into two main sections: the first section deals with the general theory of the subject, and the second section deals with the special theory of the subject.

# CHAPTER 1

## INTRODUCTION

### 1.1. MOTIVATION

Engineering systems such as ships, aircrafts, vehicles, pressure vessels, and nuclear power plants are extremely complex with many thousands of components. In the construction of such systems it is impossible to completely avoid the presence of flaws such as cracks. A crack in a structural or a machine component can be due to initial defect in a material or it can develop during machining or manufacturing. The presence of a crack in a component may weaken it so that it fails by fracturing into two or more pieces. This can occur at stresses below the material's yield strength, where failure would not normally be expected.

In engineering design, materials and design details can be carefully chosen so that designs is relatively tolerant to the presence of cracks, and design can include redundancy, so that fracture of one component does not cause catastrophic failure of the whole machine, vehicle or structure. In the classical approach, design is based on the assumption that the material is homogeneous and defect free. This makes the material, which may contain a small defect or flaws, useless. In recent years improvement in design and safety assurance have been greatly influenced by advances in the discipline of fracture mechanics, especially linear elastic fracture mechanics (LEFM).

If the load applied to a member containing a crack is too high, the crack may suddenly grow and cause the member to fail by fracturing in a brittle manner, that is, with little plastic deformation. From the theory of fracture mechanics, a quantity called the stress intensity factor,  $K$ , can be defined to characterize the severity of the crack situation as affected by crack size, stress, and geometry. In defining  $k$ , the material is assumed to behave in a linear-elastic manner according to Hooke's law, so that the approach being used is called linear-elastic fracture mechanics (LEFM). Fracture of engineering material originating from a crack is well understood provided the deformation is linear elastic. In the case of brittle material, an unstable crack extension occurs mostly immediately upon initiation. Such extension falls within the scope of LEFM. The direction of initial crack extension, the fracture load and the unstable crack path could be easily predicted to a reasonable degree of accuracy by applying any one of the predictive criterion – the criteria of maximum tangential stress (MTS); strain energy density (SED), maximum tangential strain (MTSN) and maximum tangential principal stress (MTPS)- to the stress-strain field existing at the onset of crack extension.

In ductile materials, such as many metals, large plastic deformations occur in the vicinity of the crack tip. The region within which the material yields is called the plastic zone. It is significant that the region of yielding, plastic zone must not be excessively large if the LEFM theory is to be applied. Most metals give rise to plastic deformation at the tip of a crack, the extent of which is more than what could be accounted for by the LEFM. This has led to development of elastic-plastic fracture mechanics (EPFM). In many metals due to the plastic zone formation, the crack grows stably before instability sets in. The instability occurs at a load level higher than the initiation load ( $P_i$ ). A design

based on the initiation load ( $P_i$ ) may lead to under-utilization of the material. To exploit the full potential of the material it is necessary to obtain data and characterize the stable crack growth (SCG).

A crack in every stage of development will turn into a direction in which it experiences only mode I loading, unless it is prevented from doing so by geometrical confinement. For this reason, fracture mechanics is generally confined to mode I. As a result a considerable amount of work has been directed to developing analytical and experimental methods to quantify the stress-crack relationships under this type of loading. Practical structures are not only subjected to tension but also experience shear and torsion loading. Cracks therefore are exposed to tension and shear, which lead to mixed mode cracking. The combination of tension and shear gives a mixture of mode I and II. Generally if a crack surface is not normal to the applied stress, or if there is a complex state of stress, a combination of fracture modes I, II, and III may exist, for example, a situation involving combined modes I and II. is complex because the crack may change direction so that it does not grow in its original plane, and also because the involved fracture modes do not act independently, but rather interact. The direction of crack extension is then an unknown over and above the fracture load. In this context, the mode I stable crack growth has received a considerable attention, but not the mixed mode, which is a more general problem. Some investigators have considered the mixed mode stable crack growth (SCG) problems but a general accepted analysis has not yet developed. Both theoretical and experimental investigations on mixed mode SCG are lacking.

One of the most important modes of failure in metals is crack propagation arising at regions of high stress (stress raiser) such as, notches, holes, fillets or any other discontinuities. Cracks tend to grow under loading and when reach a critical size they propagate in unstable manner causing failure of the part in which they are located. The issue of stable growth of cracks arising from a stress raiser is very scanty. The stable crack extension behavior through AISI 4340 alloy steel is also lacking. These issues have provided a motivation for the present work.

## **1.2 AIMS AND OBJECTIVES**

The present investigation is an attempt to obtain data on stable crack growth through aircraft quality alloy steel AISI 4340 or SAE 4340. The (SCG) fracture behavior was characterized through a series of fracture tests conducted on 8 mm thick compact tension (CT) specimen in mode I and mixed mode (I and II). Data pertaining to load – load line displacement diagram, crack initiation load, maximum fracture load, crack blunting, crack front geometry (tunneling), fracture surface and scanning electron microscope fractographs is presented.

Some work has also been carried out using the Finite Element Method. This includes the computation of initial stable crack direction, equivalent stress and size of the plastic zone a head of crack tip around initiation load. The commercial finite element package “ANSYS” version 5.4 was used for the finite element analysis.

Keeping these in view the present study has been carried out with the following objectives

- 1- To carry out the tensile test on AISI 4340 steel alloy to get its mechanical properties.
- 2- To carry out experimental studies on mode I stable crack growth through compact tension specimens.
- 3- To carry out experimental studies on mixed mode I and II stable crack growth through compact tension specimens.
- 4- To carry out finite element analysis to verify some of the experimental results.
- 5- To study the stable crack growth characteristics through AISI 4340 alloy steel.

### **1.3 OUTLINE OF THE DISSERTATION.**

The dissertation is divided into six chapters, in chapter one, the present chapter, the motivation of study, aims and objectives and an outline of dissertation are presented. The relevant literature on the linear elastic fracture mechanics (LEFM) and elastic-plastic fracture mechanics (EPFM) are reviewed in chapter two. The literature on the use of Finite Element Method in predicting of the crack direction is also reviewed in this chapter. In chapter three the experimental procedure (material, specimens' geometries and test procedure) is discussed. Mode I and Mixed mode stable crack growth experimental studies are presented in chapter four and five respectively. Chapter six presents a discussion of the results, general conclusion and suggestions for future study.

# Chapter two

## LITERATURE REVIEW

### 2.1 INTRODUCTION

The first part of the literature review is devoted to the study of the mechanical behavior of materials under stress. This part covers the topics of stress-strain relationships, fracture mechanics, and fatigue. The second part of the literature review is devoted to the study of the mechanical behavior of materials under impact. This part covers the topics of impact strength, Charpy impact, and pendulum impact.

### 2.2 FRACTURE MECHANICS

Fracture mechanics is a branch of mechanics that deals with the study of the mechanical behavior of materials under stress. It is concerned with the study of the mechanical behavior of materials under stress, and the study of the mechanical behavior of materials under impact. Fracture mechanics is a branch of mechanics that deals with the study of the mechanical behavior of materials under stress.

Fracture mechanics is a branch of mechanics that deals with the study of the mechanical behavior of materials under stress. It is concerned with the study of the mechanical behavior of materials under stress, and the study of the mechanical behavior of materials under impact. Fracture mechanics is a branch of mechanics that deals with the study of the mechanical behavior of materials under stress.

Fracture mechanics is a branch of mechanics that deals with the study of the mechanical behavior of materials under stress. It is concerned with the study of the mechanical behavior of materials under stress, and the study of the mechanical behavior of materials under impact. Fracture mechanics is a branch of mechanics that deals with the study of the mechanical behavior of materials under stress.

Fracture mechanics is a branch of mechanics that deals with the study of the mechanical behavior of materials under stress. It is concerned with the study of the mechanical behavior of materials under stress, and the study of the mechanical behavior of materials under impact. Fracture mechanics is a branch of mechanics that deals with the study of the mechanical behavior of materials under stress.



## CHAPTER 2

### LITERATURE REVIEW

#### 2.1. INTRODUCTION

In this chapter literature relevant to linear elastic fracture mechanics (LEFM), crack extension through brittle materials elastic plastic fracture mechanics (EPFM), and mode I and mixed mode (I and II) stable crack growth are reviewed.

#### 2.2. FRACTURE MECHANICS

Where cracks are difficult to avoid, a special methodology called fracture mechanics can be used to aid in selecting materials and designing components to minimize the possibility of fracture.

Fracture mechanics is a subset of solid mechanics that deals with the behavior of solid systems containing one or more cracks. Fracture mechanics is a relatively new area of solid mechanics research, with its foundation laid in the early 20<sup>th</sup> century. Already it has broad application in systems ranging in size from micrometer length scales (thin films, MEMS) up to kilometer length scales (earthquake fault lines). Some fracture mechanics problems may relate to configuration effects, such as cracks affected by weak bond lines, material anisotropy, or specimen inhomogeneity. These experiments may be performed with “model” materials having properties idealized for the experiment. However, one important job for fracture mechanics is to evaluate the performance of

imperfect material for engineering use. In this case the experimental models and methods must be extended and tailored to suit the material, and not the other way around.

The study and use of fracture mechanics is of major engineering importance simply because cracks or crack-like flaws occur more frequently than we might think. For example, the periodic inspections of large commercial aircraft frequently reveal cracks, some times numerous cracks that must be repaired. Cracks or crack-like flaws also commonly occur in ship structure, in bridge structures, in pressure vessels and piping, in heavy machinery, and in ground vehicles. They are also a source of concern for various parts of nuclear reactors.

### **2.3. HISTORICAL REVIEW**

Strength failures of load bearing structures can be either of the yielding-dominant or fracture-dominant types. Defects are important for both types of failure, but those of primary importance to fracture differ in an extreme way from those influencing yielding and the resistance to plastic flow. These differences are illustrated schematically in Figure 2.1

For yielding-dominant failures the significant defects are those which tend to warp and interrupt the crystal lattice planes, thus interfering with dislocation glide and providing a resistance to plastic deformation that is essential to the strength of high strength metals. Examples of such defects are interstitial and out-of-size substitution atoms, grain boundaries, coherent precipitates and dislocation networks. Larger defects like inclusions, porosity, surface scratches and small cracks may influence the effective net section bearing the load, but otherwise have little effect on resistance to yielding.

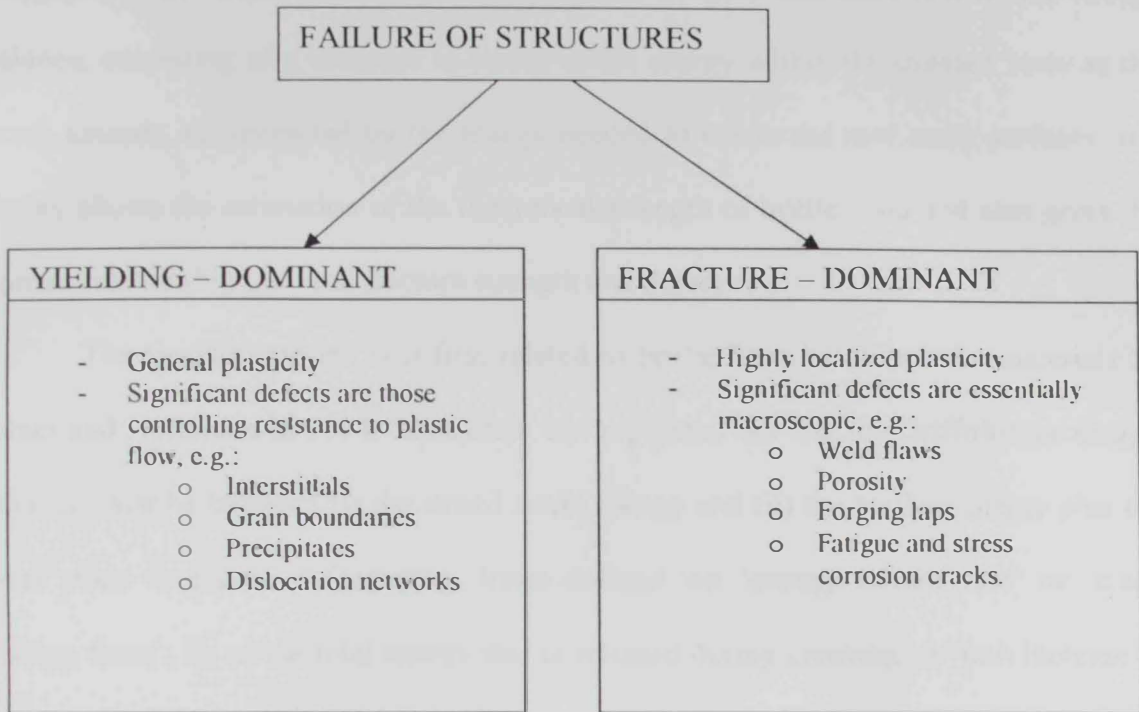


Figure 2.1. Types of structural failure.

For fracture-dominant failures, i.e. fracture before general yielding of the net section, the size scale of the defects, which are of major significance, is essentially macroscopic, since general plasticity is not involved but only the local stress strain fields associated with the defects. The minute lattice-related defects, which control resistance to plastic flow, are not of direct concern. They are important insofar as the resistance to plastic flow is related to the material's susceptibility to fracture. [1]

Fracture mechanics, is concerned almost entirely with fracture-dominant failure. The first commonly accepted successful analysis of a fracture-dominant problem was that of Giffith in 1920, who considered the propagation of brittle cracks in glass. Griffith formulated the now well-known concept that an existing crack will propagate if thereby

the total energy of the system is lowered, and he assumed that there is a simple energy balance, consisting of a decrease in elastic strain energy within the stressed body as the crack extends, counteracted by the energy needed to create the new crack surfaces. His theory allows the estimation of the theoretical strength of brittle solid and also gives the correct relationship between fracture strength and defect size.

The Griffith concept was first related to brittle fracture of metallic materials by Zener and Hollomon in 1994. Soon after, Irwin pointed out that the Griffith-type energy balance must be between (i) the stored strain energy and (ii) the surface energy plus the work done in plastic deformation. Irwin defined the 'energy release rate' or 'crack driving force',  $G$ , as the total energy that is released during cracking per unit increase in crack size. He also recognized that for relatively ductile materials the energy required to form new crack surface is generally insignificant compared to the work done in plastic deformation.

In the middle 1950s Irwin contributed another major advance by showing that the energy approach is equivalent to stress intensity ( $K$ ) approach, according to which fracture occurs when a critical stress distribution ahead of the crack tip is reached. The material property governing fracture may therefore be stated as critical stress intensity,  $K_c$ , or in terms of energy as a critical value  $G_c$ .

Demonstration of the equivalence of  $G$  and  $K$  provided the basis for development of the discipline of Linear Elastic Fracture Mechanics (LEFM). This is because the form of the stress distribution around and close to a crack tip is always the same. Thus tests on suitably shaped and loaded specimens to determine  $K_c$  make it possible to determine if cracks or crack-like flaws are tolerable in an actual structure under given conditions.

Furthermore, materials can be compared as to their suitability in situations where fracture is possible. It has also been found that the sensitivity of structures to subcritical cracking such as fatigue crack growth and stress corrosion can, to some extent, be predicted on the basis of tests using the stress intensity approach.

The beginnings of Elastic-Plastic Fracture Mechanics (EPFM) can be traced to fairly early in the development of LEFM, notably Well's work on Crack Opening Displacement (COD), which was published in 1961. In 1968 Rice introduced an elastic-plastic fracture parameter with a more theoretical basis: the J integral. Although both COD and J are now well-established concepts, EPFM is still very much an evolving discipline. The reason is the greater complexity of elastic-plastic analyses. Important topics are:

- The description of stable ductile crack growth (tearing), which is the subject of this dissertation.
- The development of failure assessment methods that combine the affects of plasticity and fracture.

As opposed to using the above-mentioned global fracture mechanics parameters, fracture problems are also increasingly being tackled by means of local fracture criteria.

In studying material containing cracks, a whole hierarchy of models, tools, and techniques exist with differing complexity and generality. The simplest model with sufficient descriptive/predictive power is obviously the best model to use. For engineering materials, model choice should be made carefully and must be justified.

A brief description of two relevant tip models and failure criteria follows. As these concepts are elemental to fracture mechanics, a more complete description can be obtained from any good text on the subject, such as Anderson [2].

## 2.4. LINEAR ELASTIC FRACTURE MECHANICS (LEFM)

When possible, fields around a single crack tip are analyzed using Linear Elastic Fracture Mechanics (LEFM) as this is the simplest model. Within LEFM any arbitrary crack tip stress state in a linear elastic isotropic homogeneous material can be decomposed into the unique linear combination of the three mutually orthogonal modes: symmetric in plane (mode I), antisymmetric in-plane (mode II), and out-of-plane (mode III). In other words, the cracked body can be loaded in any one or a combination of the three loading (displacement) modes that are schematically depicted in Figure 2.2. Mode I is called the opening or tensile mode, where the crack walls, faces, move directly apart. Mode II, the sliding or in-plane shearing mode, where the crack faces slide over, and relative to, one another in a direction perpendicular to the leading edge of the crack. Finally, Mode III, the tearing or antiplane shearing mode, where the crack faces slide away from each other in a direction parallel to the leading edge of the crack [2]. Mode I is caused by tension loading, where as the other two are caused by shear loading in different directions as shown in Figure 2.2. If a crack surface is not normal to the applied stress, or if there is a complex state of stress, a combination of fracture modes I, II, and III may exist. Thus, combinations of loading that involve more than one crack-tip mode are referred to as mixed mode.

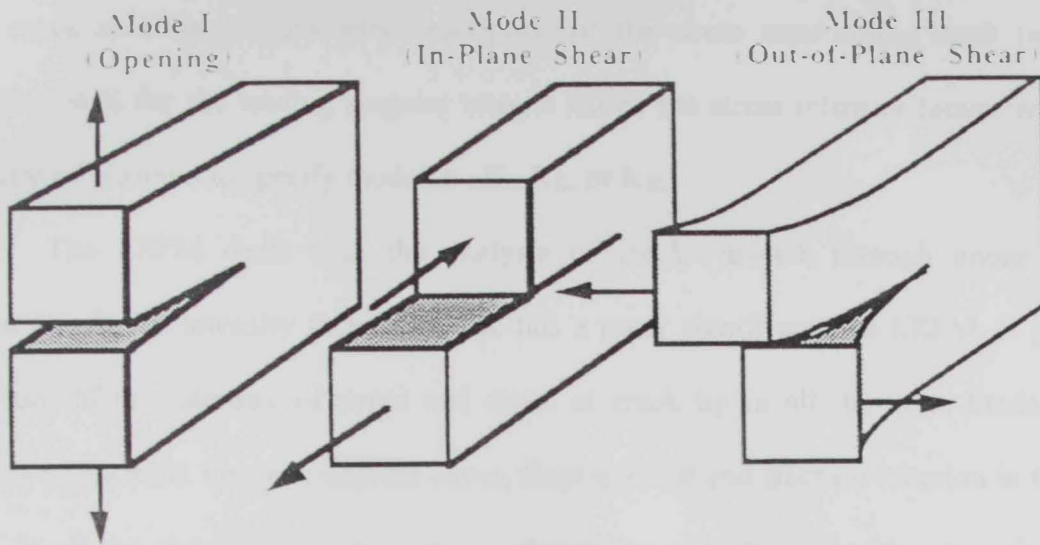


Figure 2.2 The basis modes of loading (crack surface displacement) that can be applied to a crack. [1]

For each mode, stress-field satisfying the boundary condition of having stress-free crack faces are asymptotic with unknown coefficient reflecting unspecified far-field boundary conditions (Westergaard [3], Irwin [4], Sneddon [5] and Williams [6]) are of the form:

$$\sigma_{ij} = \left( \frac{K}{\sqrt{2\pi r}} \right) f_{ij}(\theta) + \sum_{m=0}^{\infty} A_m r^{\frac{m}{2}} g_{ij}^{(m)}(\theta) \quad (2.1)$$

where  $\sigma_{ij}$  is the stress tensor,  $r$  and  $\theta$  coordinates with respect to the usual crack tip coordinate system  $f_{ij}$  and  $g_{ij}$  are functions of  $\theta$ , and  $K$  and  $A_m$  are the coefficients of the singular and higher order terms respectively. The term  $f_{ij}$  is a universal function and holds for all cracks propagating at speed much slower than the material's shear wave speed, including stationary cracks.

For each mode the leading asymptotic term is singular and thus dominates near the crack tip. Because of this dominance, the leading term's coefficient (or magnitude) can serve as a single parameter description of the stress state at the crack tip. The coefficient  $K$  for the leading singular term is called the stress intensity factor, which is usually subscripted to specify mode i.e.,  $K_I$ ,  $K_{II}$ , or  $K_{III}$ .

The LEFM deals with the analysis of cracks growth through linear elastic materials. Stress intensity factor (SIF)  $K$  has a great significance in LEFM. It gives a measure of the intensity of stress and strain at crack tip in all the three fundamental modes of fracture. One can express stress, displacement and fracture criterion in term of 'K'. In all the three modes, stress has a singularity of order  $1/\sqrt{r}$ . The stress intensity factor determines the magnitude of local stresses and it gives a clear picture of stress-strain environment at the crack tip. It has a critical value at the point of onset of unstable extension, and crack stress field for a complex problem can be obtained easily through superposition. The critical value of stress intensity factor at which the crack extension begins is known as fracture toughness. The fracture toughness is a material parameter and it can be determined experimentally [7]. The crack tip severity can also be expressed in terms of energy release rate  $G$ ,  $J$  integral, and COD ( $\delta$ ). The fracture condition can be expressed in terms of three parameters. All criteria indicate that crack growth occurs when the basis parameter reaches a critical value. It's quite known that the parameters are related, e.g.  $G = J = (1 - \nu^2) K^2 / E$  under plane strain and  $G = J = K^2 / E$  under plane stress, where  $E$  is the elastic modulus and  $\nu$  is the Poisson ratio. [8]

Real material cannot support the theoretical infinity stresses at the tip of a sharp crack, so that upon loading the crack tip becomes blunted and a region of yielding,



crazing, or microcracking forms. Due to yielding within the plastic zone, the stresses are lower than the values from the elastic stress field equations. LEFM can be used as long as the plastic zone is small, which is the case when the stress is low with respect to the yield stress ( $\sigma = 0.8 \sigma_y$ ). When the stresses are higher the plastic zone will spread beyond the point at which it can be expressed uniquely as a function of K, so that K is no longer useful as a similitude parameter. Such high stress occurs at the point of fracture if the toughness is very high [8].

## 2.5. UNSTABLE PATH OF CRACK EXTENSION

The unstable crack extension takes place mostly immediately upon initiation through brittle materials. Therefore, it is of importance to know the initiation load, direction of initiation crack growth initiation and unstable crack path can be predicted. A number of criteria are available for the prediction of brittle fracture load ( $P_c$ ) and direction of initial crack initiation ( $\theta$ ). All these are defined using some aspects of stress-strain field existing prior to the start of propagation. The criteria that are widely used are:

- 1- The maximum tangential stress (MTS) criterion [9]
- 2- The maximum tangential principal stress (MTPS) criterion [10]
- 3- The maximum tangential strain (MTSN) criterion [11]
- 4- The strain energy density (SED) criterion [12]

According to the MTS criterion, the crack extended in a radial direction perpendicular to the direction of maximum tangential stress, and the extension starts when the maximum tangential stress reaches a critical value. The maximum tangential principal stress criterion states that the crack extends in a radial direction perpendicular to the

direction of maximum tangential stress, or the direction of zero shear stress. The extension starts when the maximum tangential stress reaches a critical value. Maximum tangential strain criterion is identical to the MTS criterion except that the basis is strain rather than stress. According to the strain energy density the crack extended in a radial direction of minimum strain energy density.

## 2.6. SMALL SCALE YIELDING

A stress singularity at the crack tip as predicted by LEFM cannot exist in materials with finite strength. Instead the highly stressed material yields and plastically deforms. To first order the size of the plastic zone for mode I is:

$$r_p = \frac{1}{2\pi} \left( \frac{K_I}{\sigma_{YS}} \right)^2 \quad (2.2)$$

where  $\sigma_{YS}$  is the material yield stress. The actual shape of the plastic zone depends on crack tip triaxiality. Linear Elastic fracture Mechanics (LEFM) can deal with only limited crack tip plasticity, i.e. the plastic zone must remain small compared to the crack size and the cracked body as a whole must still behave in an approximately elastic manner. If this is not the case then the problem has to be treated elasto-plastically. However, if the size of the plastic zone is sufficiently small as compared to the size of crack and any other geometrical dimensions (small scale yielding), the elastic singularities fields still give good approximation to the actual field in an annular region surrounding the crack tip

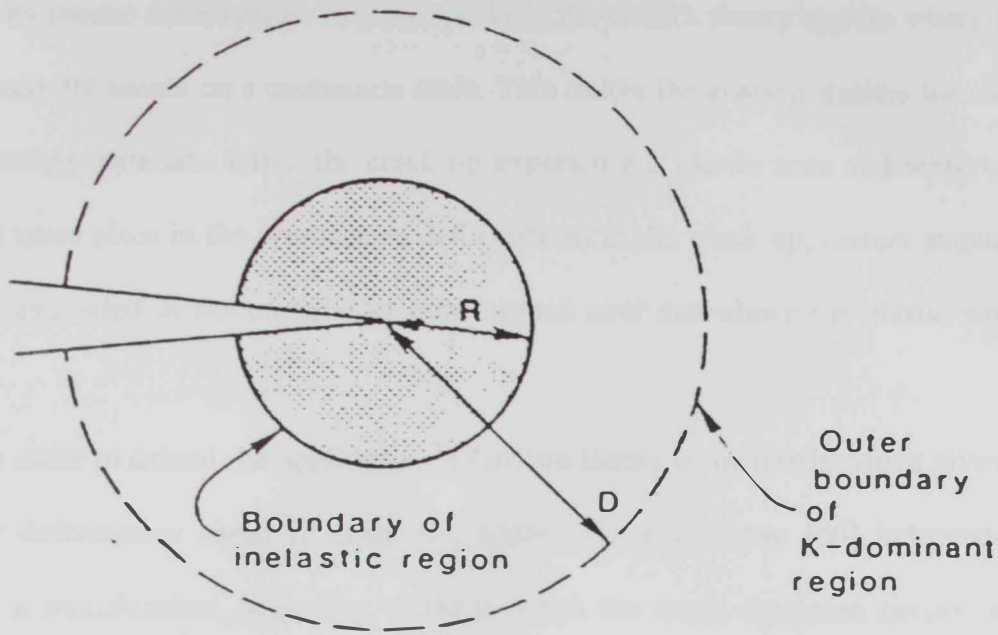


Figure 2.3 Basic of Linear Elastic Fracture Mechanics

In materials that are well modeled by LEFM, the plastic zone is small enough to be completely surrounded by an annulus in which stresses are described by the  $K$ -field (leading term in the asymptotic expansion Equation. 2.1). The outer limit of the  $K$ -field dominated annulus is due to the increasing relative contributions of higher order asymptotic stress field terms. However since a  $K$ -dominated annulus completely bounds the crack tip,  $K$  is still a single parameter description of the crack tip stress state in that it describes the entire boundary conditions of the crack tip. This concept that LEFM can still describe crack tip fields in such materials despite crack tip yielding is called small scale yielding (S.S.Y.) (Freund [13], Freund and Rosakis [14]).

There are many materials in which crack growth initiation and/or extension is preceded by plastic deformation. Strictly speaking the Griffith theory applies where non-linear effects are absent on a continuum scale. This makes the analysis useless for almost all engineering materials. Often the crack tip experience a plastic zone and when crack extension takes place in the presence of deformations at the crack tip, certain amount of energy is expended in the creation of new surface over and above the elastic surface energy.

In order to extend the application of Griffith theory to materials which gives rise to plastic deformation ahead of crack tip, Irwin [15] and Orwan [16] independently proposed a modification. According to them, when the crack extension occurs in the presence of the plasticity effects, a certain amount of energy is expended in the irreversible deformation process, for plastic deformation around the crack tip over and above the elastic energy for creation of new surfaces. In fact, the elastic energy required is very negligible compared with the plastic work. Later Irwin, Kies and Smith [17] proposed the first method of quantitative accounting for the effect of the plastic zone at the crack tip. They proposed that the physical crack length can be amended by a correction factor, which depends on the extent of plastic deformation, and the problem can be treated mathematically as linear elastic. Gradually, efforts have been made to accommodate more plasticity effects than what is possible by their approaches.

Thus, the early attempts to model the plastic deformation attending the crack tip were based on extension of LEFM. However if the size of plastic zone is large then assumption of small scale yielding no longer holds good. To include the influence of this significant plastic deformation that may accompany crack initiation and subsequent stable

crack growth one has to go in for elastic-plastic fracture mechanics EPFM. The development in the EPFM, which deals with such cases, is rather slow. One of the reasons for this is that it is difficult to obtain precisely the stress-strain field in the presence of plastic deformation.

## **2.7. ELASTIC-PLASTIC FRACTURE MECHANICS**

EPFM is used when the crack tip is not sharp and there is some crack-tip plasticity (blunting). EPFM is used to design materials such as lower-strength, higher-toughness steels. For such more ductile material the assumption of small scale yielding may not be met disallowing LEFM analysis. The next level of fracture modeling is Elastic-Plastic Fracture Mechanics (EPFM). In such cases the problem has to be treated elasto-plastically. Due to its complexity the concepts of Elastic-Plastic Fracture Mechanics (EPFM) are not so well developed as LEFM theory, a fact that is reflected in the approximation nature of the eventual solutions.

### **The Dugdale Model**

Dugdale [18] analyzed the plastic zone size ahead of a mode I crack by treating it as a strip of yielded materials and using the complex variable formulation of elasticity. For elastic-perfectly plastic material, Dugdale found very good agreement between predicted and experimental results; later Hahn and Rosenfield [19] confirmed the accuracy of Dugdale predictions experimentally. The plastic zone size given by Dugdale model tallied with the results of Bilby, Cottrell and Swiden [20], who treated the crack as a continuous distribution of dislocations. The Dugdale approach has been later applied by

other investigators [19, 21, 22] to determine the crack opening displacement (COD). In the presence of a small-scale plasticity, crack growth can take place stably till the instability; such phenomenon under plane stress condition has been sometimes studied by the concept of resistance (R) curves [8].

### Crack Opening Displacement Approach.

The approach of Irwin, Kies and Smith [17] was suitable where plasticity at the crack tip occurs on a small scale. In 1963 Wells [23] introduced the crack opening displacement (COD) approach as an alternate approach which is useful, even in the case of a large scale plastic deformation. This approach focuses on the strains in the crack tip region instead of the stresses, unlike the stress intensity approach. In the presence of plasticity a crack tip will blunt when it is loaded in tension. Wells proposed to use the crack flank displacement at the tip of a blunting crack, the so-called crack tip opening displacement (CTOD) as a fracture parameter Figure 2.4 .

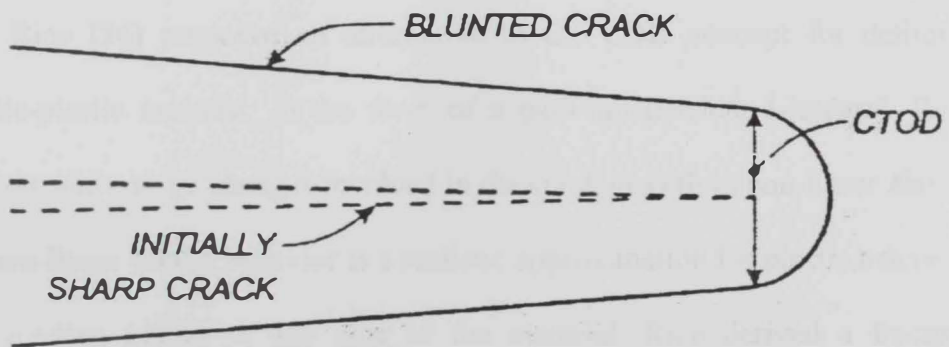


Figure 2.4. Cracked tip opening displacement

Even for tougher materials exhibiting considerable plasticity critical CTOD values could be defined corresponding to the onset of fracture. Such critical CTOD values could then be used to qualify the materials concerned for a given application. However, initially it was proved difficult to determine the required CTOD for a given load and geometry or alternatively to calculate critical crack lengths or loads for given material. Burdekin and Stone [24] showed the validity of the criterion by conducting experiments with milled steel in tension and bending. This work provided the basis for COD approach in design under contained yielding conditions. There are some difficulties associated with the COD approach. It is a problem to define precisely the point at which the COD should be measured. Turner [25] noted that there are two values of CODs; one ( $\delta_i$ ) associated with the initiation of crack extension and the other ( $\delta_m$ ) corresponding to the maximum load.  $\delta_i$  is more nearly independent of geometry than  $\delta_m$  but the numerical values of  $\delta_i$  at crack initiation are small.

### **J Integral Approach**

In 1968 Rice [26] proposed an alternative to the COD concept for defining fracture in elastic-plastic material, in the form of a path-independent J-integral. Rice considered the potential energy changes involved in the crack growth in non-linear elastic material. Such non-linear elastic behavior is a realistic approximation for plastic behavior provided no unloading occurs in any part of the material. Rice derived a fracture parameter called J, a contour integral that can be evaluated along any arbitrary path enclosing the crack tip, as illustrated in Figure 2.5. He showed J to be equal to the energy release rate for crack in nonlinear elastic material, analogous to G for linear elastic

material. With this key paper, Rice laid the groundwork for the bulk of the applications in elastic-plastic fracture mechanics and for crack-tip characterization in a variety of other applications.  $J$  is given by,

$$J = \int_{\Gamma} \left( W dy - T_i \frac{\partial u_i}{\partial x} ds \right) \quad (2.3)$$

where  $\Gamma$  is an arbitrary path counter-clockwise around the crack tip,  $T_i$  are components of the traction vector perpendicular to  $\Gamma$ ,  $u_i$  are displacement vector components,  $W$  is the strain energy density and the  $y$  direction is taken normal to crack line as shown in Figure 2.5.

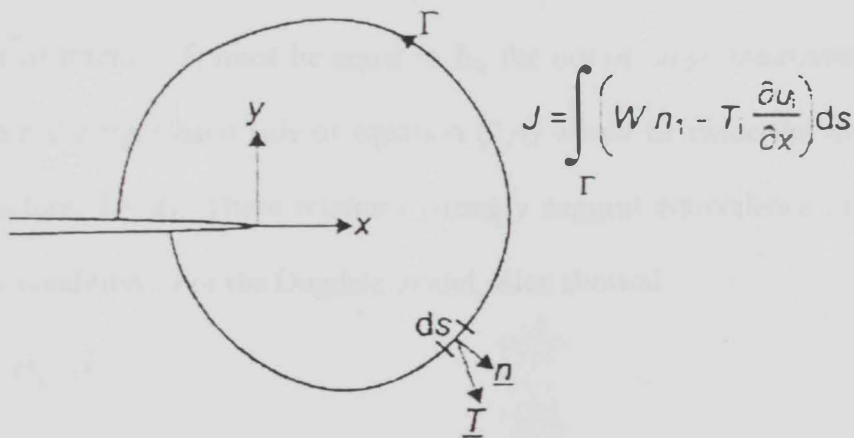


Figure 2.5.  $J$  contour integral along arbitrary path  $\Gamma$  enclosing a crack tip in non-linear elastic material.  $W$  is strain energy density along,  $\underline{n}$  is outward-directed unit vector normal to  $\Gamma$ ,  $\underline{T}$  is traction acting on and  $\underline{u}$  is the displacement along  $\Gamma$ .

For a nonlinear elastic material the  $J$ -integral was shown to be a parameter characterizing the crack-tip mechanical environment.  $J$  is interpreted as the rate of change



of potential energy for nonlinear constitutive behavior and it can give the potential energy release associated with crack advance [8].  $J$  is used to define fracture in elastic-plastic fracture mechanics closely parallel to  $K$ , stress intensity factor, in the LEFM. The role played by  $J$  in unifying LEFM is explained by Rice with aid of Barenblatt's model. By taking  $\Gamma$  to be contour that just circumscribes the cohesive zone in Barenblatt's model, Rice readily found that

$$J = \int_0^{\delta_t} \sigma(\delta) d\delta \quad (2.4)$$

where  $\sigma$  = cohesive stress and

$\delta_t$  = separation distance at crack-tip

At the onset of fracture,  $\delta_t$  must be equal to  $\delta_c$ , the out-of-range interatomic separation distance. Then the right-hand side of equation (2.4) would be twice the surface energy. Thus for fracture,  $J_c = 2\gamma$ . These relations strongly suggest equivalence in  $J$  and  $G$  for linear elastic conditions. For the Dugdale model, Rice showed

$$J = \sigma_y \cdot \delta_t \quad (2.5)$$

where  $\sigma(\delta)$  is equal to  $\sigma_y$  and  $\delta_t$  is the crack tip opening displacement. From energy release rate interpretation of  $J$ , it can also be shown that

$$J = - \frac{\partial \pi}{\partial a} = G \quad (2.6)$$

where  $\pi$  denotes potential energy of cracked body. Thus equations (2.5) and (2.6) show the equivalence of all of the popular fracture mechanics parameter under linear elastic conditions.

The characterization of crack tip stress-strain field and path independence of  $J$  was based on the assumption of a nonlinear elasticity. Upto the onset of crack extension there is a simple monotonic loading of the body and no element of material unloads. Till this point both a non-linear elastic material and an elastic plastic material obeying the deformation theory of plasticity are identical. For both, the stress-strain state depends on the final state and not on the path of loading. Based on this argument  $J$ -integral is considered useful for elastic-plastic situations. The assumption of a deformation theory of plasticity does not lead to a serious limitation of the  $J$ -integral as shown by Budiansky [27]. This is because, when nearly a proportional deformation occurs, the difference between the deformation theory of plasticity and the incremental theory of plasticity is negligible. However this cannot be true for a growing crack in a real elastic-plastic material as elastic unloading and non-proportional loading occurs near the crack-tip and none of these processes is adequately represented by the deformation theory of plasticity. In this type of situation an analysis based on the incremental theory of plasticity is called for.

Though  $J$  is considered to represent the energy release rate, it is not valid under elastic-plastic situations because of two reasons. First, loading and unloading curves are different. Second, there is some energy absorbed in the plastic deformation. In spite of all these,  $J$  is used for the characterization of crack-tip stress-strain field and crack extension is associated with a critical value of  $J$ .

For simple geometries and load cases the  $J$  integral can be evaluated analytically. However, in practice finite element calculations are often required. In spite of this  $J$  has found widespread application as a parameter to predict the onset of crack growth in

elastic-plastic problems. Later it was found that  $J$  could also be used to describe a limited amount of stable crack growth. [1]

## 2.8 CRACK TIP FIELD:

### 2.8.1. Crack Tip Field for a Stationary Crack in Ductile Material

The elastic-plastic stress-strain field around a stationary crack was first determined by Hult and McClintock [28] for a mode III crack using the deformation theory of plasticity. They showed that there is a strain singularity of order  $r^{-1}$  in the case of elastic-perfectly plastic material. Similar solution for mode I stationary crack was obtained by Hutchinson [29] and Rice and Rosengren [30]. They showed that the stresses and strain in the vicinity of the crack tip under both small scale yielding and fully plastic conditions may be presented by

$$\sigma_{ij} = \sigma_Y \left( \frac{EJ}{\sigma_Y^2 I_n r} \right)^{\frac{1}{n+1}} \bar{\sigma}_{ij}(\theta, n)$$

$$\varepsilon_{ij} = \frac{\sigma_Y}{E} \left( \frac{EJ}{\sigma_Y^2 I_n r} \right)^{\frac{n}{n+1}} \bar{\varepsilon}_{ij}(\theta, n) \quad (2.7)$$

where

$J$  = Rice's  $J$  integral

$\sigma_Y$  = yield stress

$E$  = elasticity modulus

$n$  = hardening exponent of Ramberg-Osgood relationship

$r, \theta$  = polar co-ordinates referred to the crack tip

$\overline{\sigma}_{ij}(\theta, n), \overline{\varepsilon}_{ij}(\theta, n)$  = Known dimensionless functions of  $\theta$  and hardening exponent  $n$  and,

$I_n$  = a constant, which is function of  $n$  only.

$J$  is the amplitude of the stress and strain singularities in equation 2.7.

For a fully plastic material ( $n=\infty$ ), the strain fields exhibit a  $r^{-1}$  singularity. In this case the equation (2.7) becomes

$$\begin{aligned} \sigma_{ij} &= \sigma_Y \overline{\sigma}_{ij}(\theta, n = \infty), \text{ and} \\ \varepsilon_{ij} &= \frac{\alpha \delta_t}{I_n r} \overline{\varepsilon}_{ij}(\theta, n = \infty) \end{aligned} \quad (2.8)$$

where  $J = \alpha \sigma_Y \delta_t$

$\delta_t$  = Crack tip opening displacement (COD), and

$\alpha$  = a parameters of order unity.

Equation (2.7) and (2.8) are known as the Hutchinson, Rice and Rosengren (HRR) singularity field and  $J$  and  $\delta$  are field parameters. When HRR field encompasses the fracture process zone, the HRR parameters,  $J$  and  $\delta$  are likely to characterize the fracture process to the onset of the crack growth. There is evidence that under both small and large scale yielding at the onset of crack growth initiation for certain crack configurations; the HRR zone embeds the fracture process zone.  $J$  or  $\delta$  can therefore be used to define fracture in EPFM closely parallel to  $K$ , the stress intensity factor in LFM.

The above crack tip fields are obtained using the  $J_2$ -deformation theory of plasticity as opposed to the incremental theory, which is more valid for metallic materials and assuming that geometric changes are negligible or small deformation theory is valid.

The obtained stress-strain state is independent of loading path according to the

deformation theory but it is not so as per the incremental theory. The above characterization of the crack-tip field in terms of  $J$  and the path independence of  $J$  count on this load-path independence. Up to the onset of crack extension there is simple monotonic loading of the body and no element of material unloads. More or less a proportional loading exists and difference between the two theories is negligible [25-27]. Based on this argument  $J$  is considered suitable for materials obeying incremental theory of plasticity. The path independence of  $J$  for real elastic-plastic materials is not yet established analytically. This has been shown only by finite element computations [31-32]

The crack tip fields have been analyzed by the slip line field theory by McClintock [33] and Rice and Johnson [34]. In the strain hardening materials under small or large scale yielding, the HRR singularity dominates over a significant distance always greater than 4 to 6 times the crack opening displacement, a head of the crack tip when the uncracked ligament is subjected primarily to bending [31, 35-37]. It is also reported [31, 35-38] that when the ligament is primarily in tension, the HRR does not dominate over any region of appreciable dimensions.

### **2.8.2 Crack-Tip Field for a Propagating Crack in Ductile Material**

After the onset of crack growth, further propagation, in an elastic-plastic material takes place with an increasing load. For a growing crack both an elastic unloading and a non-proportional loading occur near the tip. This is schematically shown in Figure 2.6. None of these processes is adequately representable by the deformation theory of

plasticity. These make the determination of crack tip field a head of an extending crack difficult mathematically.

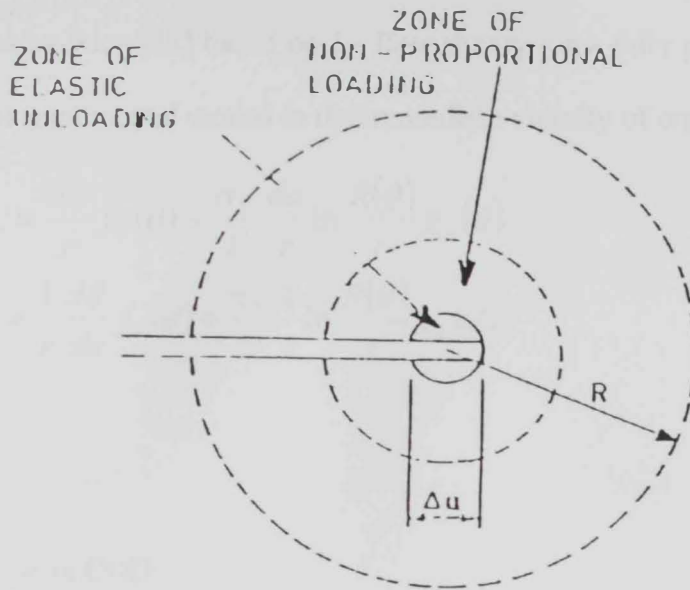


Figure 2.6 Schematic for the field surrounding a growing crack

A study of mode III problem was first reported by McClintock and Irwin [41], and a full solution, subjected to corrections by Rice [42] and Broberg [43] was given by Chitaley and McClintock [44]. The general form of the solution for a plane strain mode I crack extending through an elastic-perfectly-plastic material was first given by Rice [42]. He used the  $J_2$  deformation theory of plasticity. Similar results for rigid-plastic materials was given by McClintock [33, 45], and Chitaley and McClintock [44]. At the tip of crack growing through an elastic-perfectly-plastic material there is a logarithmic,  $\ln|/r$ , strain singularity, which is much weaker than a  $r^{-1}$  singularity in the case of a stationary crack. This reduced strain singularity partly explains the phenomenon of stable crack growth.

Rice's analysis [42] has been extended by Cherepanov [46] for general non-steady growth, Amazigo and Hutchinson [47] for steady-state growth through an isotropically hardening solid with flow strength increasing linearly with strain.

The studies by Rice [42] based on  $J_2$ - flow theory for a fully plastic material ( $n = \infty$ ) showed that the incremental strains in the immediate vicinity of crack tip are given by

$$d\varepsilon_{ij} = \frac{d\delta}{r} f_{ij}(\theta) + \frac{\sigma_Y}{E} \frac{da}{r} \ln \frac{R(\theta)}{r} g_{ij}(\theta)$$

2.9

$$\text{or } \frac{d\varepsilon_{ij}}{da} = \frac{1}{r} \frac{d\delta}{da} f_{ij}(\theta) + \frac{\sigma_Y}{E} \frac{1}{r} \ln \frac{R(\theta)}{r} g_{ij}(\theta)$$

where

$d\delta$  = increase in COD

$da$  = incremental of crack extension,

$g_{ij}(\theta)$  = dimensionless function of order unity,

$f_{ij}(\theta) = \alpha \bar{\varepsilon}_{ij}(\theta, n = \infty) / I_n$ , {see equation. 2.8}, and

$R(\theta)$  = a measure of the distance from the crack tip to the elastic-plastic boundary.

The first term in equation. (2.9) represents the additional strains due to crack tip blunting if the crack tip doesn't advance during load/displacement increments. The second term in equation. (2.9) represents the additional plastic strains caused by the advance of stress field through the material. In many cases, the first term dominates over a significant interval compared to  $\delta_1$  (equation.2.7), except right at the crack tip where the  $(1/r) \ln(R/r)$  singularity dominates [48]. In another words, the strains at the crack tip are uniquely characterized by the crack tip opening angle

$$\frac{ds}{da}, \text{ if } \frac{d\delta}{da} \gg \frac{\sigma_0}{E} \ln \frac{R(\theta)}{r}$$

Hutchinson and Paris [49] based on the  $J_2$  deformation theory of plasticity, for a fully plastic material ( $n=\infty$ ), obtained the incremental strains during the crack growth in the form.

$$\begin{aligned} d\varepsilon_{ij} &= \frac{1}{\alpha\sigma_Y} \frac{dJ}{r} f_{ij}(\theta) + \frac{J}{\alpha\sigma_Y} \frac{da}{r^2} \beta_{ij}(\theta) \\ \text{or } \frac{d\varepsilon_{ij}}{da} &= \frac{1}{\alpha\sigma_Y} \frac{dJ}{da} \frac{1}{r} f_{ij}(\theta) + \frac{1}{\alpha\sigma_Y} \frac{1}{r^2} \beta_{ij}(\theta) \end{aligned} \quad 2.10$$

where  $\beta_{ij}(\theta)$  is a dimensionless quantity of order unity. This relation indicates the  $J$  uniquely characterizes the near field if  $(dJ/da) \gg (J/r)$ .

The similarity in the structure of the two equations (2.3 and 2.4), derived distinctly from the different approaches is notable. Their first terms represent proportional increments in the strain field due to an increase in the strength of the HRR singularity, while the second terms show the non-proportional strain increments due to an advance of the HRR field with an exceeding crack. Therefore, if the HRR field increase in strength more rapidly that it advances then the crack tip opening angle,  $(d\delta/da)$  and  $dJ/da$ , describe the crack-tip environment. This means that when the fracture process zone is enclosed by the region dominated by  $(d\delta/da)$  or  $(dJ/da)$  equations (2.9 and 2.10) and together with restraints,  $d\delta/da \gg (\sigma_Y/E) \ln(R(\theta)/r)$  and  $(dJ/da) \gg J/r$  provide the basis for COD-based and J-based resistance approach to stable crack growth.

Basing on theses type of characteristics Paris et al. [50]. Introduced non-dimensional parameter  $T_{mc}$  called tearing modulus defined by



$$T_{mc} = \left( \frac{E}{\sigma_Y^2} \right) \left( \frac{dJ_R}{da} \right) \quad (2.11)$$

As a material parameter, signifying the material's resistance to crack growth. In above relationship  $J_R$  vs.  $a$  is a resistance curve and  $dJ_R / da$  is its slope. The condition for instability is given by

$$T_m \geq T_{mc} \quad (2.12)$$

where  $T_m = \left( \frac{E}{\sigma_Y^2} \right) \left( \frac{dJ}{da} \right)$ , and is known as the crack driving force.

Accordingly to Paris et al. [50] during the stable tearing extension,  $T_m$  remains constant and the value of  $T_{mc}$  is dependent on specimen geometry, loading, etc. The tearing modulus can also be based on  $\delta$ -resistance curve.

$$T_{mc}(\delta) = \left( \frac{E}{\sigma_Y} \right) \left( \frac{d\delta_R}{da} \right) \quad (2.13)$$

Under a J controlled growth  $T_{mc}$  and  $T_{mc}(\delta)$  are related [51] by

$$T_{mc}(\delta) = \frac{n}{n+1} d_n T_{mc} \quad (2.14)$$

where  $d_n$  is a constant in  $J = \left( \frac{1}{d_n} \right) \sigma_Y^2 \frac{dJ}{da}$ .

This relation indicates that, for an extension under a constant COA,  $(d\delta/da)$ , the J-resistance curve is straight-line. Further, the relation is valid subjected to the two conditions First,  $ndJ/J \gg da/r$ . Second, the amount of crack extension  $\Delta a$  is small compared with the size of the HRR singularity dominated region. The first condition stipulates the J-dominance around the crack-tip during the extension. This, in turn, ensures the dominance of proportional loading over the non-proportional part due to

elastic unloading. When the proportional loading is significant the difference between the deformation theory and the incremental theory is negligible. Since the situations under consideration is dominated by the proportional loading, they can be analyzed using the deformation theory and they must involve small crack growth compared with the size of the HRR singularity zone, and hence the second condition. Shih [51] has corroborated the existence of a constant  $T_m$  during stable tearing and the validity of relation (2.14) based on the experimental data of a number of investigators [e.g.52].

Recently, Ma et al [53] have proposed a plane strain mixed mode crack-tip stress fields characterized by a triaxial stress parameter and a characteristic length based a plastic deformation extent. Based on physical observation from controlled crack growth experiments in ductile materials, they have performed a series of numerical and theoretical studies. The finite element models indicated that, for the full range of mode mixity and constraint conditions, the proposed, self-similar family of mixed mode crack-tip fields accurately represents the stress fields for all fracture specimens considered.

Chen et al. [54] have investigated the plane-stress asymptotic field near a crack tip for elastic-plastic materials with strain gradient effects. They have established that, at a fixed distance  $r$  to the crack tip, the maximum shear stress is more than three times its counter part in the HRR field in mode II, and is nearly doubled in mode I. The increases are consistently larger than those observed in plane strain, namely 2.5 times in mode II and 1.7 times in mode I. Though this increase in stress level is not large enough to explain the atomistic fracture process in ductile metals discussed in [55], it has shed some light that the strain gradient plasticity theory based on rotation and stretch gradient of

deformation [18] may link macroscopic fracture behavior to atomistic fracture processes in ductile metals.

In order to improve upon continuum models for understand the origins of ductile versus brittle response in materials, an accurate assessment of the stress fields near a crack tip must be developed. Existing continuum models have considered the crack tip to be perfectly sharp in order to use convenient analytical solutions for the crack tip. The physical reality of a blunted crack configuration has motivated limited attempts at evaluating its effect and determining what to extent its stress field differ from the sharp crack stress fields [e.g. Schiøtz and co-workers [56,57], Gumbsch and co-workers [58,59], and Thomson [60]]. Fisher and Beltz have [61] reported, upon reviewing current models for quantifying ductile versus brittle fracture behavior, that changes in the crack tip geometry will significantly affect the stress fields around the crack tip, which can change the favorability of crack advancement or dislocation emission. They have presented a two-dimensional finite element models to evaluate the stress fields at a blunt crack tip subjected to loading. Stress fields have been calculated for mode I loading as well as for self-stress due to the presence of dislocation near a crack tip. They have compared these calculated stress fields with analytical solutions for appropriate limiting cases. Recently, Fisher and Belz [62] have used the available closed form stress fields solution for a crack tip of elliptical geometry to calculate the thresholds for dislocation nucleation and atomic decohesion.

## **2.9. CRITERIA FOR CRACK GROWTH**

There has been a considerable advances in the understanding of mode I crack growth initiation, stable crack growth and instability. The advances are founded on the solutions for crack tip fields for stationary and growing cracks. A review of the criteria is given in [63].

### 2.9.1 Crack Growth Initiation

In the approach of Wells [23] the condition for fracture initiation is given in terms of a crack opening displacement (COD). This has also been considered relevant for the post initiation stage [see 63]. It is assumed that a characteristic displacement behind the crack tip triggers the crack extension at all stages starting from initiation to collapse. The foundation for the application of the COD approach to fracture in design is mostly due to Burdekin and Ston [24]. There are two values of COD; one ( $\delta_i$ ) is associated with the initiation of crack extension and the other ( $\delta_m$ ) corresponds to the maximum load [25]. A design calculation based on  $\delta_i$  does imply an unrealistic degree of conservatism in relation to the final fracture, where as  $\delta_m$  might or might not coincide with the onset of unstable crack growth.

The use of  $J$  as a HRR field parameter has been confirmed by the experimental observations of different investigators, e.g. [64,65].  $J$  does not represent the energy release rate with crack advance for a real elastic-plastic material because of two reasons. First, loading and unloading curves for a material element are different. Second there is some energy absorbed in plastically deforming an element. In spite of all these,  $J$  is used for the characterization of the crack tip stress-strain field and the onset of crack extension. The onset of crack growth is given in terms of  $J$  reaching a critical value provided that certain limits relating to specimen dimension are exceeded. Such limits are

close, for example, to the ones for the plane strain fracture toughness ( $J_{IC}$ ) testing. Thus characterization of initiation of crack growth is possible in terms of  $J$  and COD.

### 2.9.2. Stable Crack Growth

McClintock and Irwin [41] first stated that a crack extends stably when strain at a characteristic distance ahead of crack tip reaches a critical value. Anderson [66,67], de Koning [68], Luxmoore et al, [69], Newman [70], Kanninen et al. [71], Wang [72], etc., have shown that the condition for the continuing mode I stable crack extension can be specified in terms of a COA behind the crack tip. There is a difficulty with such a parameter. The crack assumes a curvilinear profile proportional to  $r \ln r$ . The profile has a vertical tangent at the crack-tip and hence an ambiguous value of the COA. At a finite distance from crack-tip, however, there is a finite slope and hence a meaningful definition of the parameter is possible. Shih et al. [35] and Kanninen et al. [71] have shown that COA at initiation is higher than the value at the later stage of stable growth. Some investigators [e.g. 73] have shown that the mode I initiation can be specified in term of  $J_c$  or  $\delta_c$  and the stable extension is governed by a constant COA.

Maiti and Mourad [74,75], Mourad and Maiti [76-81] and Mourad [82] work of Mourad definition used by Newman [70] is adopted. The COA is the ratio of COD and the distance behind the crack tip at which the crack opening is considered. There is a very good agreement between the predicted and the experimental results. Similar results were presented by Wang [72]. In Koledink [82] it was worked out clearly that two parameter are needed to describe a ductile fracture process: the crack growth initiation toughness and the crack growth toughness. Shan et al. [83] have indicated that, the critical crack tip

opening displacement,  $CTOD_i$ , for the crack growth initiation and the critical crack tip opening angle,  $CTOA_c$ , for the stable crack growth are applied as the input data for the numerical simulation of the fracture process.

### 2.9.3 Finite Element Analysis of Stable Crack Growth

In case of elastic-plastic material a load increment beyond the yield point will give rise to both elastic as well as plastic strains. Thus, total strain increment can be written as

$$d\varepsilon = d\varepsilon^e + d\varepsilon^p \quad (2.15)$$

For the elastic part if the material is isotropic, stress-strain relationship is given by Hook's law as

$$\{\sigma\} = E [D]^e \{\varepsilon\} \quad (2.16)$$

Similar relations can be written for the plastic strain but then  $[D]^p$  matrix will no longer be matrix of constants. It will have some strain dependent terms.

Marcial and King [cited in 63] proposed a method in which mean stiffness is used for the element, which yields in the next increment of loading. This method doesn't have any restriction on increment of loading and uses an iterative procedure for the determination of 'the partial stiffness coefficients' or the stress-strain matrix. Yamada et al. [cited in 63] first gave explicitly the stress-strain matrix for an elastic-plastic element. They also proposed an algorithm, which works with small load increments. All the above schemes can be interpreted as the variants of Newton-Raphson scheme for the solution of nonlinear equations.

The Newton-Raphson scheme required modification of the coefficient matrix at each iteration. The modified Newton-Raphson scheme can be adapted to avoid this problem and solution time can be reduced considerably. But this scheme may require a large number of iteration within a load step. The general steps followed in the finite element analysis of stable crack growth are reported in [63]

## 2.10. MIXED MODE STUDIES

Very few studies [e.g. 74-81, 84-91] investigated the mixed mode problems; and most of them deal with the initiation phase. Shih [86] has examined the direction of initial crack extension and critical load under very small-scale yielding and plane strain condition. He showed that MTS criterion [9] can be used to predict the results on metals [86]. Ahmad, Barnes and Kanninen [84] have studied, theoretically and experimentally, the crack initiation problem under both static and dynamic loading and tried to specify the condition for the onset of fracture in terms of  $\int$  integral.

Mourad and Maiti [75, 76], Mourad and Maiti [e.g., 77, 78] and recently Mourad [81] have examined both experimentally and theoretically the mode I and mixed mode stable crack growth through different specimens' configuration. In these studies, TPB specimen with inclined edge crack, TPB specimens with offset edge crack and CT specimens have been employed. They have also studied mode II stable crack growth through compact-shear specimen [79]. They have carried out both experimental and theoretical investigation considering doubly stiffened and/or unstiffened, 8mm thick specimens of D16AT aluminum alloy to examine the possibility of characterizing the whole stable crack growth from initiation to maximum load under various modes of two

dimensional loading in terms of COA criterion. They have concluded mainly based on the agreement between theoretical and experimental load-displacement diagrams that the whole crack growth from the initiation to instability can be characterized in terms of a single COA. Recently Maiti and his coworker [80] examined the SCG through thin sheet employing COA criterion. Otsuka et al. [78] performed a mixed mode fracture test on a cracked tensile strip specimen of carbon sheet and measured COD and stretch zone width (SZW) of an angled crack. They observed a correlation between the COD and SZW and proposed a COD based criterion for mixed mode fracture initiation. Applicability of  $J$  and  $\hat{J}$  integrals to mixed mode fracture of ductile materials has also been attempted by many investigators [e.g., 84, 85]. Sakata et al. [85] have done experiments and finite element analysis for an angled crack problem in a compact tension specimen. They have found that  $\hat{J}$  is a global fracture parameter. Further, they have observed that  $\hat{J}$  is related to SZW, which is a local parameter. And shown [85] that experimental results for mixed mode testing coincide with those for mode I.

Maccagno and Knott [88], Hallback and Nilson [89], Maiti and his co-workers [eg. 74-81], have looked into the possibility of unifying the fracture over the whole range, pure mode I to mode II. Knott and his coworkers [e.g. 88] and Hallback and Nilsson [89] have reported that a criterion based on the shear band localization can explain the initiation of fracture in the whole range. Mourad and Maiti [78] / have shown the suitability of the COA criterion in the same context and the stable crack growth. They have, also considered the pure mode II loading.



Sutton and his Coworkers, [92, 93] have recently shown that flaws in ductile materials under local mixed mode I/II conditions will change direction and undergo stable crack growth along directions that can be shown to be predominantly either mode I or mode II. One model [92, 93] that has been shown to adequately predict the direction and onset of crack extension is crack opening displacement (COD). This model predicts that (a) mode I crack growth will occur in a direction that maximizes the opening component of crack opening displacement ( $COD_I$ ) and (b) mode II crack growth will occur in the direction of maximum shear – type crack displacement ( $COD_{II}$ ). Based on recent experimental studies, they have shown [94] also that, a critical crack opening displacement (COD) has the potential to be a viable parameter for predicting the onset of crack growth in thin sheet 2024-T3 aluminum under combined tension (mode I) and in-plane shear (mode II) loading conditions.

There have been attempts to study the initiation and growth under mode I and mixed mode using the continuum damage mechanics approaches. It appears that the onset of initiation can be explained in terms of a critical void volume fraction. The direction of initial crack extension can also be predicted through such methods [63]. Reference may be made to for more literature details in this method of analysis.

## **2.11. EFFECT OF CRACK BLUNTING ON SUBSEQUENT CRACK GROWTH**

The effects of crack blunting on the brittle and ductile crack behavior and subsequent crack growth have been studied by some investigators [e.g., 56, 57, 61 and 62]. When a sharp crack in a material is loaded until it deforms plastically at the crack

tip, two fundamentally different modes of deformation can occur: cleavage and dislocation emission. The crack may propagate (possibly leading to cleavage of the specimen), or it may emit a dislocation. In the first case the material is said to be intrinsically brittle, in the second it is intrinsically ductile. Schiøtz et al. [56, 57] studied the effects of blunt crack geometries on crack propagation. They have shown that blunt cracks have a stronger tendency to emit dislocation than do sharp cracks. This may be important in intrinsically brittle materials, where the nature tendency for a sharp crack is to propagate by cleavage rather than to emit dislocations. In these materials a dislocation may be blunted by absorbing a dislocation from a near by source and thereby turned into an emitting crack preventing further cleavage. It is obviously also relevant to cracks in more ductile materials where the crack itself may emit dislocations. They have investigated the effect of crack blunting on the subsequent crack propagation and they have shown that as the crack is blunted, a small but noticeable increase in the crack loading needed to propagate the crack. Schiøtz. et al [ ]. has also examined the behavior of blunted cracks under mode I and mode II loading. The mode I results indicate a new mechanism for enhanced ductility in some materials. They have found that blunting the crack increases the force required to propagate the crack, but only by a surprisingly modest amount. The relative modest magnitude of the effect can be attributed to the sharp corner of the blunt crack, where the stress singularity under mode I loading is almost as strong as for a sharp crack. Despite the small effect on the cleavage criterion, for many force laws the blunting causes the crack to change behavior and to start emitting dislocations instead of propagating. This has the consequence that if a crack in such a material absorbs a dislocation at the crack tip, a segment of the crack will locally be

arrested, leading to an increase in the microscopic crack tip toughness, which further may lead to a much larger increase in the macroscopic toughness of the material. The blunting effects presented here may thus, in combination with the effect of attracting dislocations to the crack tip, cause an increase in the fracture toughness of materials by many orders of magnitude.

Numerous experimental observations have indicated that an atomically sharp crack is very rare and that crack tip blunting can precede or accompany crack propagation. Several methods have been proposed to predict whether a sharp crack tip will blunt, possibly leading to ductile failure, or continue to clear in a brittle fashion. Fisher et al. [61] discussed the positive-dislocation–emission behavior of a crack, in an attempt to understand if the nucleation of a single dislocation will always lead to a ductile response or if subsequent brittle propagation can occur, they have obtained elastic solutions of the stresses near the blunted crack tip for two type of loading.

The role of crack blunting in ductile versus brittle response of crystalline material has been investigated by Beltz et al. [Cited in 62]. They have used continuum concepts to evaluate the competitions between crack advance and dislocation nucleation at the tip of the crack having a finite tip curvature. Recently Fischer and Beltz [62] have examined the effect of crack blunting on the competition between dislocation nucleation and cleavage. They have accomplished this by assuming that the crack geometry is elliptical, which has the primary advantage that the stress field are available in close forms these stress field solutions are then used to calculate the threshold for dislocation nucleation and atomic decohesion. These calculations have been carried out for various crack tip geometries to ascertain the effects of crack tip blunting. These calculations have been carried for

various crack tip geometries. From results comparisons, four possible type of material fracture behavior are identified: intrinsically brittle, quasi-brittle, intrinsically ductile, and quasi-ductile. Finally, they have discussed real material examples. Farkas [Cited in 62] have suggested that blunting of a sharp crack tip can significantly modify the stress field around the crack tip, and/or change the favorability of crack advances or dislocation nucleation.

## 2.12 CRACK FRONT TUNNELING

From postmortem evaluation of the fracture specimens it was clear that the crack growth process was somewhat different along the specimen centerline [75-81, 84]. Mourad and Maiti [76-81] have examined the crack front tunneling through different specimens' configuration of D16AT aluminum alloy and due to various modes of two-dimensional stable crack growth. There was a considerable amount of tunneling at initiation and as stable growth progresses in the case of mode I and mixed mode loading; however, the front is more or less straight at the end of both fatigue precracking and stable crack growth in case of mode II loading. It may be noted here that, in the case of mode I, the tunneling was linked to a non-uniform distribution of SIF along the crack front [95]. Ahmad, Barnes and Kanninen [84] have reported that there is a considerable amount of tunneling as stable crack growth progresses; the extent of tunneling is as high as 8 mm for steels. Shan et al. [83] examined the stable crack growth in CT specimens made of high strength steel SAE 4340 and observed that in the tested specimens the crack grows mainly in the center region of the specimens. In the investigated crack extension range (in the specimen center  $\Delta a \approx 6\text{mm}$ ) no stable crack growth occurs in the surface region of the

specimens. The slight crack extension near the specimen surface is caused by the blunting of the crack tip. Therefore, a careful study of both the centerline and surface crack profiles should be undertaken to quantify the amount of stable crack growth along the crack front as the crack proceeds as well as the direction during the early stage of growth.

## 2.14 CLOSURE

The condition for crack initiation in a mode I can be given in terms of COD or J integral and the stable crack growth can be characterized in terms of COA or tearing modulus. When crack grows under J controlled conditions, the COA and tearing modulus are linearly related. The condition for the mixed mode stable crack growth initiation can be given in terms of J and  $\hat{J}$  integral. It also appears that under a very contained yielding, the condition for the onset of crack extension can be given in terms of the MTS and MTPS criteria, which are very successful in linear elastic fracture mechanics.

Mixed mode problems are more general. Though the elastic mixed mode problems have received some attention, the literature on the elastic-plastic case is very scanty. Few attempts have so far been made to measure the changes in initiation and maximum loads with the loading angle and the increased load bearing capacity with the crack growth. Thus there is need for more experimental as well as theoretical studies.

Through properly designed CT specimens it is possible to get a variety of combinations of mode I and mode II. It may be difficult to achieve a pure mode II unless a special fixture is used.

The study of stable crack growth initiated from fine notches as per crack, the associated crack blunting and crack front tunneling are very lacking. It is therefore necessary to examine these issues.

In view of all theses, the present study has been carried out with the objectives, which are indicated in section 1.2.

# Chapter three

## CHAPTER 3

# EXPERIMENTAL PROCEDURE

### 3.1. INTRODUCTION

This chapter reports on: the selected material for the present investigation and its properties, the geometry of the specimens used for both tensile test and fracture test as well as procedure of fabrication, and testing.

### 3.2 MATERIAL

The material selected for the present investigation is an aircraft quality AISI 4340 steel alloy which is heat treatable, low alloy steel containing nickel, chromium and molybdenum. It is known for its toughness and capability of developing high strength in the heat-treated condition while retaining good fatigue strength. It also combines deep hardenability with good ductility as well as good toughness and strength. It has sufficient carbon and alloy content to necessitate the application of preheat if cracking is to be avoided in a weld and associated heat affected zone. The material has numerous applications; typical applications are for structural use, such as aircraft landing gear, power transmission gears, shafts and other structural parts.

The material was supplied by Hillfoot Steel Group Ltd, UK. It was available in the form of round bar of 180 mm diameter (forged and annealed). The chemical



composition determined by micro prop is presented in Table 3.1, along with reference values as per ASTM A29/A29M./1992.

### **3.3. SPECIMENS PREPARATION**

#### **3.3.1 Tensile Specimens Preparation**

The tensile test specimen was made as per ASTM E8/1990 (Test Methods for Tension Testing of Metallic Materials) recommendations. The geometry of the tensile test specimen is shown in Figure 3.1

#### **3.3.2 Fracture Specimens Preparations**

So far there is no standard specimen configuration and test procedure available for mode I and mixed mode stable crack growth studies. The different configurations employed are compact tension (CT) specimens, three point bend (TPB) specimens, crack bend bar, etc. The compact tension (CT) specimen was employed by some workers [74-79] for both mode I and mixed mode stable crack growth study. The specimen offers some advantages, e.g. ease of fabrication and pre-cracking. It has one limitation that mode I loading always dominate and pure mode II can not be attained easily. This specimen has been used here for both experimental and theoretical investigations in mode I and mixed mode (I and II).

The specimens are prepared from a round bar of 180 mm in diameter. The specimens were configured in T-T orientation. The T-T is defined by orienting the crack and the load perpendicular to the axis of the rod. To minimize variation due to the material, all specimens were taken from the same lot of AISI 4340 steel alloy rod. The

rod firstly was cut in small segments of 250 mm in length, and then it was machined and flattened to a bar of 120X120 mm cross-section. The bar was then cut into slices (plates) of 10 mm thickness, and ultimately the plate's thickness was reduced to 8 mm by a milling. The specimens were finally made in size of 120 mm x 120 mm x 8 mm thick. For fixing these dimension and manufacture of the specimens some of the ASTM E399 (1990) guidelines were followed. Specimens were first made with 3 mm wide notch and 40 mm length straight slot terminated as a V shape of 60° angle. Then a pre-crack pre-notch with root radius of 0.05 mm using a wire-cutting machine was introduced. The extent of the pre-crack was from 1mm up to 5 mm to produce different initial crack length ( $a_0$ ) to width ( $w$ ),  $a_0/w$ , ratio (0.41, 0.42, 0.43, 0.44, and 0.45). The pre-cracking for all specimens was introduced using cutting wire of 0.1 mm diameter. The knife-edges were machined at the crack mouth of the specimen for clip gauge installation purpose. The required holes for different modes of loading were also machined. Load inclinations,  $\psi = 75^\circ, 65^\circ, 60^\circ,$  and  $50^\circ$ , with the crack are considered for different combination of mode I and mode II.  $\psi = 90$  corresponding to mode I. The specimen configuration is shown in Figure 3.2. The notch and pre-cracking were done in Cosmoplast Industrial Co.W.L.L., Al-Sharjah by wire cutting machine (FANUC, Japan, Model: (w-2)).

### 3.4. FIXTURE

A fork-type fixture was designed and fabricated from AISI 4340 steel alloy material. The design based on the rigidity of the fixture. This fixture was designed so that both mode I and mixed mode fracture tests can be accommodated. Figure 3.3 shows a photograph the fork type fixture.

## **3.5. TEST PROCEDURES**

### **3.5.1. Tensile Test**

Tensile tests were conducted on standard 6 mm wide rectangular tension specimens as shown in Figure 3.1. Specimens were tested in the longitudinal (L) and the transverse (T) directions. The tensile test was conducted according to ASTM E8/1990 standard (Test Methods for tension testing of metallic material). The mechanical test was performed in tension at room temperature on a 100 kN MTS machine (model), which is displacement controlled. The cross-head speed was 0.5 mm/min according to the ASTM procedure. Young's modulus and yield stress and ultimate tensile strength were determined from the result. The measured mechanical properties are presented in Table 3.2.

### **3.5.2. Fracture Test**

All fracture tests were conducted on a full computerized 100 kN MTS machine under displacement control. Experimental setup is shown in Figure 3.4. The specimens were loaded quasi-statically (with over-head displacement range of 0.1 mm/min) to the maximum load and beyond. The load line displacement was measured by a clip gauge (Figure 3.5) as the crack proceeds. The clip gauge must be attached carefully to the sharp knife-edges. The calibration curve of the clip gauge is shown in Figure 3.6. The load and the load line displacement were recorded at suitable intervals during the test. The load and the load line displacement were eventually plotted to obtain the load- displacement diagrams. The load overhead displacement variation was also obtained directly from the testing machine.

The fracture tests were performed for different combination of loading angle  $\psi$  and  $a_0/w$  ratio. Five different angles of loading ( $\psi = 50^\circ, 60^\circ, 65^\circ, 70^\circ, 75^\circ$ ) and Five different  $a_0/w$  ratios ( $a_0/w = 0.41, 0.42, 0.43, 0.44$  and  $0.45$ ) were tested. The loading angle represents the angle between the loading direction and the centerline of the specimen (Figure. 3.2). Thus, the specimen is under Mode I condition when  $\psi = 90^\circ$ . Mode I tests were performed for all  $a_0/w$  ratios. However mixed mode tests were performed for  $a_0/w$  ratio of 0.42 and 0.43 only. At least 2 up to 5 specimens were tested for each case to ensure the repeatability of the results.

Table 3.1: Chemical composition of AISI 4340 steel alloy.

Elements	Standard limits as per ASTM A29/A29M (%)	Test results (%)
Carbon ( c )	0.38 – 0.43	0.40
Manganese (Mn)	0.60 – 0.80	0.608
Phosphorus (p) max.	0.035 max.	0.009
Sulfur ( S ) max.	0.040 max.	0.029
Silicone (Si)	0.15 – 0.35	0.247
Chromium ( Cr )	0.70 -0.90	1.169
Nickel (Ni)	1.65 – 2.0	1.348
Molybdenum (Mo)	0.20 – 0.30	0.217
Copper ( Cu )	0.35 max.	0.218
Iron ( Fe )	Remainder	Remainder

Table 3.2: Mechanical properties of AISI 4340 steel alloy (at room temperature)

Modulus of elasticity GPa	Tangential modulus GPa	Yield strength MPa	Ultimate Strength MPa	Percentage elongation %	reduction in area %
198	10	487	662	20	50

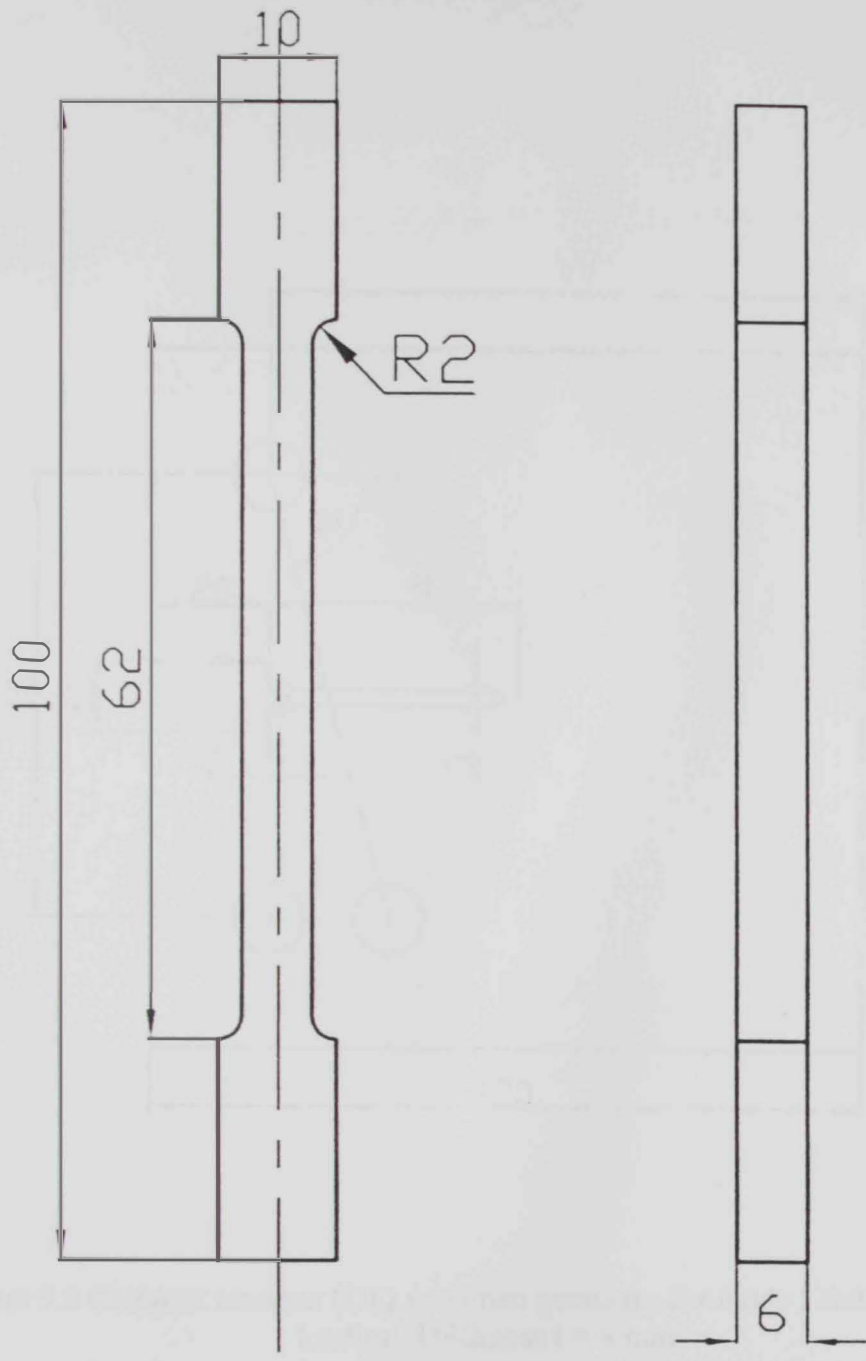


Figure 3.1 Tensile test specimen geometry

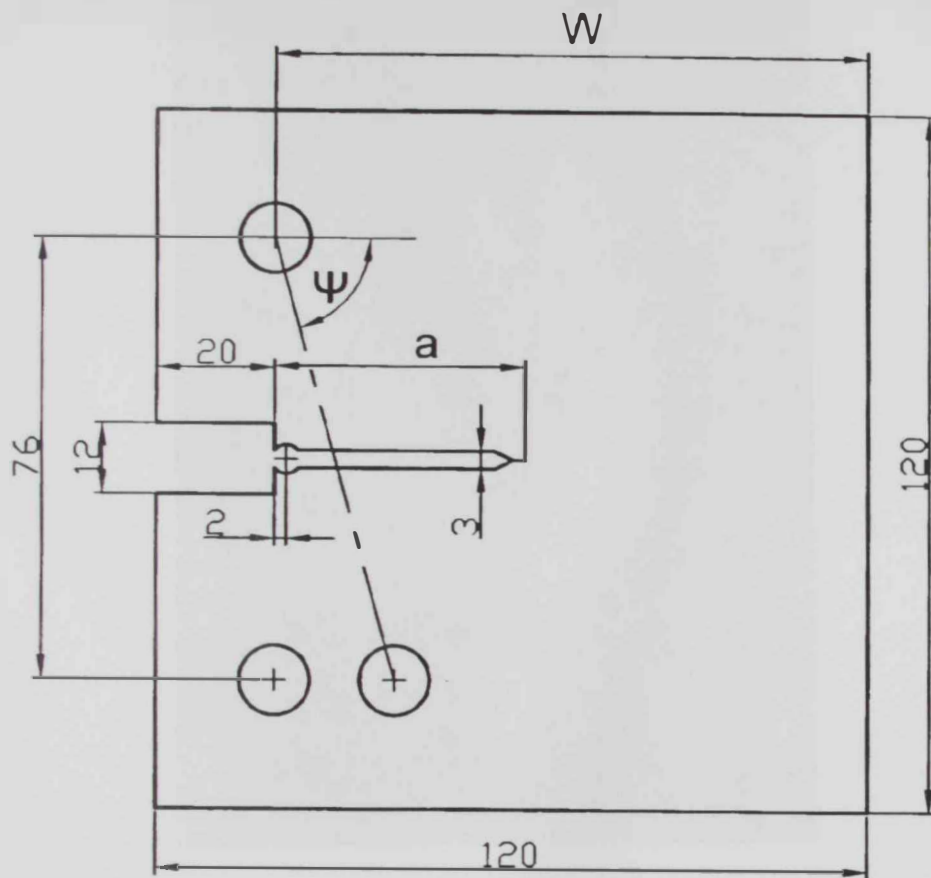


Figure 3.2 Compact tensions (CT) specimen geometry for mode I and mixed mode loading. Thickness  $t = 8$  mm.



Figure 3.3 Photograph showing the fork-type fixture





Figure 3.4 Experimental setup.

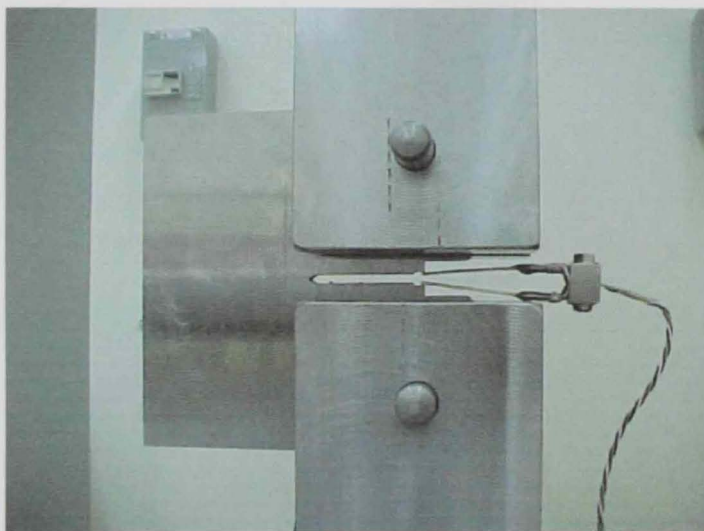


Figure 3.5 Photograph showing the clip gauge position.

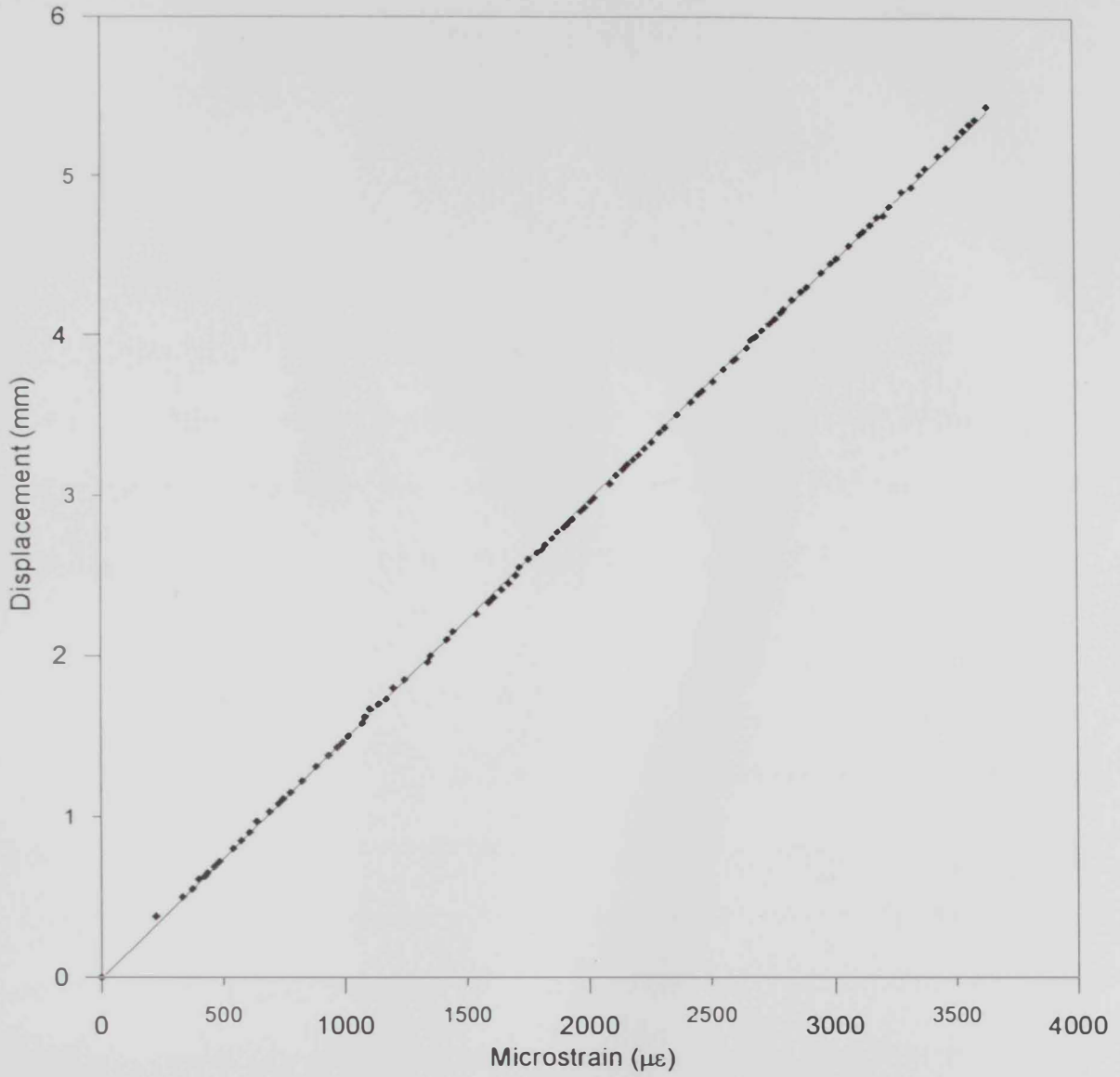


Figure 3.6 Calibration curve of the clip gauge

# Chapter four

## MODE-III STABLE CRACK GROWTH

### 4.1. INTRODUCTION

In this chapter the authors have presented a detailed study on the problem of mode-III crack growth in a ductile material. The authors have shown that the crack growth rate is a function of the applied stress intensity factor and the crack length. The authors have also shown that the crack growth rate is a function of the applied frequency and the crack length. The authors have also shown that the crack growth rate is a function of the applied amplitude and the crack length.

### 4.1.1. REVIEW OF LITERATURE

The authors have reviewed the literature on mode-III crack growth in a ductile material. The authors have found that the crack growth rate is a function of the applied stress intensity factor and the crack length. The authors have also found that the crack growth rate is a function of the applied frequency and the crack length. The authors have also found that the crack growth rate is a function of the applied amplitude and the crack length. The authors have also found that the crack growth rate is a function of the applied frequency and the crack length. The authors have also found that the crack growth rate is a function of the applied amplitude and the crack length.

## CHAPTER 4

### MODE I STABLE CRACK GROWTH

#### 4.1. INTRODUCTION

In this chapter Mode I experimental measurement of initiation load, maximum fracture load, load – load line displacement curves, range of stable crack growth, fracture surface, crack front tunneling, and crack blunting are presented. Finite element analyses were done to predict, at initiation, the plastic zone and equivalent stress.

#### 4.2. EXPERIMENTAL STUDIES

The compact tension (CT) specimen for mode I stable crack growth is shown in Figure 4.1. The test was conducted on 100 kN MTS machine under displacement controlled conditions. The specimens were loaded quasi-statically to the maximum load and beyond. The loading was done with a head speed of 0.1 mm/min. The load Vs load line displacements were recorded at suitable intervals of loading. The data were plotted to obtain the load-load line displacement diagrams. The loading was interrupted at suitable intervals, to facilitate measurements. A spot light was focused on the instantaneous crack tip to augment visibility through a magnifier of 10 times magnifications. A magnifier was used to detect the onset of crack initiation and the range of stable crack growth.

## Load- Displacement Data

Five different values of  $a_0/w$  ratios were used (0.41, 0.42, 0.43, and 0.44). Three specimens at least were tested for each  $a_0/w$  ratio to ensure the results repeatability. Figure 4.2 present mode I specimen after fracture which shows that the direction of crack growth under mode I is perpendicular to the loading direction. At the point of onset of crack extension, it was observed that the crack blunts appreciably. Some of the specimens were loaded until the load starts to decrease after maximum load, and the others were loaded until the full separation of the specimen. Figures 4.3 through 4.8 show the different load-load line displacement diagrams. The load-over head displacement diagrams are shown in appendix 4.A.

Initially the load is varying linearly with the displacement till a certain point at which the curve deviates from its linearity. There was a change in the slope of the load-load line displacement record around the commencement of the crack extension corresponding to the initiation load  $P_i$ . As the crack proceeds the slope of the curve decreases till it reaches the maximum load  $P_{max}$ . Crack blunting was observed around the point at which the curve deviates from its linearity, and then the crack was observed to initiate and extended stably up to the instability point. The crack tip locations corresponding to initiation and maximum load are marked on the surface of the specimen using a sharp tipped pin. The distance between the two is measured to obtain the space of the stable crack growth. The range of stable crack growth was observed to be from 2 mm up to 4 mm. The amount of stable crack growth (SCG) is reduces as the  $a_0/w$  ratio increases.

The initiation load ( $P_i$ ) and the maximum load ( $P_{max}$ ) of all  $a_0/w$  ratios are recorded and presented in Table 4.1. The maximum load is from 2 to 2.5 times the initiation load. A comparison of load displacement diagrams of different  $a_0/w$  ratios is shown in Figure 4.8. Figure 4.9 shows the variation of both the maximum and initiation loads with  $a_0/w$  ratio. Both  $P_{max}$  and  $P_i$  are decreasing as  $a_0/w$  ratio increases. They are varying mostly in a linear relationship with  $a_0/w$ .

### **Crack Front Tunneling**

Small quantity of a red dye penetrate was applied, near the crack tip, on the surface of a few specimens around the initiation and maximum load. These specimens were broken up as soon as the dye penetrate dried up. Figures 4.10 through 4.12 show sample photographs of the fractured surfaces and the extents of the crack front tunneling. There is a considerable curving of the crack front or tunneling. The extents of the tunneling around the initiation and maximum loads are approximately, 4:6 and 8:12 respectively. The tunneling was reported by some investigators (e.g. Newman [53] and Ahmad et al. [84]). The later investigators indicated a magnitude of 5 to 8 mm (for steels). This tunneling results in a large crack opening displacements. The tunneling was also reported by Maiti and Mourad [74, 75] and Mourad and Maiti [76-79]. In fact they indicated different magnitudes for different specimens and different modes of loading (For D16AT aircraft grade aluminum alloy). The effect of crack front tunneling on the fracture behavior was discussed by other investigators [e.g. 96, 97]

## Examination of fracture surfaces

The images in this section are of the entire fracture surfaces of several representative specimens. The images were taken with a digital camera of 10 x optical zoom under lighting such that flat fracture is light gray, while shear lips (if any) are angled away from the light when possible and appear darker. In all images the wire cutting notch / pre crack is on the left and appears smooth and generally dark. Adjacent to the wire-cutting pre-crack the range of stable crack growth as the crack front tunneling is visible.

Figure 4.13 shows a typical fracture surface. More photographs showing the fracture surfaces are also presented in Figures 4.10 - 4.12. The images show a mostly flat fracture surfaces. Sometimes the material develops much smaller shear lips at the region of stable crack growth but generally the shear lip is nearly non-existent. All fracture surfaces exhibit a coarse granular appearance at the region of stable crack growth, which is slightly coarser than the rest of the surface; for specimens that were broken due to a higher head speed after the maximum load. The fracture surface is also rough and non-reflective and all these are characteristics of the ductile fracture.

SEM microscopy was performed on fracture surfaces of mode I. the scanning electron micrographs of stable crack growth zone and the region of unstable crack growth are shown in Figures. 4.14 and 4.15. Both regions are rough and dominated by dimples. These observations are in agreement with other investigators [75-79, 89, 90]. Since the material was put under mode I loading, equixed dimples is the characteristic of the entire fracture surface. The two regions look similar for specimen quasi-statically loaded up to full separation. However the fracture size from the unstable crack growth region are

smaller than the same for the stable crack growth region when specimen was loaded quasistatically up to instability and followed by a higher head speed for full separation.

#### 4.3 - FINITE ELEMENT ANALYSIS

A two dimensional elastic-plastic finite element model for mode I analysis has been constructed using the program ANSYS 5.4, a commercial general purpose finite element package. The mechanical properties of the material are shown in Table 3.2. Mode I stable crack growth in isotropic material shows symmetry along crack plane, as a result only half of the specimen was modeled. The finite element has been done in order to determine the equivalent stress ahead of the crack tip, along the crack line, at the initiation of stable crack extension. To facilitate a 2-D elastic-plastic stress analyses the tensile stress-strain diagram has been approximated as a bilinear curve with elastic modulus  $E = 198$  GPa, plastic modulus  $E_t = 10$  GPa, yield stress  $\sigma_y = 662$  MPa and Poisson's ratio  $\nu = 0.3$ . A plane state of stress has been assumed in all 2-D stress analysis. The analysis has been carried out to predict the equivalent stress ahead of the crack tip for  $a_0/w$  ratio = 0.41, 0.42, 0.43, 0.44 and 0.45. Figure 4.16 shows the finite element discretization for mode I in a CT specimen of  $a_0/w = 0.43$ . The discretization for all cases have 14995 elements and 15245 nodes. 8-noded quadrilateral elements of average side length of 0.2 mm is used around and ahead of the crack tip and elements of bigger size are used else in the discretization.

Figure 4.17 presents the variation of the equivalent stress ahead of the crack tip and along the crack line at initiation load. The equivalent stress has maximum value at



the crack tip and reduces with distance from the crack tip. The crack tip experience more stress for small  $a_0/w$  ratio. The same variation has been observed [e.g. 74] through a CT specimen of D16AT aluminum alloy.

The currently active plastic zones at onset of stable crack growth and before for different  $a_0/w$  ratios are shown in Figure 4.18. The spread along the crack extension line and transverse to the crack are more for smaller  $a_0/w$  ratio as a consequence of the higher initiation load. The spreads along the crack extension are 2.6, 2.4, 2.2, 1.9 and 1.55 mm for  $a_0/w$  ratio = 0.41, 0.42, 0.43, 0.44 and 0.45 respectively. However, the transverse spreads are 1.55, 1.38, 1.20 and 1.04 respectively. The same shape of plastic zones has been predicted by some investigators [e.g. 74-82] through different specimen configurations.

The deformed shapes of the CT specimen in mode I loading for different  $a_0/w$  ratios at the onset of initiation is shown in Figure 4.19.

Table 4.1 Summary of the experimental results

$a_0/w$ ratio	$P_1$ (kN)	$P_{max}$ (kN)	$P_1/P_{max}$ ratio	Tunneling (mm) around		Extent of SCG (mm)
				$P_1$	$P_{max}$	
0.41	22	45.473	2.1	4-6	8-2	2-4
0.42	20	44.0	2.2			
0.43	18	40.4	2.2			
0.44	16	39.0	2.4			
0.45	15	36	2.5			

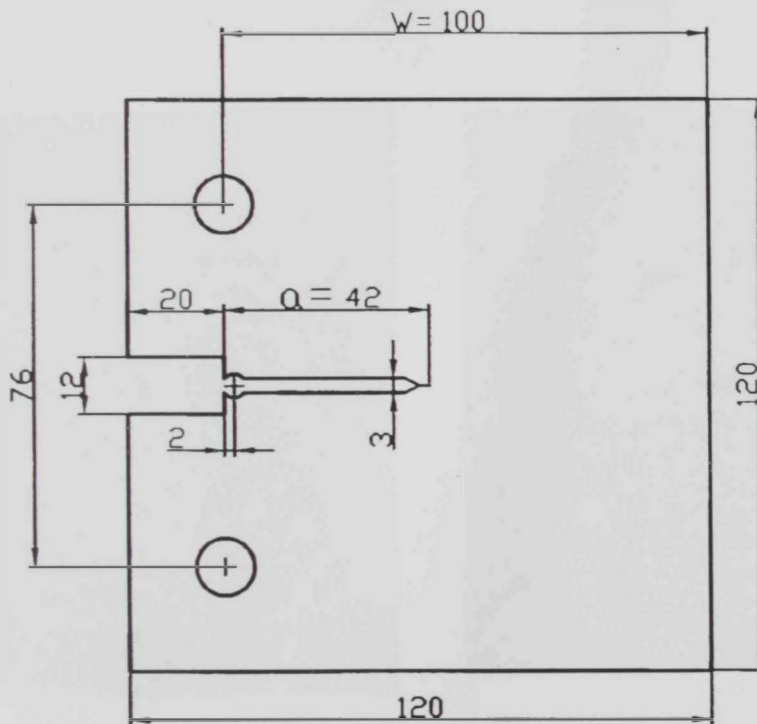
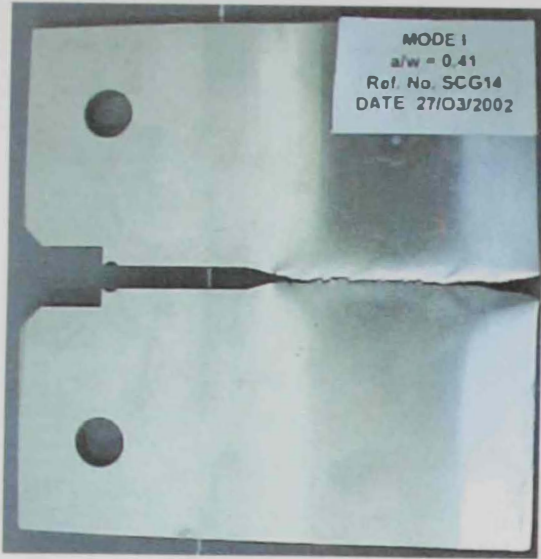


Figure 4.1 Compact tensions (CT) specimen for mode I stable crack growth specimen geometry ( all dimension are in mm)



(a)



(b)



(c)



(d)

Figure 4.2 Sample photographs for Mode I fractured specimens for different  $a_0/w$  ratios.

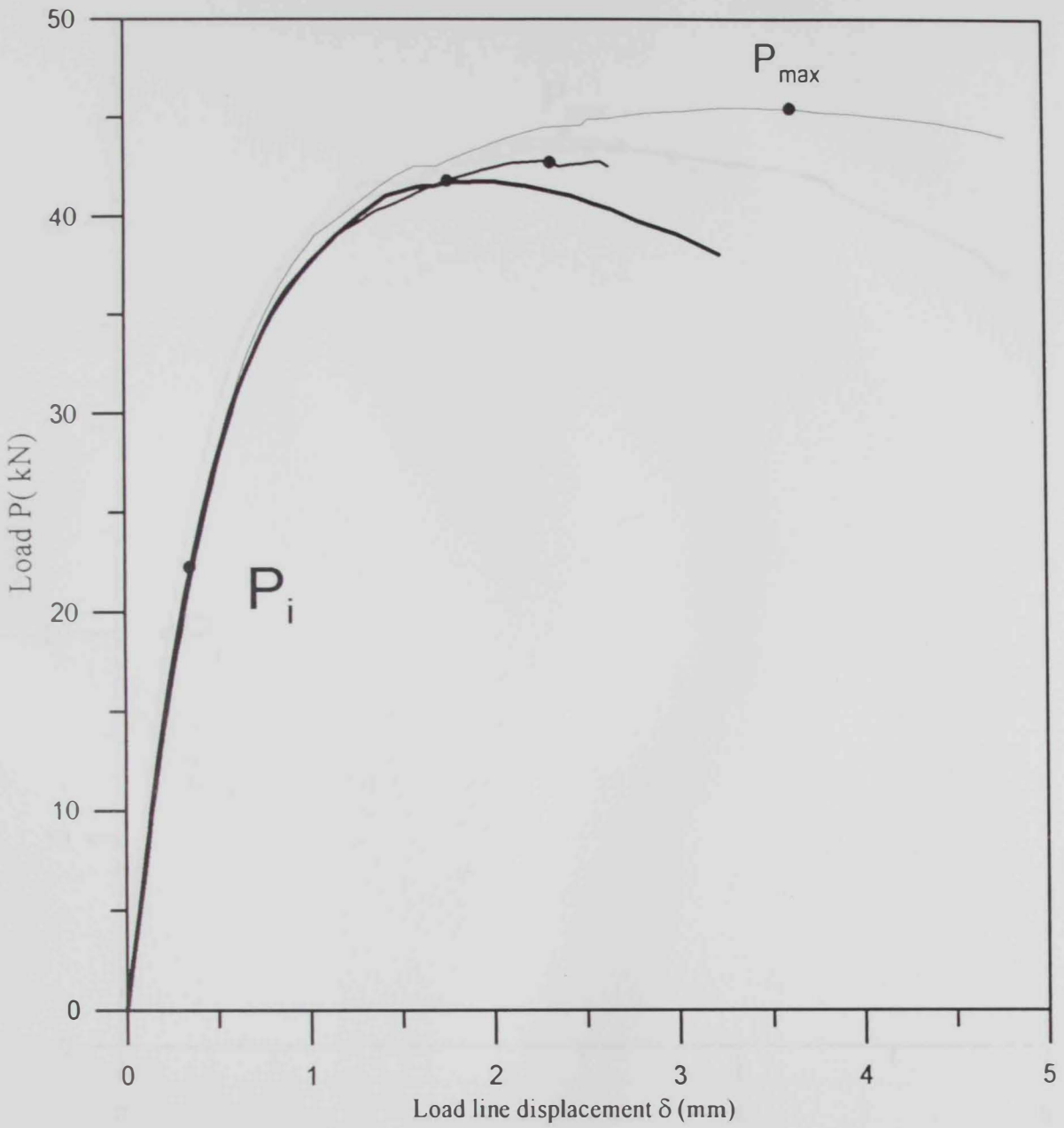


Figure 4.3 Mode I, Load - Load line displacement diagram for  $a/w = 0.41$

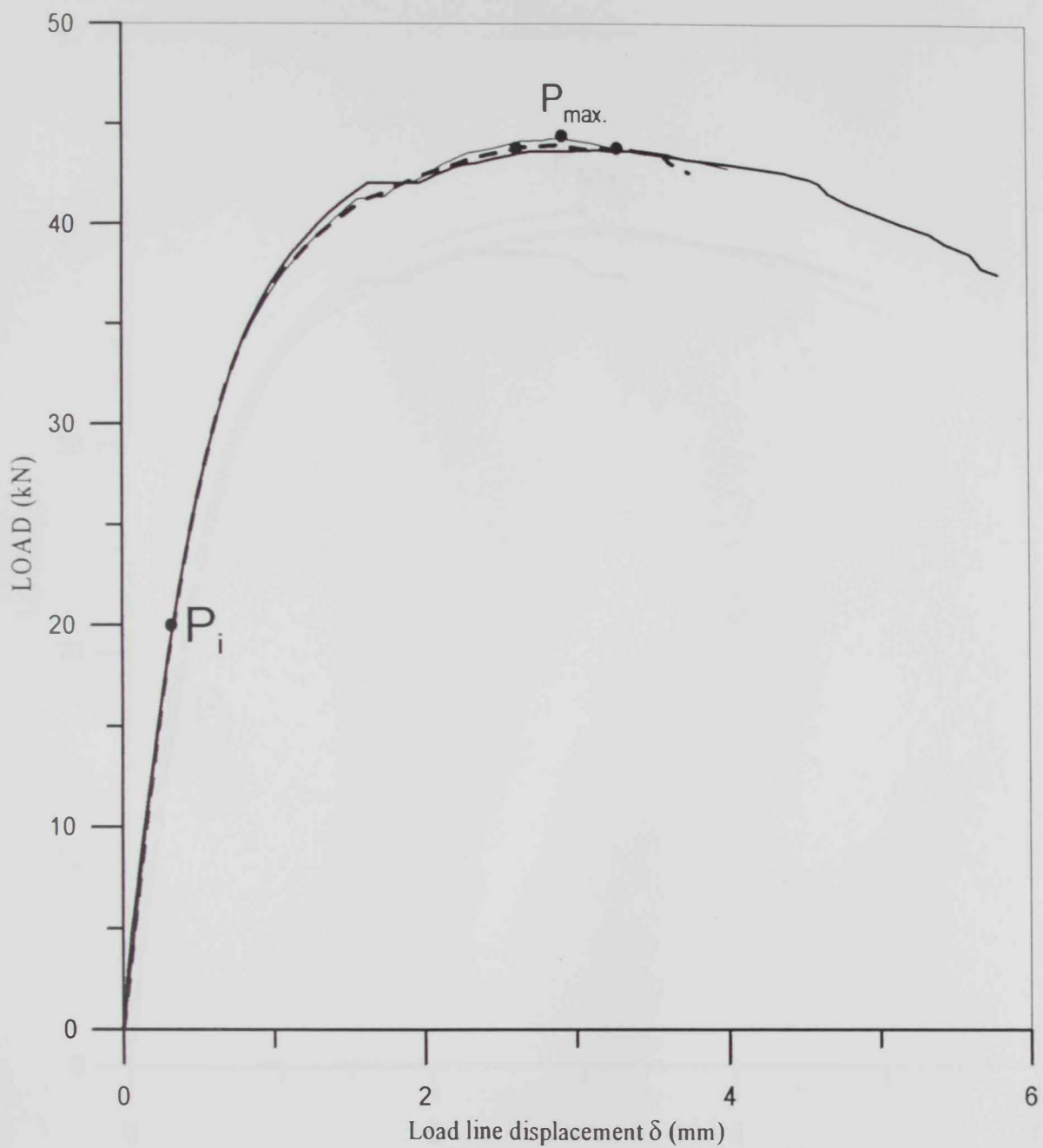


Figure 4.4 Mode I, Load - Load line displacement diagram for  $a_0/w = 0.42$

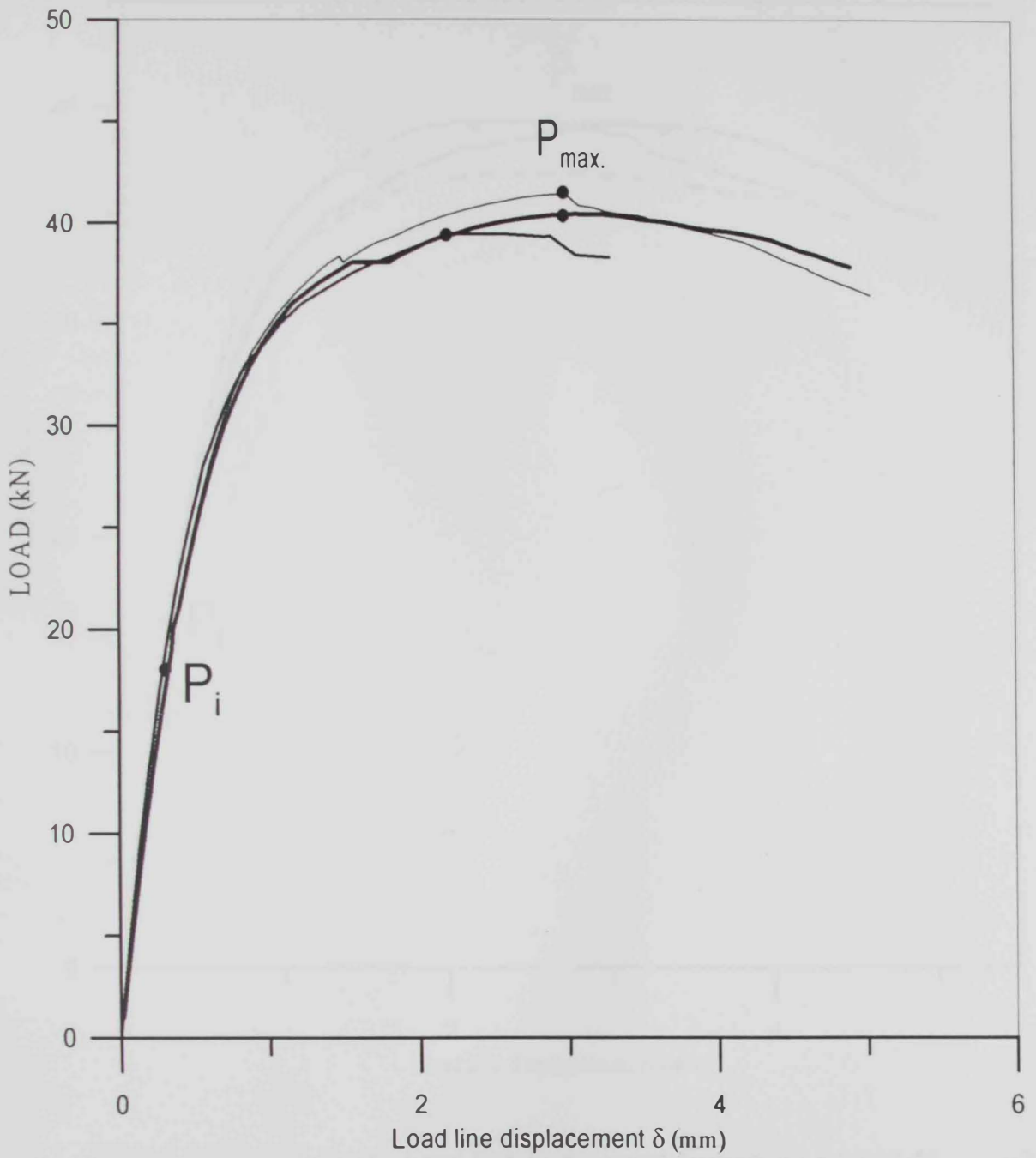


Figure 4.5 Mode I, Load – Load line displacement diagram for  $a_0/w = 0.43$

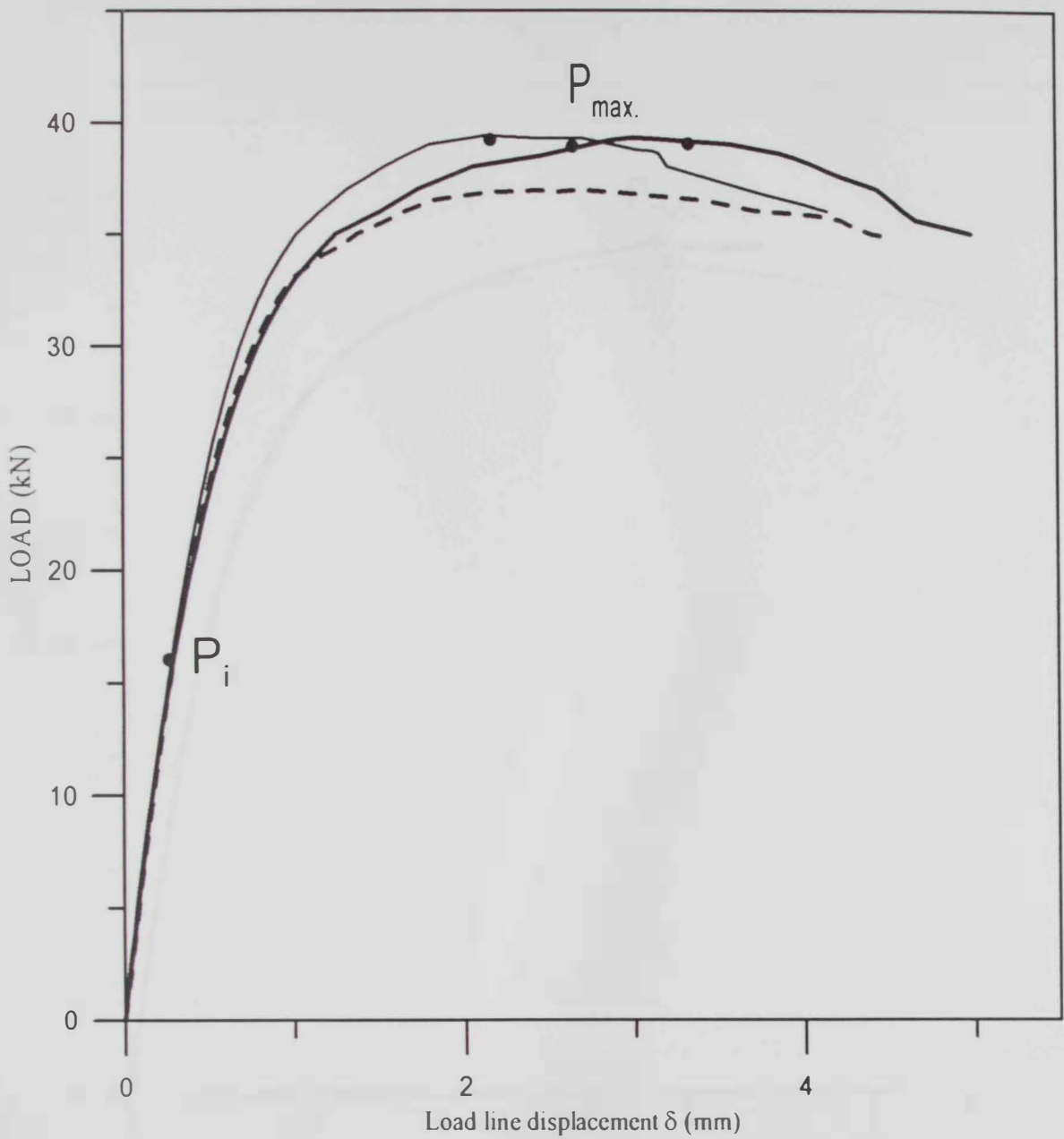


Figure 4.6 Mode I, Load – Load line displacement diagram for  $a_0/w = 0.44$

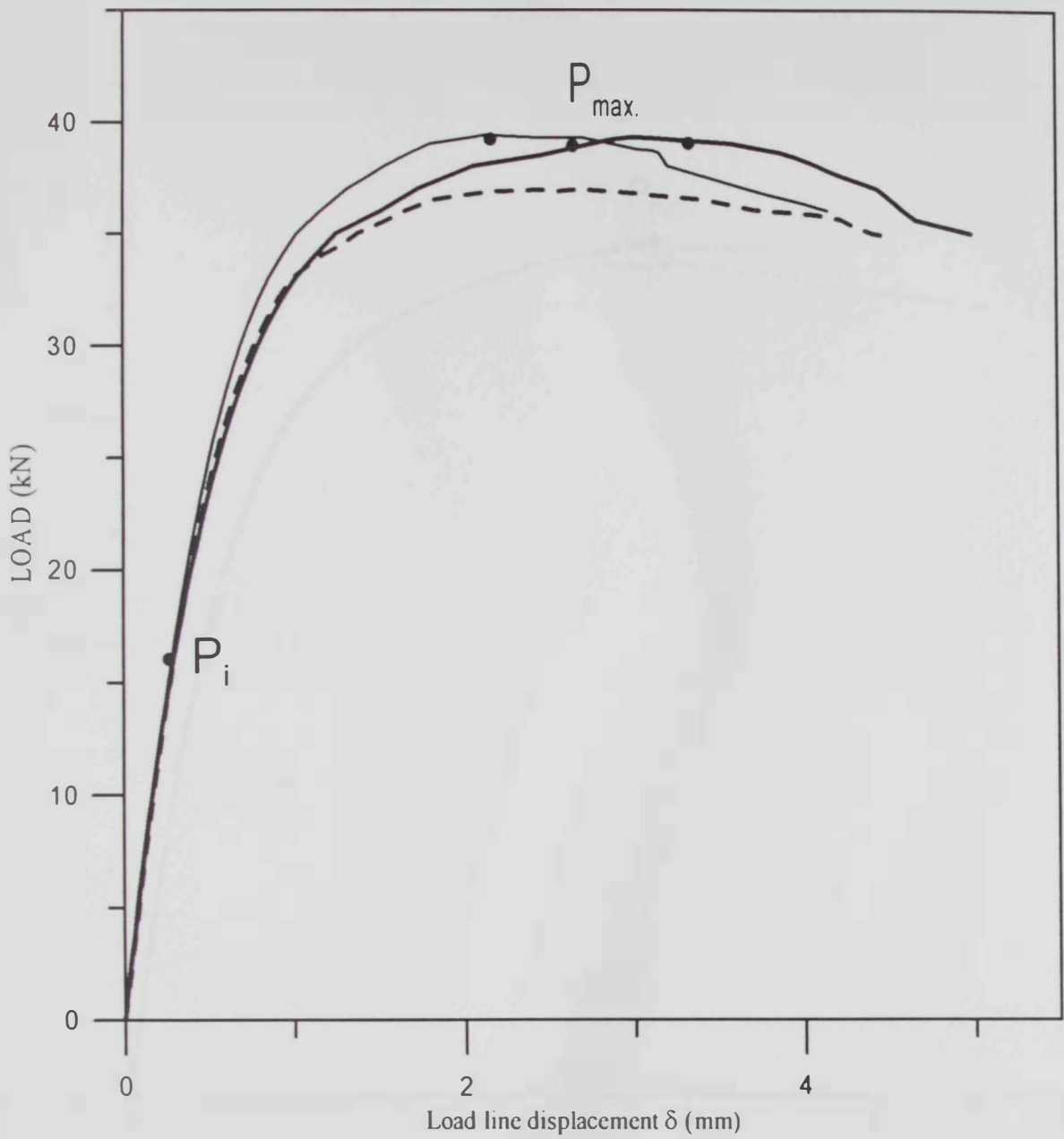


Figure 4.6 Mode I, Load - Load line displacement diagram for  $a_0/w = 0.44$



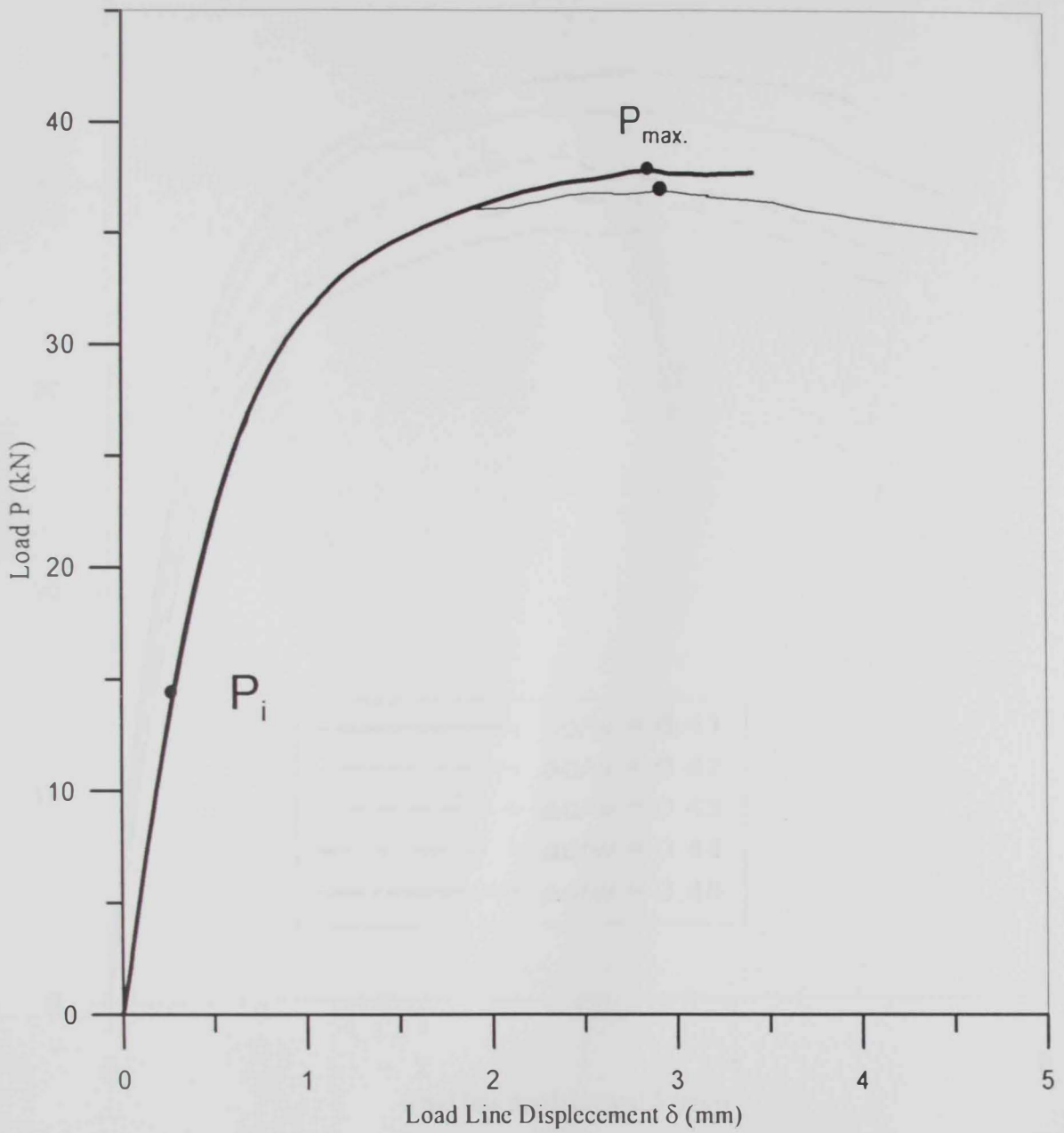


Figure 4.7 Mode I, Load - Load line displacement diagram for  $a_c/w = 0.45$

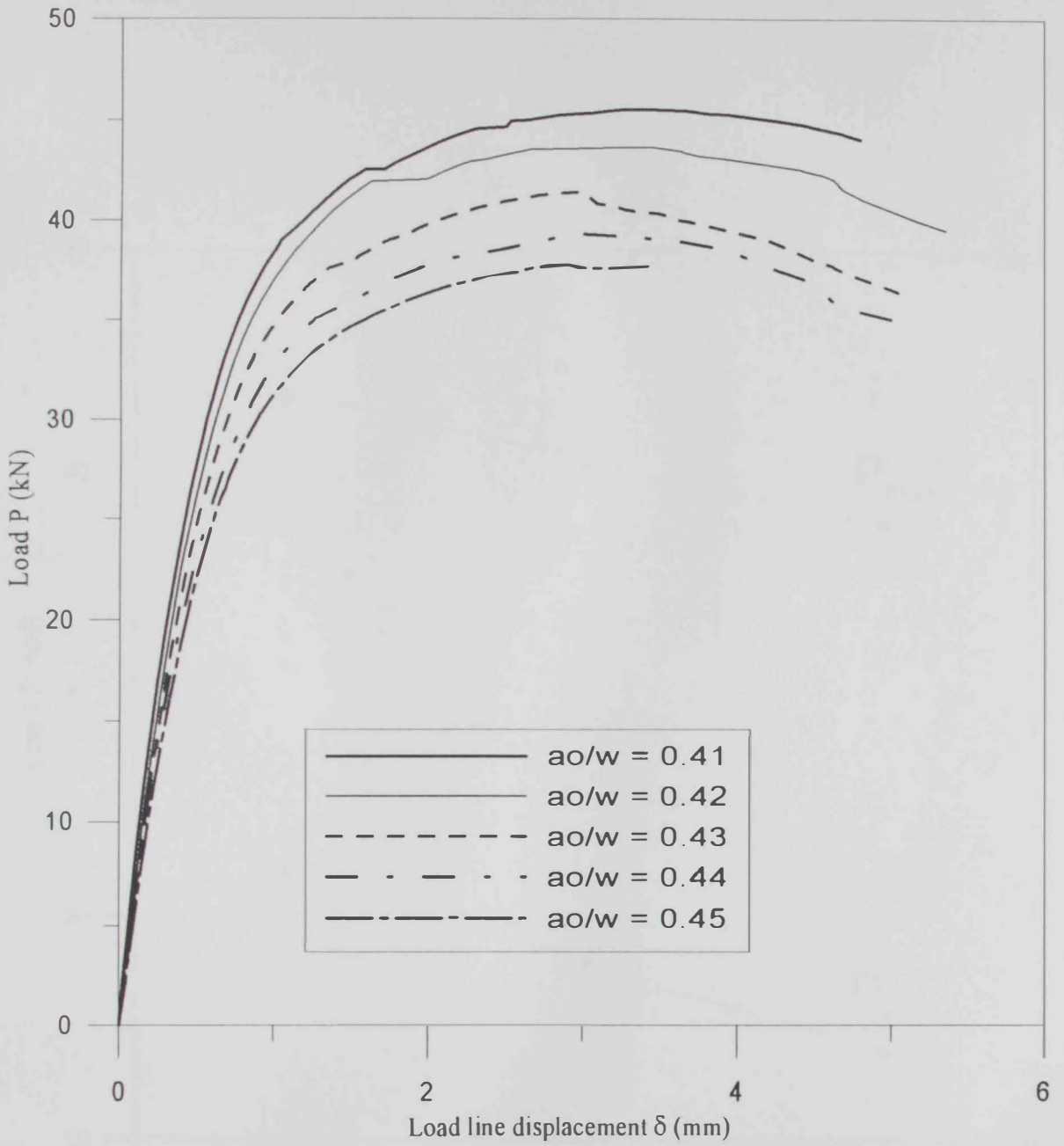


Figure 4.8 Comparison of mode I, Load – Load line displacement diagrams for different  $a_0/w$  ratios.

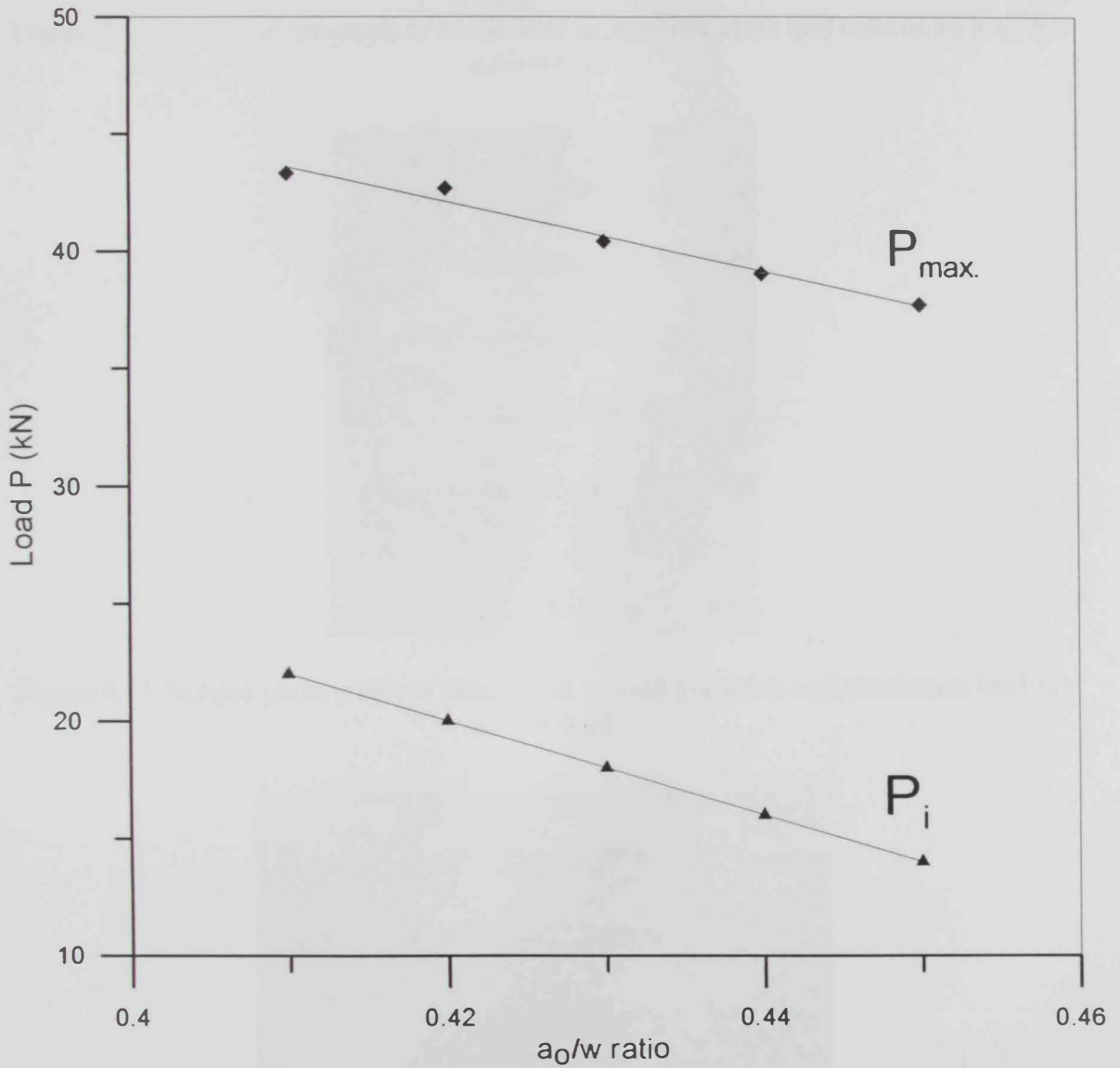


Figure 4.9 Variation of  $P_{max}$  and  $P_i$  against  $a_0/w$  ratio.

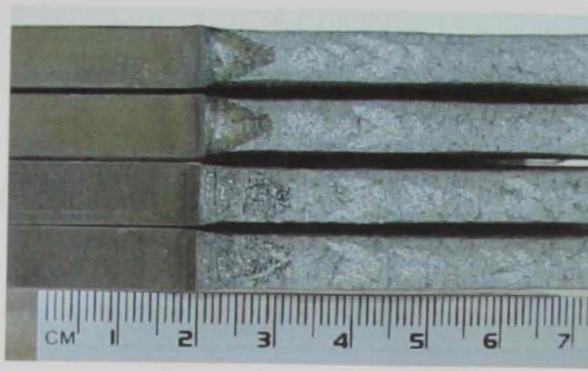


Figure 4.10 Sample photograph of crack front around initiation and maximum load for  $a_0/w = 0.41$

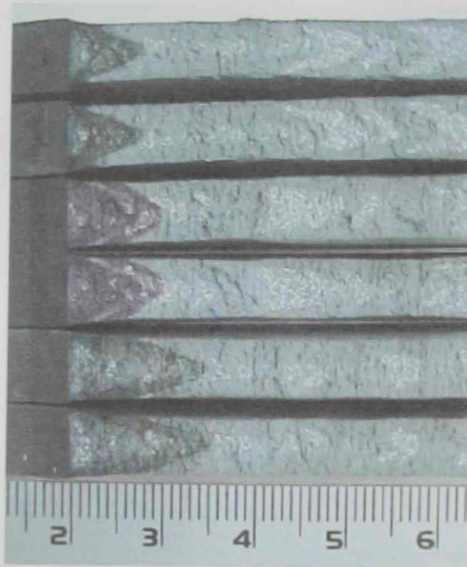


Figure 4.11 Sample photograph of crack front around initiation and maximum load for  $a_0/w = 0.42$

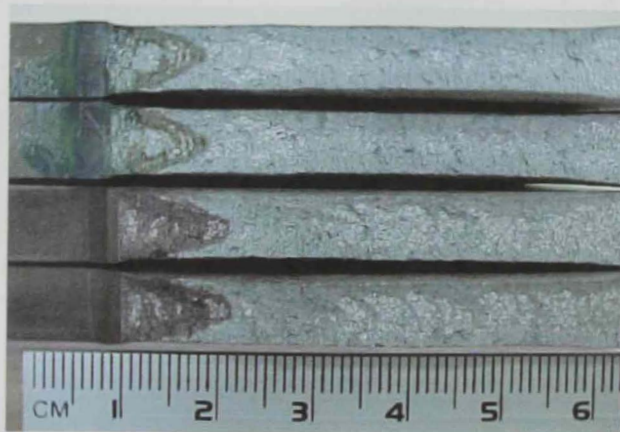


Figure 4.12 Sample photograph of crack front around initiation and maximum load for  $a_0/w = 0.43$

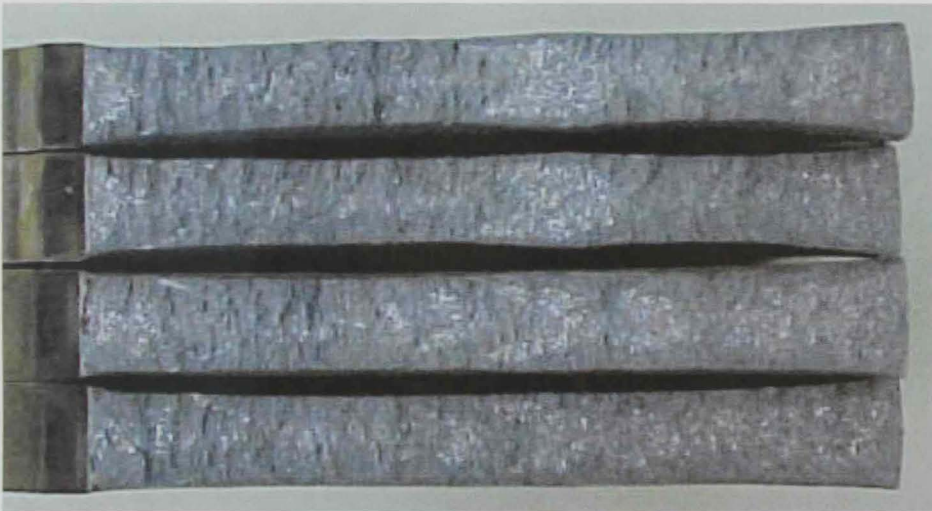
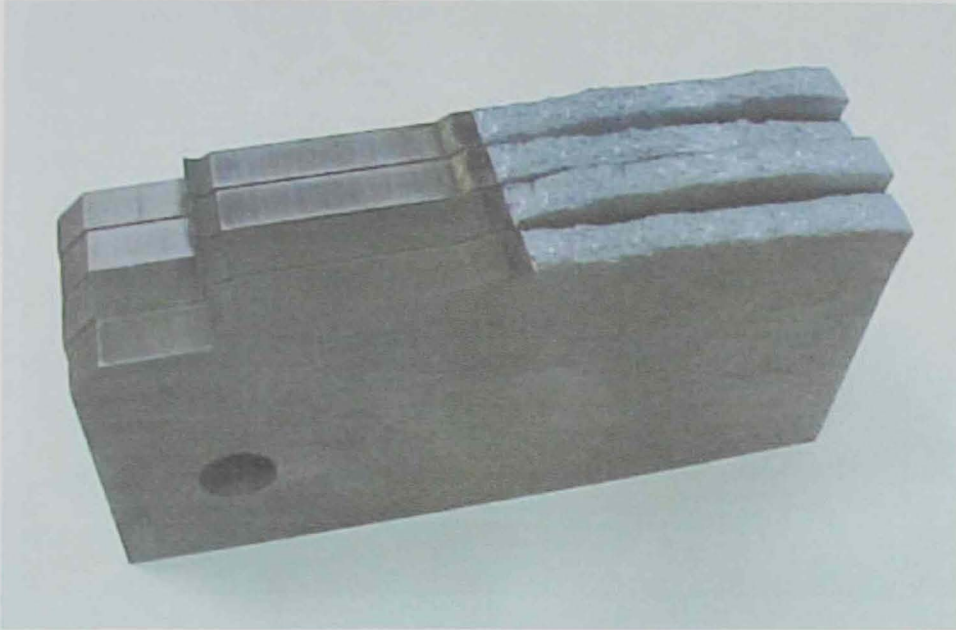


Figure 4.13 Sample photographs of fracture surfaces

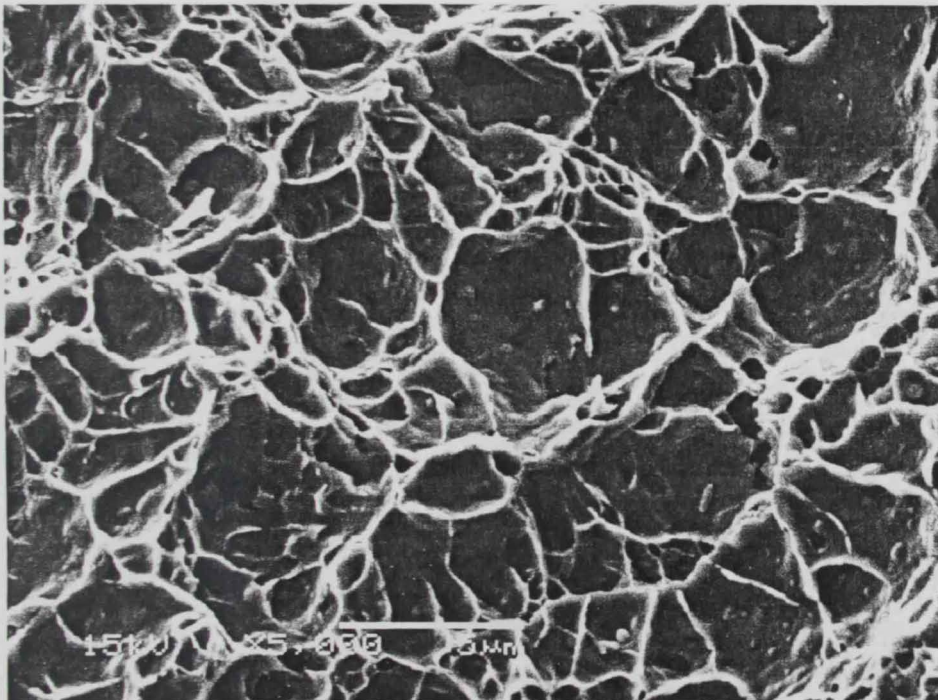
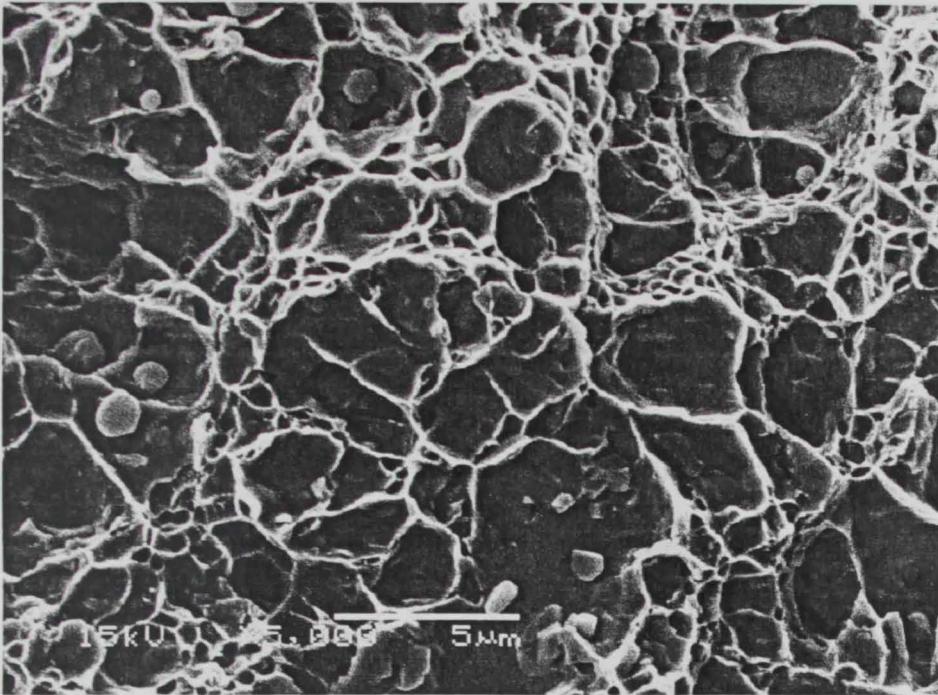


Figure 4.14 Scanning electron micrographs samples for mod I stable crack growth region

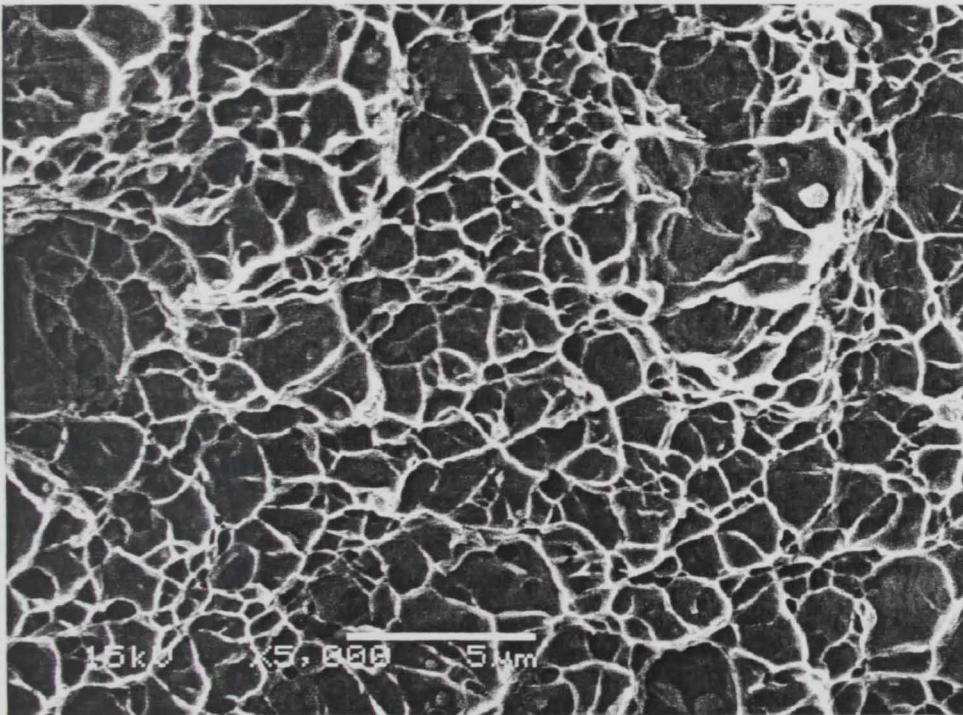
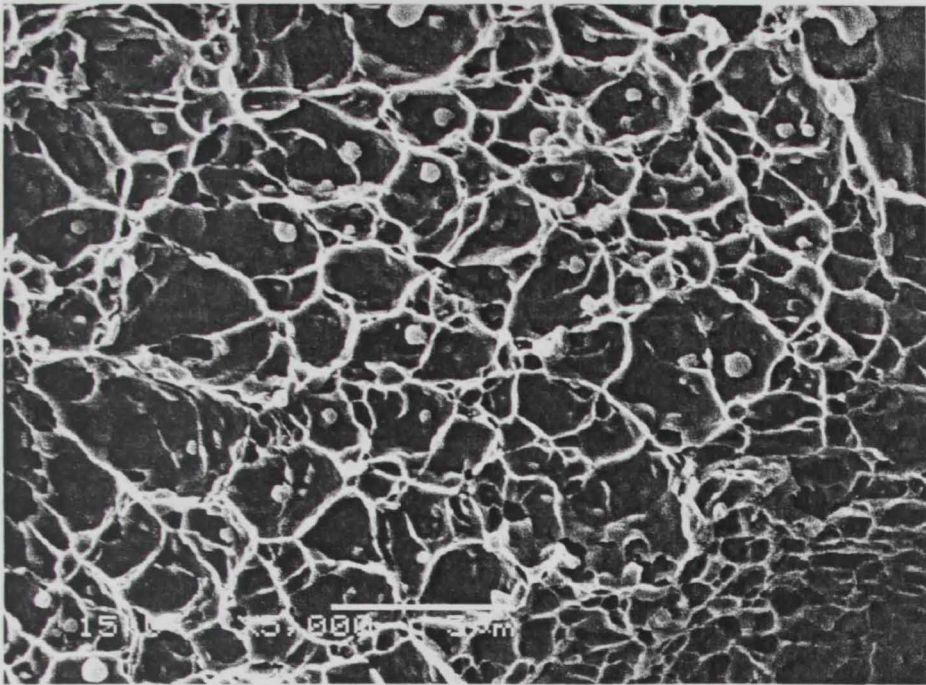


Figure 4.15 Scanning electron micrographs samples for mode I unstable crack growth region.

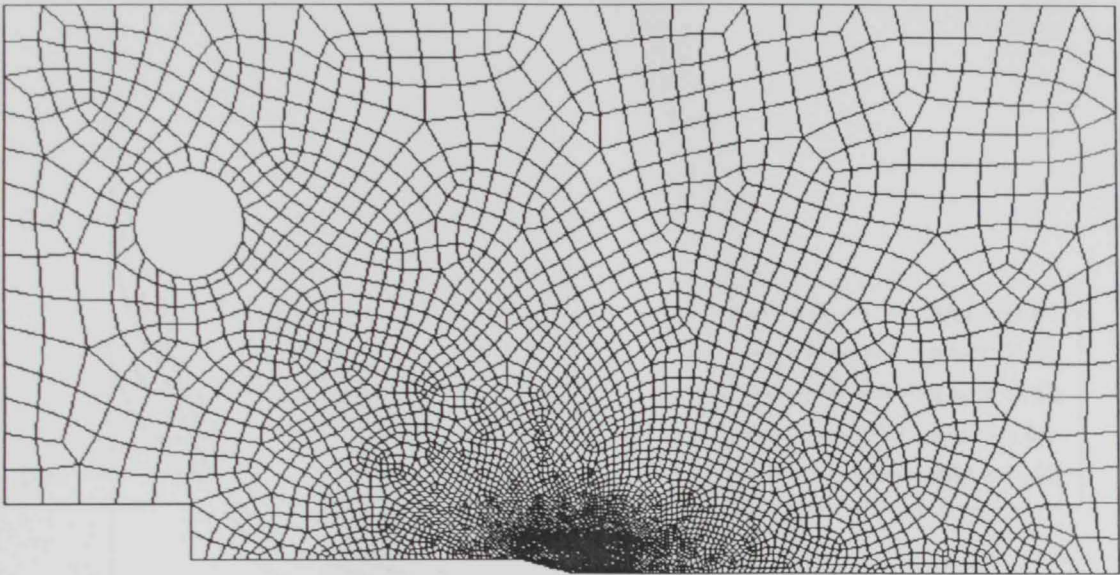


Figure 4.16 Discretisation for mode I specimen, ( $a/w = 0.43$ ). Number of nodes 15245 and number of element 4995.



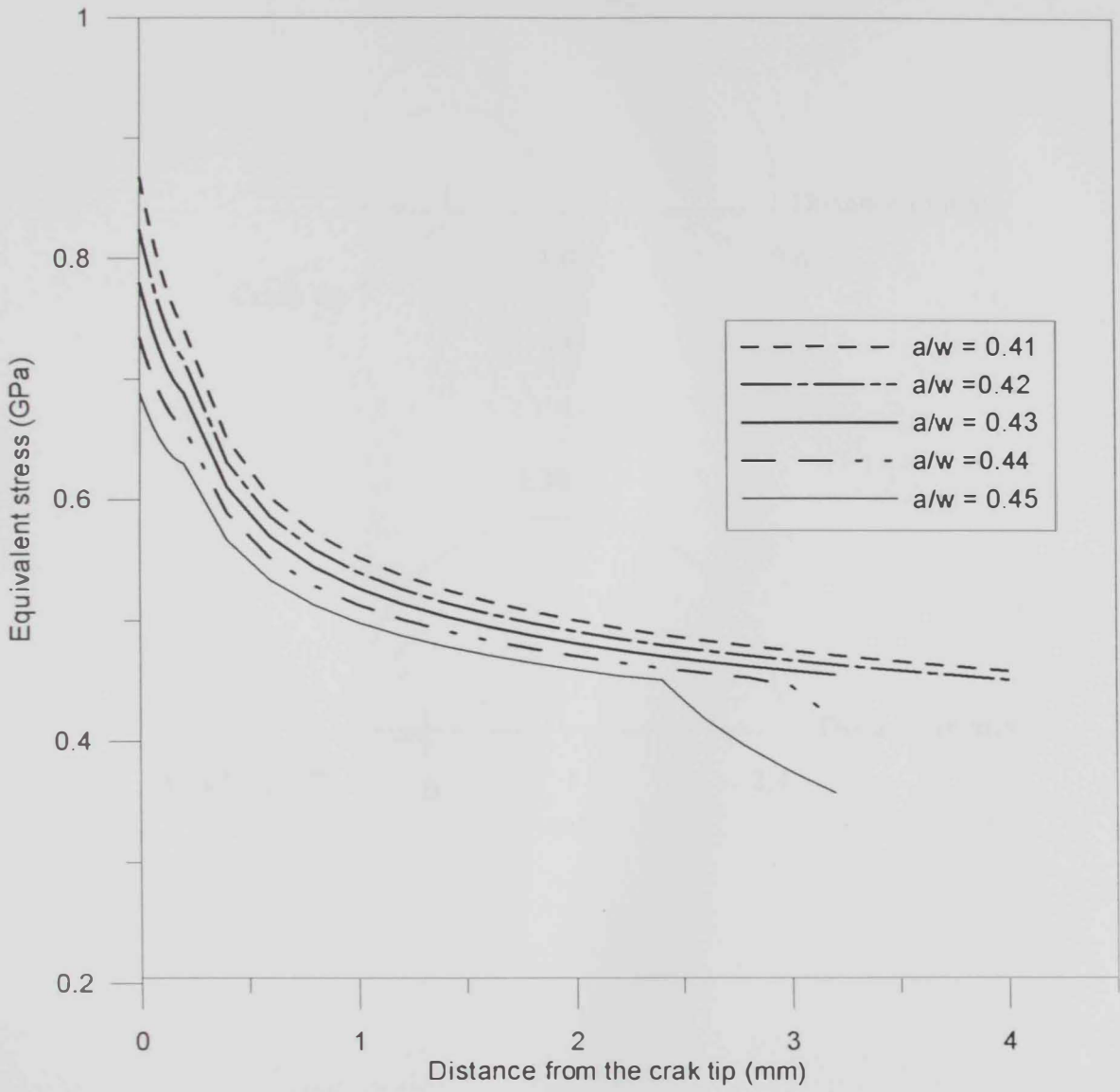


Figure 5.17 Variation of the equivalent stress ahead of crack tip at the onset of crack extension.

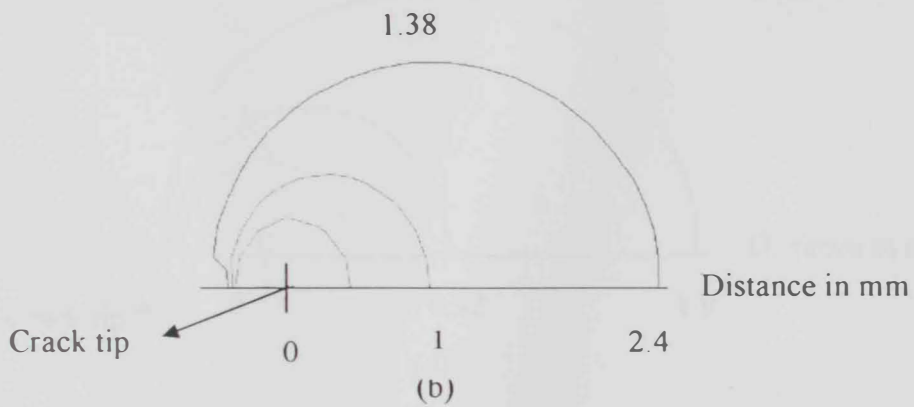
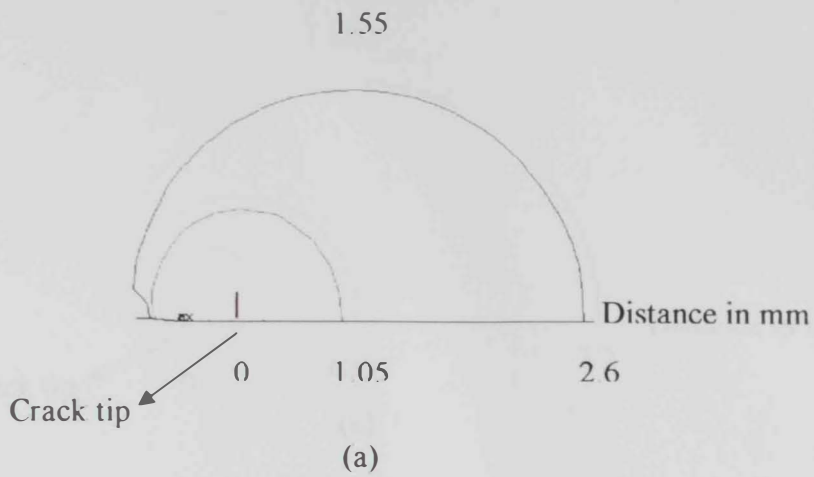


Figure 4.18 Plastic Zone in mode I at the onset of crack extension. (a)  $a_0/w = 0.41$ ,  $P_i = 22$  kN, (b)  $a_0/w = 0.42$ ,  $P_i = 20$  kN, (c)  $a_0/w = 0.43$ ,  $P_i = 18$  kN, (d)  $a_0/w = 0.44$ ,  $P_i = 16$  kN, (e)  $a_0/w = 0.45$ ,  $P_i = 14$  kN.

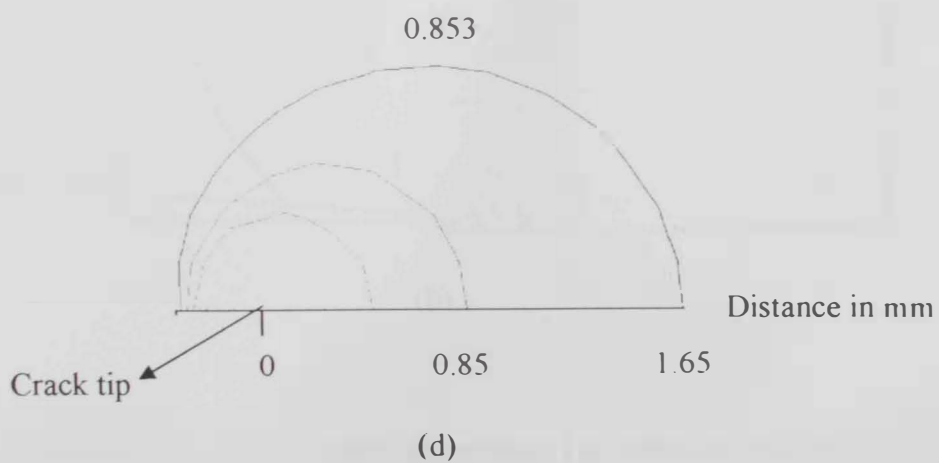
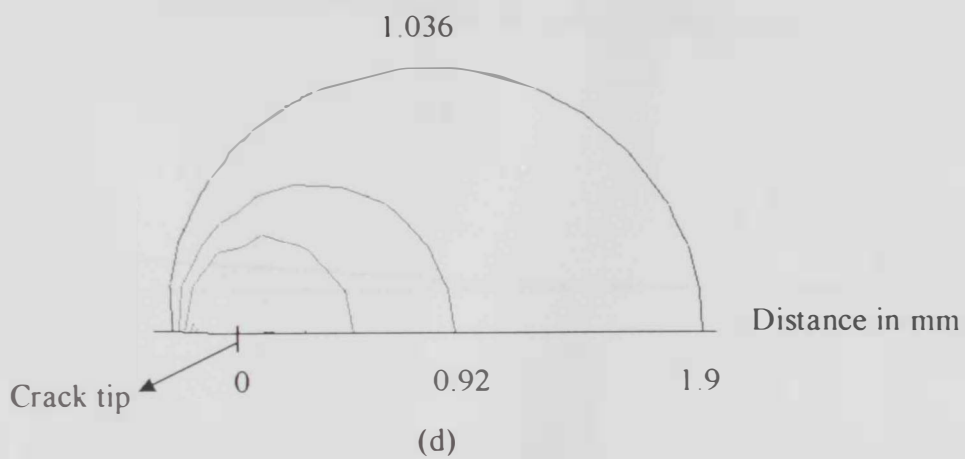
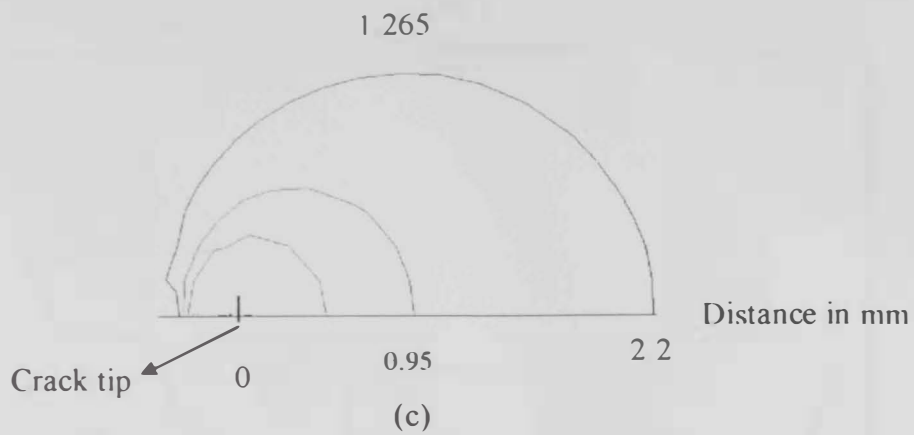
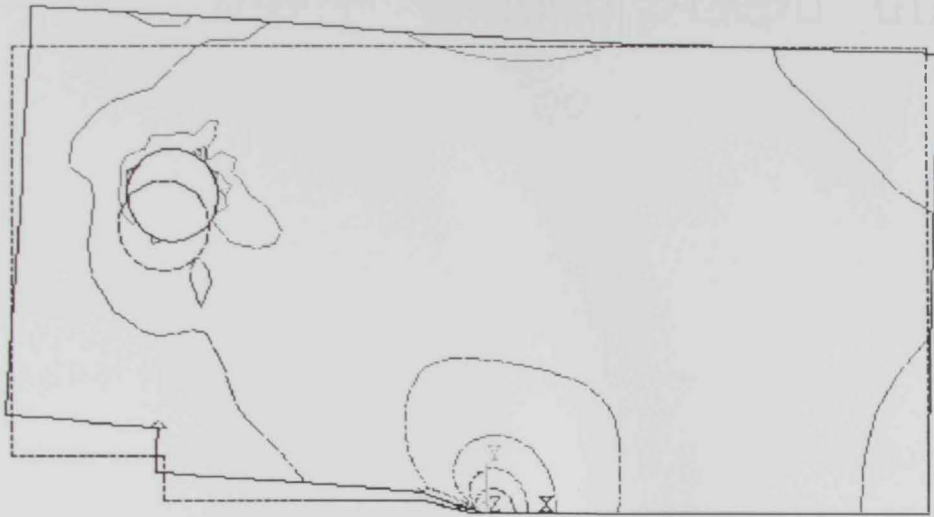
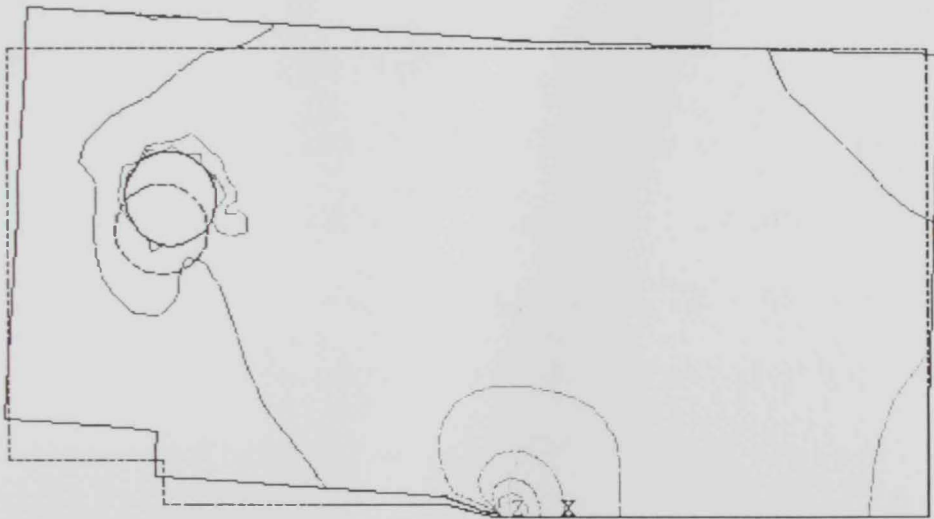


Figure 4.18 (Cont.)



(a)



(b)

Figure 5.19 Deformed shape of CT specimen in mode I at initiation load, (a)  $a_0/w = 0.42$ , and (b)  $a_0/w = 0.45$

# Chapter five

## CHAPTER 5

# MIXED MODE STABLE CRACK GROWTH

### 5.1. INTRODUCTION

The compact tension specimen was also adopted to examine the mixed mode (I & II) stable crack growth for AISI 4340 alloy steel. Both experimental and theoretical investigations were considered. Comparisons between experimental and theoretical results are presented wherever possible.

### 5.2. EXPERIMENTAL STUDIES

Figure 5.1 shows the compact tension (CT) specimen configuration for mixed mode stable crack growth. Two different  $a_0/w$  ratios (0.42 and 0.43) and four different loading angles  $\psi$  ( $50^\circ$ ,  $60^\circ$ ,  $65^\circ$ , and  $75^\circ$ ) were employed. The different combinations of  $a_0/w$  ratio and  $\psi$  that used for mixed mode stable crack growth tests are presented in Table 5.1. The specimen of loading angles  $50^\circ$ ,  $60^\circ$ ,  $65^\circ$  and  $75^\circ$  were tested with  $a_0/w = 0.43$ , while the specimens of loading angles of  $60^\circ$ ,  $65^\circ$  and  $75^\circ$  were tested with  $a_0/w = 0.42$ . Due to the limited load carrying capacity of the MTS testing machine a combination of  $a_0/w = 0.42$  and  $\psi = 50^\circ$  could not be tested.

Two specimens at least were tested to ensure the results repeatability. Some of the specimens were loaded quasi-statically to the maximum load and beyond and then broken

due to a higher head speed. Some of them were loaded quasi-statically until the full separation. The experimental results of fracture tests are summarized in Table 5.1.

### Load Displacement Data

The load- load line displacement (LLLD) records obtained for  $\psi = 60^\circ, 65^\circ$  and  $75^\circ$  with  $a_0/w$  ratio = 0.42 are shown in Figures 5.2, 5.3 and 5.4. To facilitate the comparison between the LLLD diagrams for different loading angles, a representative curve for each loading angle ( $60^\circ, 65^\circ, 75^\circ$  and  $90^\circ$ ) is plotted in Figure 5.5. Also representative load displacement records obtained for loading angle  $50^\circ, 60^\circ, 65^\circ, 75^\circ$  and  $90^\circ$  with  $a_0/w$  ratio = 0.43 are presented in Figure 5.6.

Figure 5.7 illustrates the effect of  $a_0/w$  ratio on the LLLD records for a constant loading angle. The displacement  $\delta$  represents the opening between the two points lying on the mode I load line and the opposite crack flanks.

Initially the load is varying linearly with displacement till a certain point at which the curve deviates from its linearity this point is considered as the crack initiation point. As the crack proceeds the slope of the curve decreases till it is nearly flattened at the maximum load ( $P_{max}$ ), and then the crack proceeds under approximately constant load. The maximum load ( $P_{max}$ ) is approximately 2 times the initiation load  $P_i$  and, both  $P_{max}$  and  $P_i$  for mixed mode are higher than those for mode I. As was observed in the case of mode I, the crack under mixed mode condition blunted considerably before the crack started to propagate. The effect of  $a_0/w$  ratio on the Load – Load line displacement diagrams are shown in Figure 5.7.

Figures 5.8 and 5.9 present the effect of the loading angle  $\psi$  on both initiation ( $P_i$ ) and maximum ( $P_{max}$ ) loads. Summary of the results of the experimental tests are also given in Table 5.1. Samples of the load-over head displacement curves that obtained from the MTS machine are presented in Appendix 5A.

### **Range of Stable Crack Growth**

The initiation of crack growth has been detected by monitoring the crack tip position through a magnifier continuously. These are marked by dots in the LLLD curves. The extent of stable crack growth is around 2 mm. A remarkable crack blunting was observed before the onset of stable crack growth initiation, then the crack is observed to initiate and extended stably up to the instability point. As was the case for mode I stable crack growth, it was a bit difficult to identify exactly the onset of crack initiation due to the limited magnification of the magnifier. This issue needs more investigations in order to adequately identify the onset of stable crack extension and in turns the corresponding point of  $P_i$  on the LLLD curves.

### **Crack Initiation Direction**

Typical photographs of some fractured samples are presented in Figures 5.10 and 5.11 the crack grows initially almost along a straight line, which is inclined at an angle  $\theta$  with initial crack. The direction of initial extension was measured directly or after projecting the photograph of a specimen to a large magnification. Table 5.1 presents the angle of initial crack for the different cases. Figure 5.12 shows the measured crack initiation direction under mixed mode loading versus the loading angle ( $\psi^\circ$ ).



## **Crack Front Tunneling**

The crack front tunneling was measured using a dye penetrate. A sample photograph showing the extent of tunneling at the initiation and after maximum load is shown in Figure 5.13. It is observed that the crack curving is of the order of 8 to 12 mm at the maximum load and 5 to 7 at initiation. The tunneling size at the initiation is generally lower. Also the tunneling size in the mixed mode is more than that of mode I.

## **Examination of Fracture Surfaces**

The fracture surfaces of mixed mode stable crack growth are presented in Figure 5.14. Same procedures of the case of mode I were followed while obtaining the fracture surfaces for mixed mode. Mixed mode fracture surface have more or less of the same macroscopically features.

Figures 5.15 and 5.16 show scanning electron fractographs of the stable crack growth and the unstable crack growth regions. Both regions are similar microscopically as in the case of mode I. Unlike mode I, equiaxed dimples appear, which complete rims. The dimples are elongated due to the shear component and from an oval shape. Like mode I, for the specimen separated at a higher head velocity, the feature surface of unstable region has smaller length scales and more irregular pattern than that for the stable crack growth region.

### 5.3. FINITE ELEMENT ANALYSIS

A 2-D finite element model using ANSYS 5.4, has been used to determine the directions of initial stable crack extensions. All the analysis has been performed assuming a plane state of stress. Some investigators [63, 74-76] have shown that the direction of crack extension can be determined from the elastic stress analysis using the maximum tangential principal stress or the maximum principal stress criteria. This method has been adopted for all case studies. An elastic finite element analysis in conjunction with criterion of maximum tangential principal stress has been used to predict the direction of initial crack extension. The elastic analysis has been carried out to predict the directions of initial crack growth for different combinations of  $a_0/w$  ratio and loading angle  $\psi$ . Combinations of  $a_0/w = 0.42$  with  $\psi = 75^\circ, 65^\circ$  and  $60^\circ$ , and  $a_0/w = 0.43$  with  $\psi = 75^\circ, 65^\circ, 60^\circ$  and  $50^\circ$  have been studied.

Figure 5.17 shows the finite element discretizations for different cases. The mesh is based on a simple circular crack tip mesh. The discretization has 4365 elements and 13467 nodes. At the crack tip the quarter point singularity elements are used. Each discretization consists of 32 square root singularities element around the crack tip with 0.025 mm side length. All other elements are eight noded quadratic elements. According to the maximum tangential principal stress (MTPS) criterion a crack will grow in a radial direction perpendicular to the direction of a maximum tangential principal stress. The extension starts when the maximum tangential principal stress reaches a critical value. Thereby the angle of initial crack extension is obtained. The stresses are obtained at the following radii from the crack tip; 0.025, 0.0375, 0.05, 0.05797, 0.0668, 0.0768, etc.

A comparison of the predicted and experimental directions of initial crack extension is given in table 5.1. There is a good agreement between the predicted and experimental results based on MTPS criterion. These observations agree well with some other investigators for different material [74-81].

Table 5.1 Summary of experimental and predicted results for mixed mode stable crack growth.

a <sub>0</sub> /w ratio	Loading angle (ψ) <sup>o</sup>	Initiation load (P <sub>i</sub> ) (kN)	Maximum load (P <sub>max</sub> ) (kN)	P <sub>max</sub> / P <sub>i</sub> ratio	Direction of initial crack extension (θ) <sup>o</sup>	
					Experimental	Predicted
0.42	90	22	45.473	2.1	0.0 <sup>o</sup>	0.0 <sup>o</sup>
	75	24.480	51.433	2.1	11 <sup>o</sup> - 12 <sup>o</sup>	11.1 <sup>o</sup>
	65	27.836	58.526	2.1	19 <sup>o</sup> - 19.5 <sup>o</sup>	19.1 <sup>o</sup>
	60	30.5	65.73	2.16	23 <sup>o</sup>	22.47 <sup>o</sup>
0.43	90	18.0	40.4		0 <sup>o</sup>	0 <sup>o</sup>
	75	23.0	50.288	2.0	11 <sup>o</sup> - 12 <sup>o</sup>	10.82 <sup>o</sup>
	65	27.0	57.529	2.13	18 <sup>o</sup> - 19.5 <sup>o</sup>	18.76 <sup>o</sup>
	60	29.50	63.004	2.06	22 <sup>o</sup> - 22.5 <sup>o</sup>	22.17 <sup>o</sup>
	50	33.825	75.430	2.23	26 <sup>o</sup> - 27 <sup>o</sup>	26.80 <sup>o</sup>

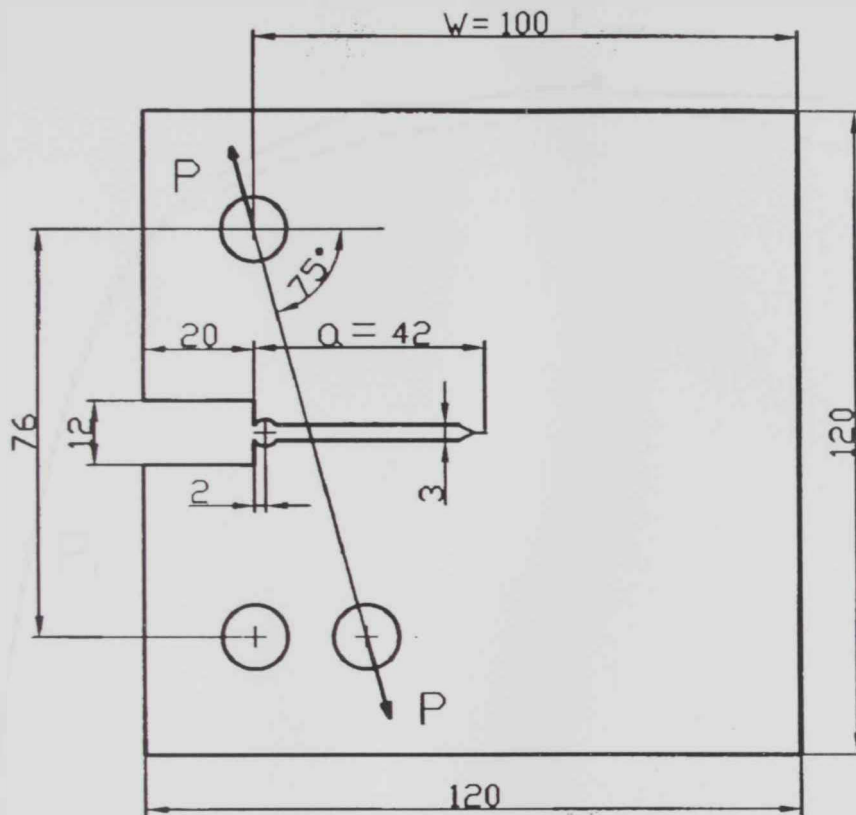
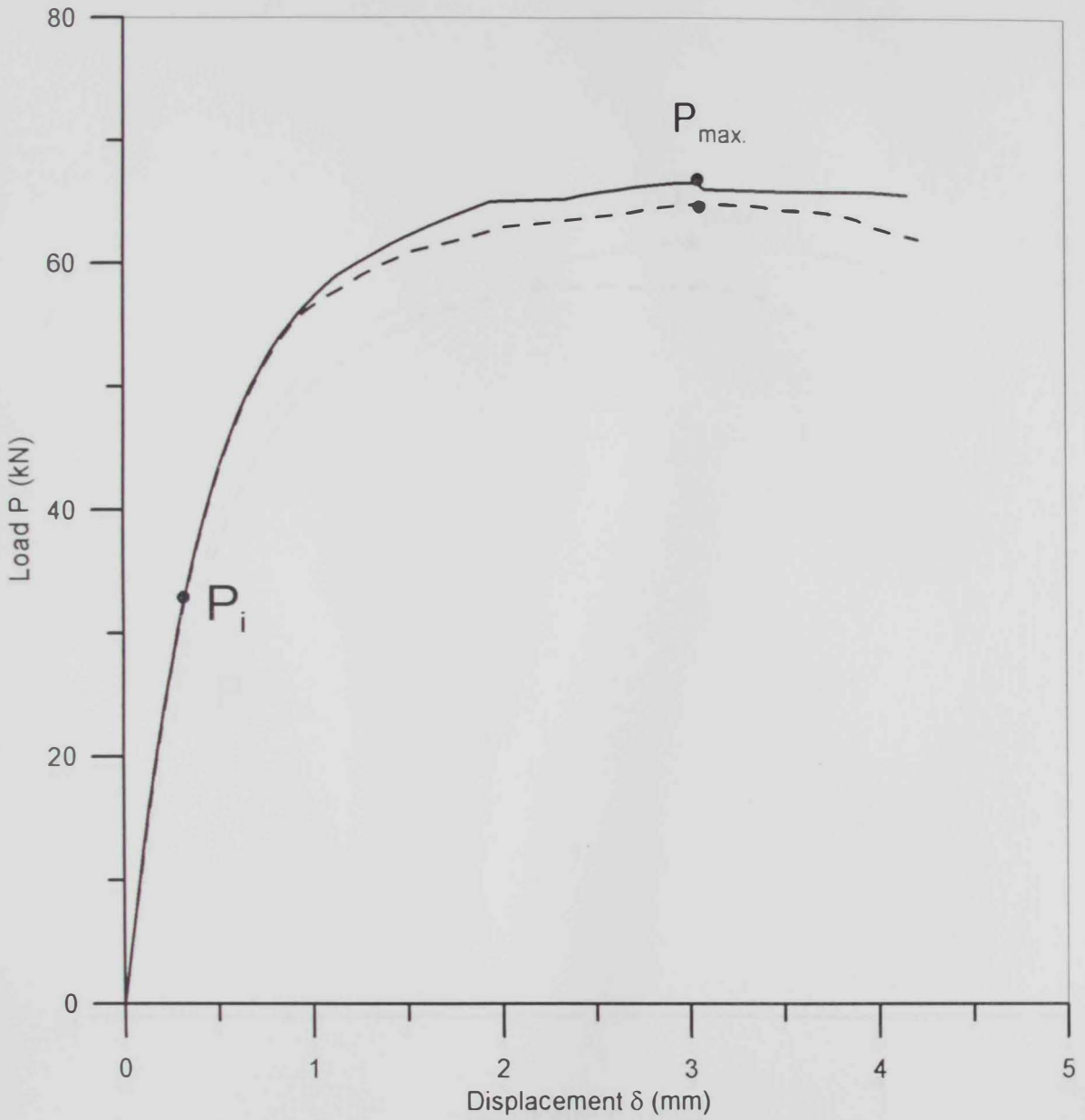
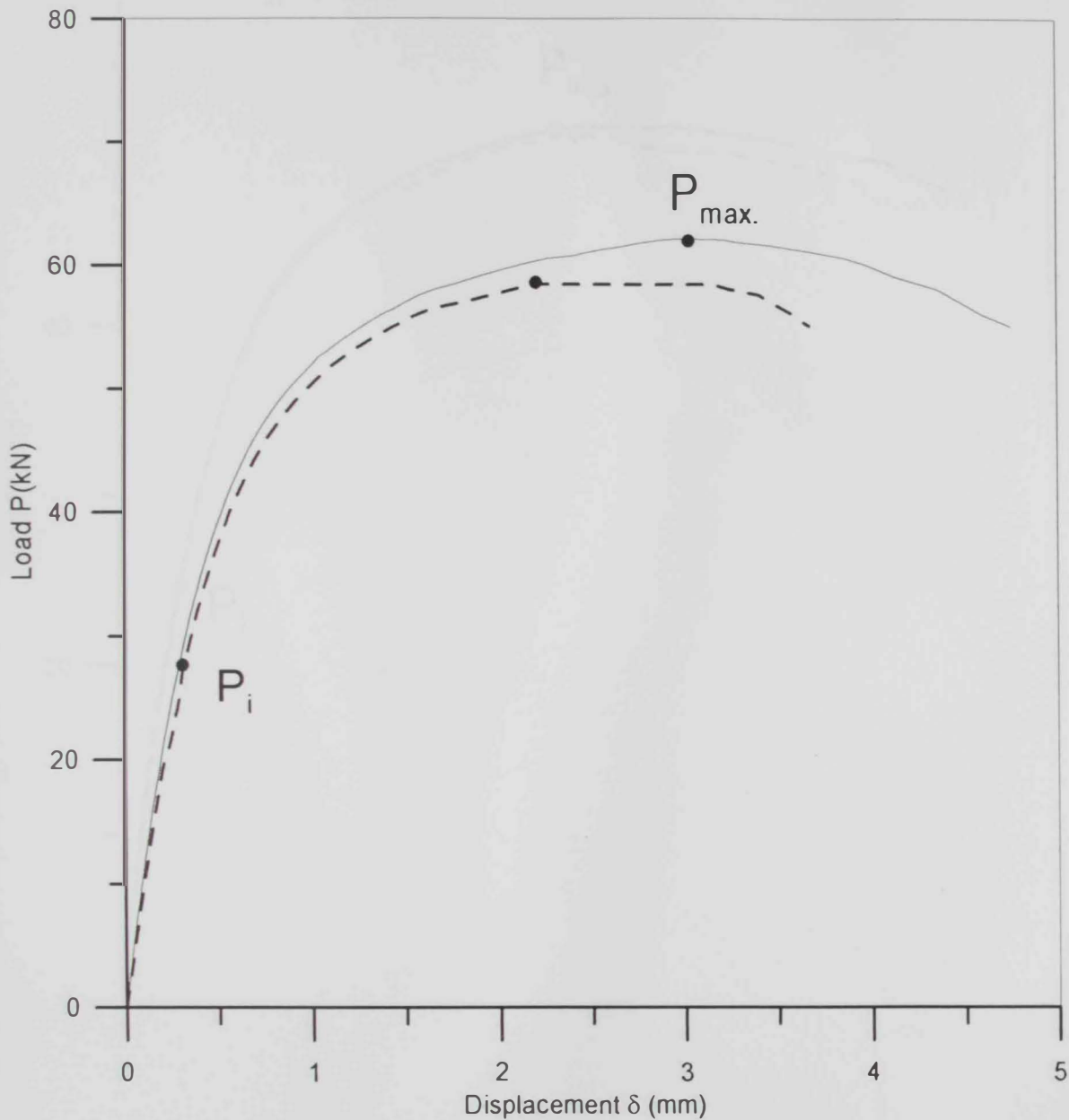


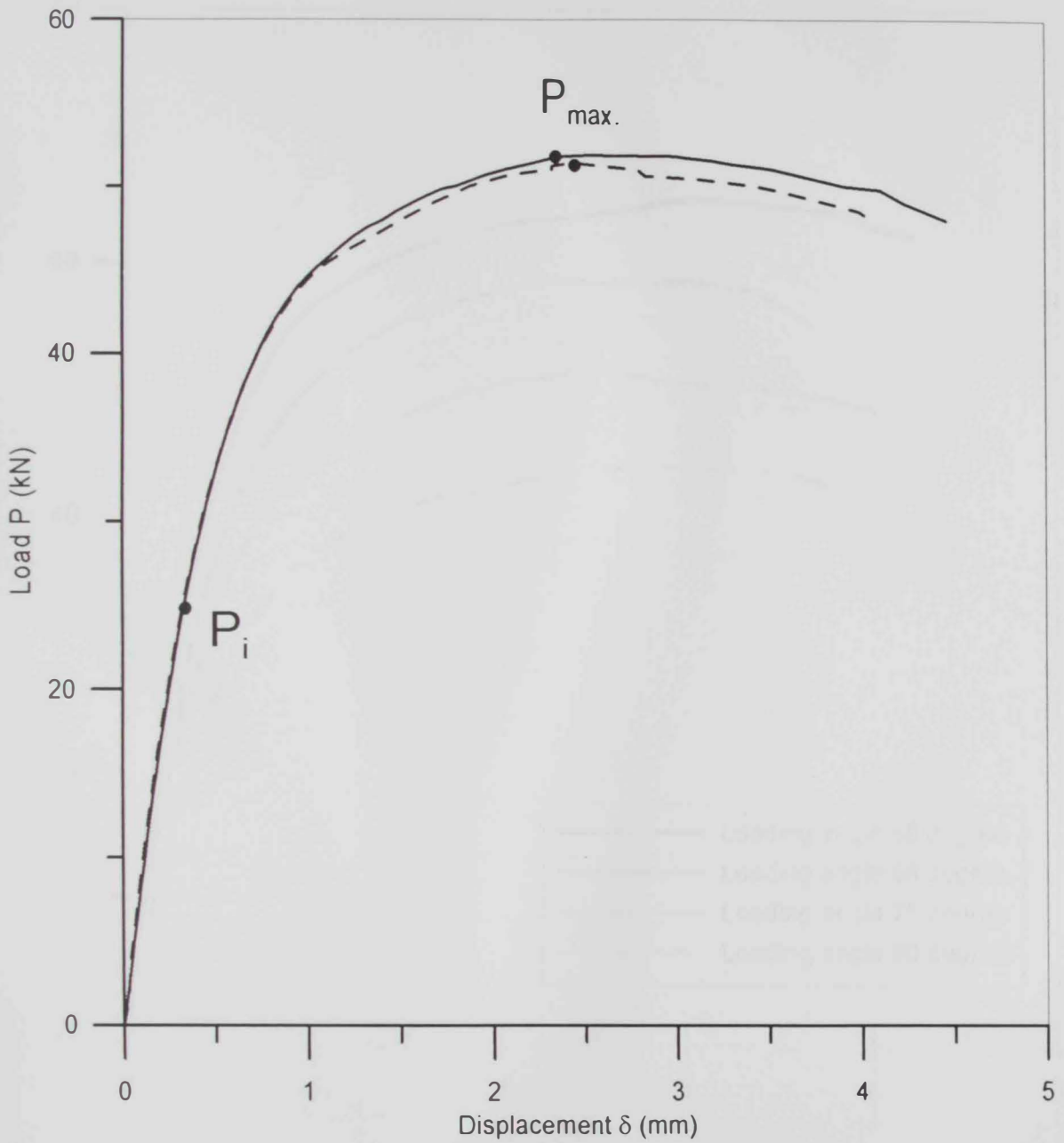
Figure 5.1. Compact tension (CT) specimen geometry for mixed modes stable crack growth.



Figures 5.2 Load - Load line displacement diagram for  $a_0/w = 0.42$  and loading angle  $\psi = 60^\circ$ .



Figures 5.3 Load - Load line displacement diagram for  $a_0/w = 0.42$  and loading angle  $\psi = 65^\circ$ .



Figures 5.4 Load – Load line displacement diagram for  $a/w = 0.42$  and loading angle  $\psi = 75^\circ$ .



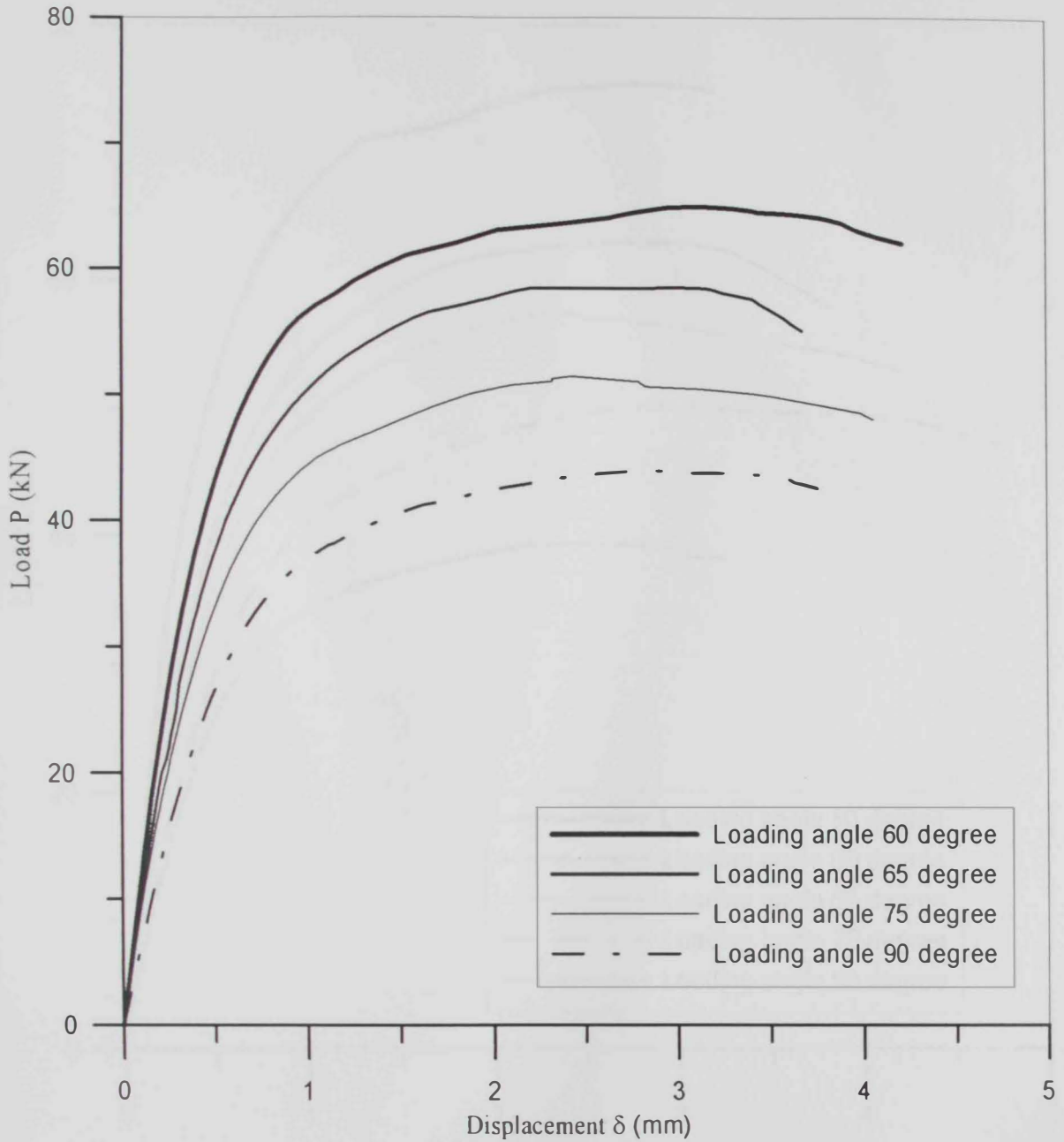


Figure 5.5 Comparison of load – load line displacement diagrams for different loading angles ( $\psi = 60^\circ, 65^\circ, 75^\circ,$  and  $90^\circ$ ) and  $a/w = 0.42$

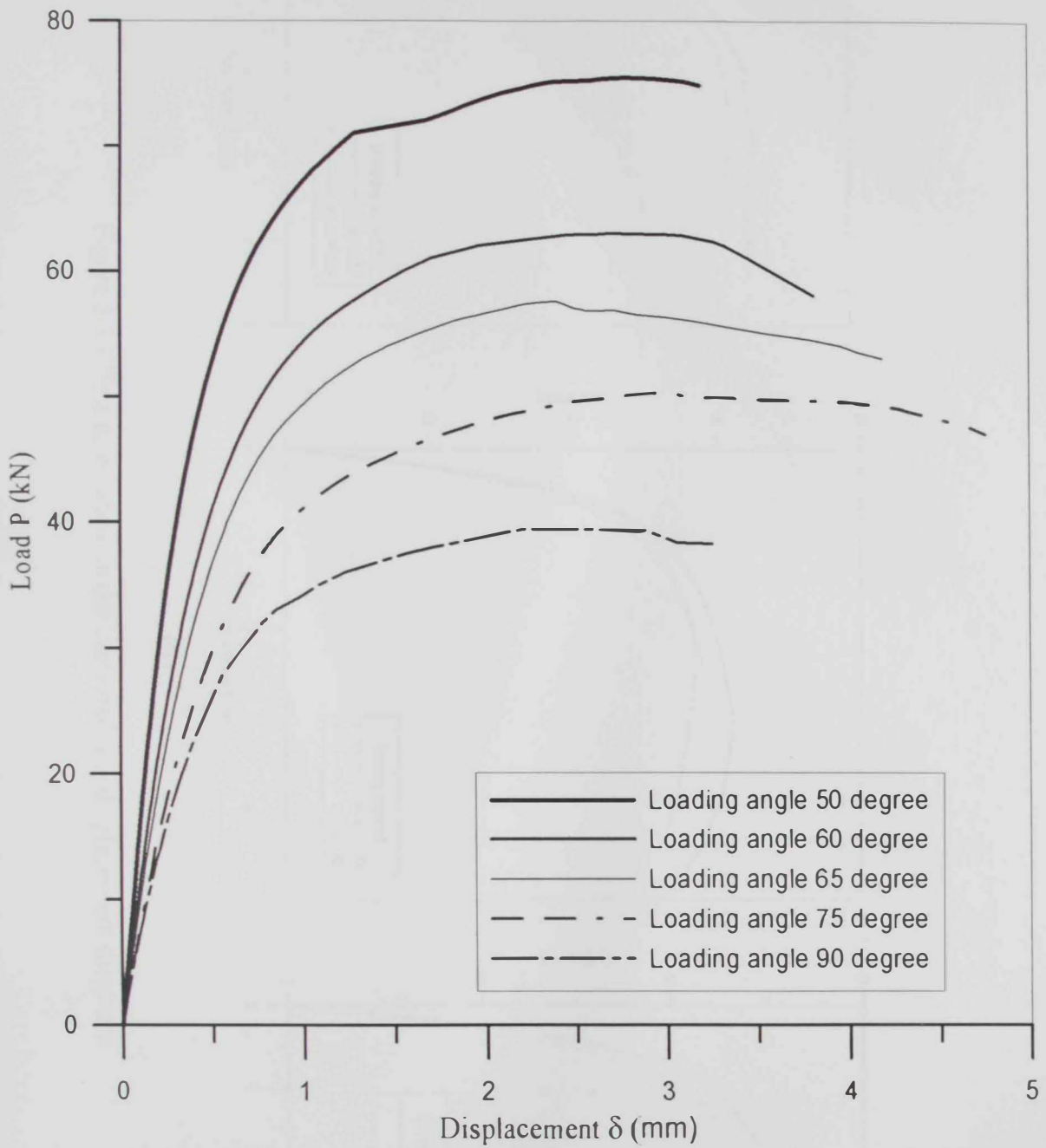
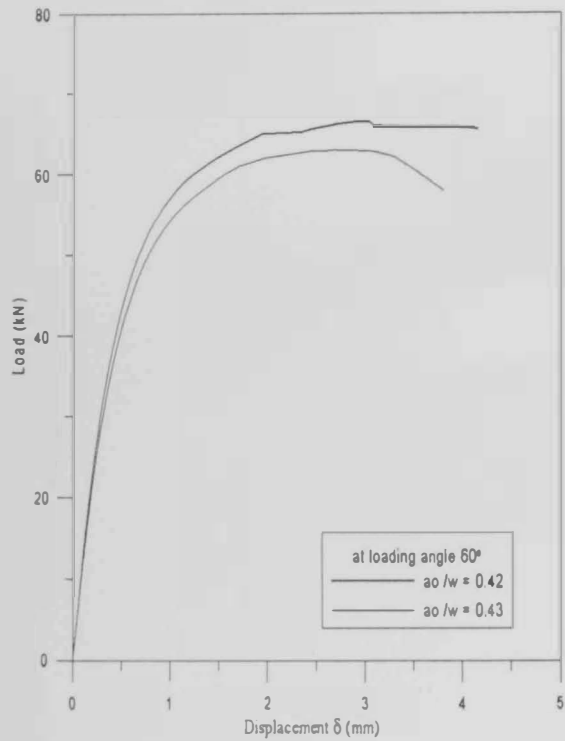
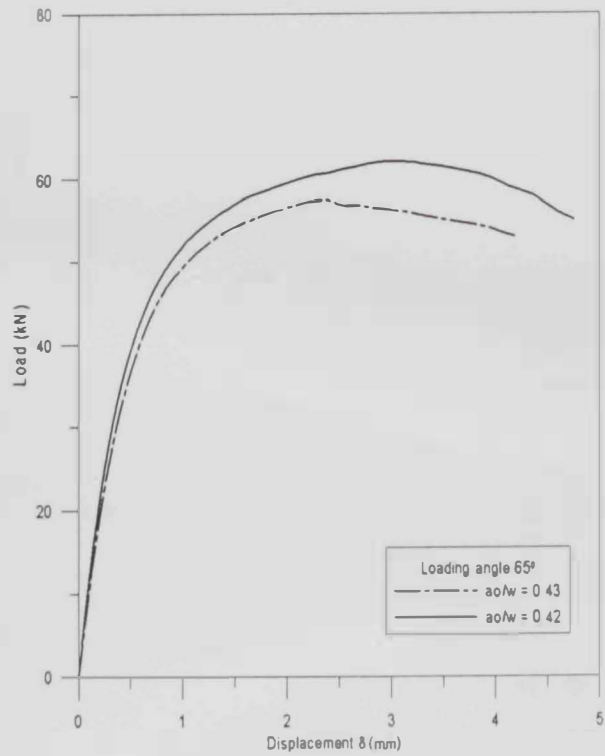


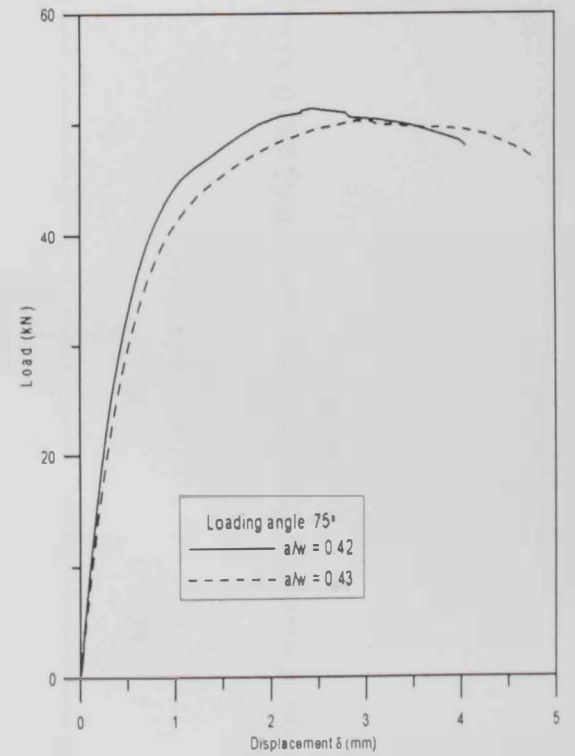
Figure 5.6 A comparison of load displacement diagrams for different loading angle ( $\psi = 50^\circ, 60^\circ, 65^\circ, 75^\circ$  and  $90^\circ$ ) and  $a_0/w = 0.43$



(a)



(b)



(c)

Figure 5.7 Effect  $a/w$  ratios on the load-load line displacement diagrams

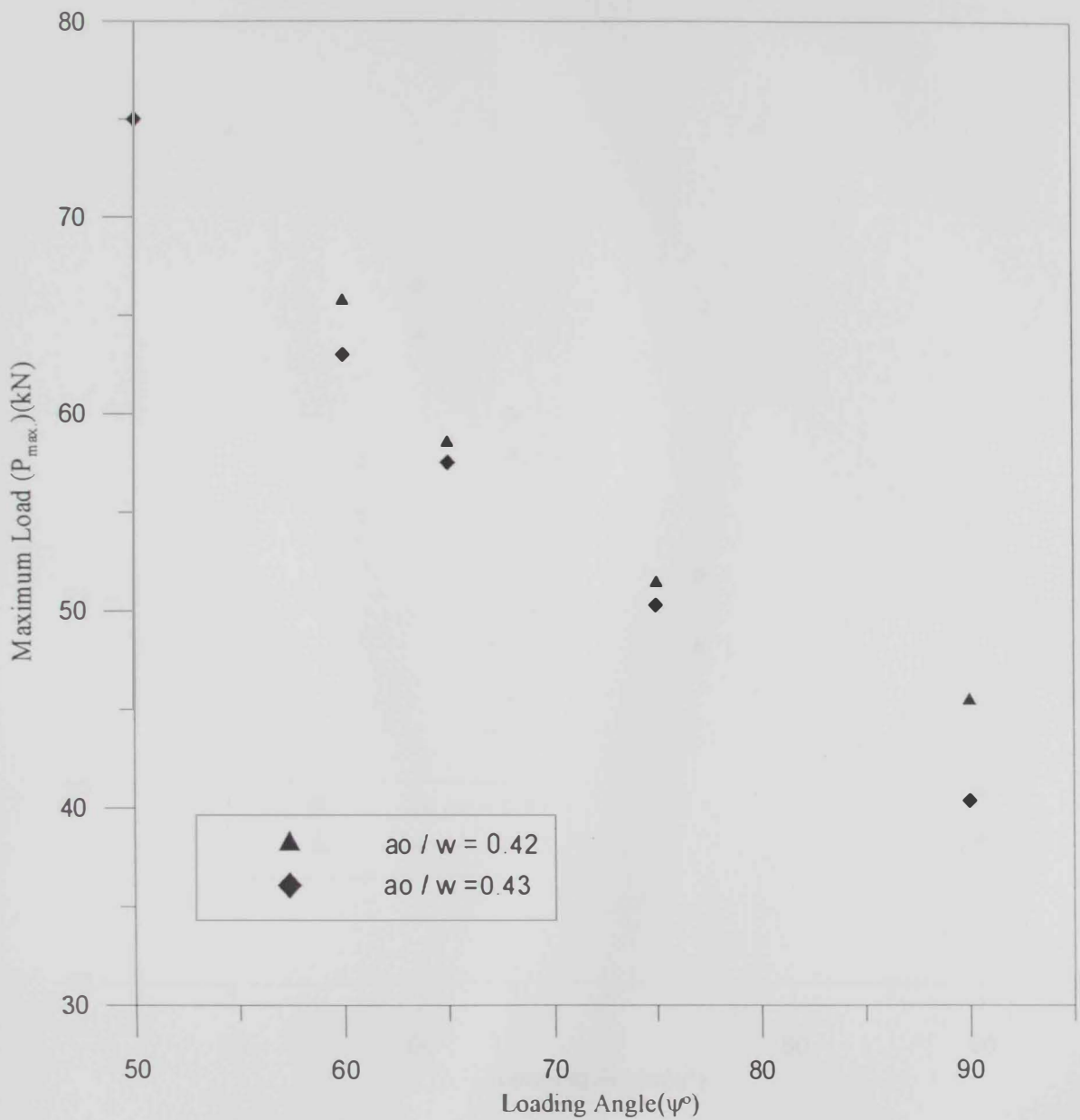


Figure 5.8 Variation of maximum load ( $P_{max}$ ) for  $a_0/w = 0.42$  and  $0.43$  against loading angle ( $\psi$ ).

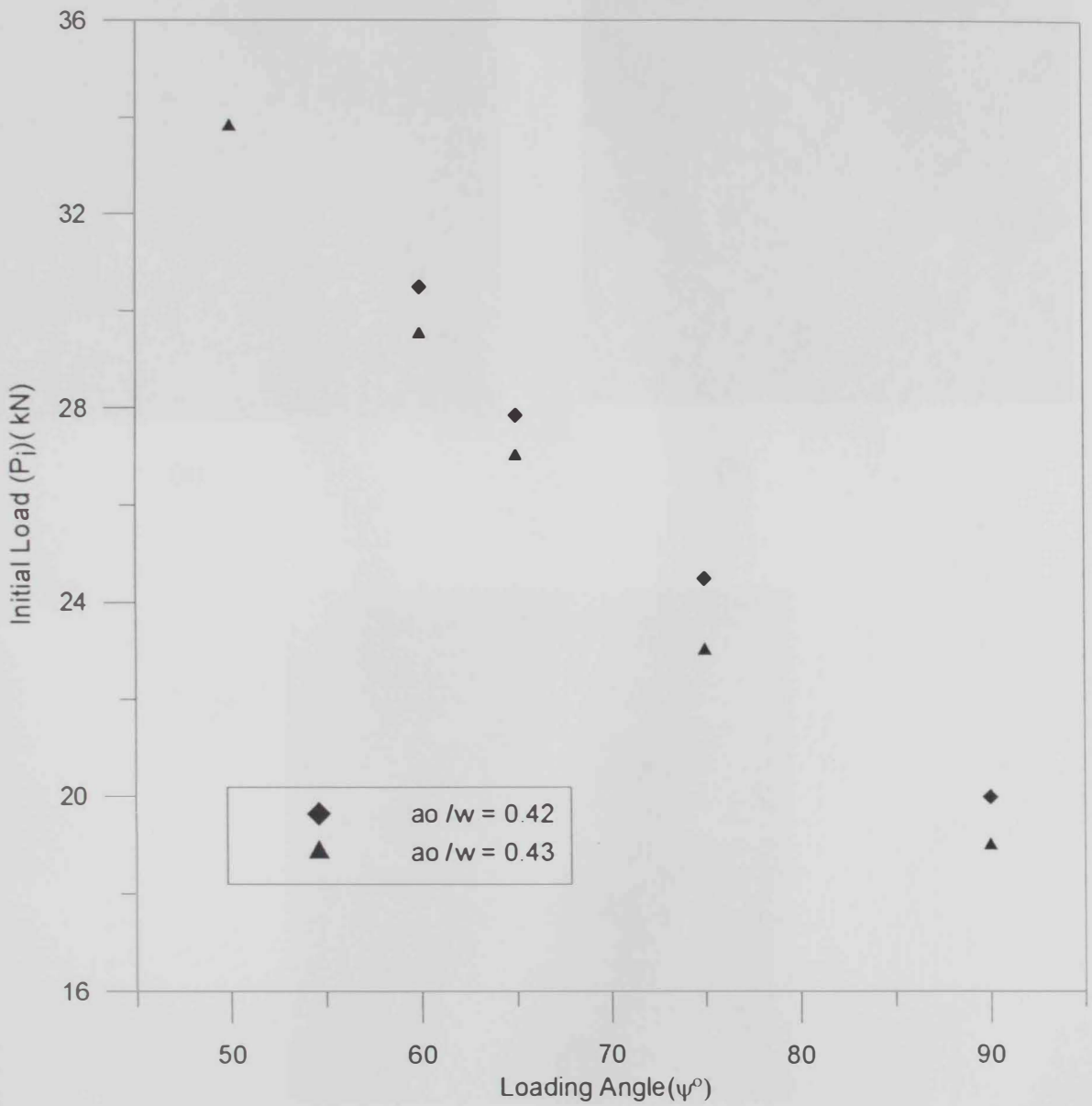
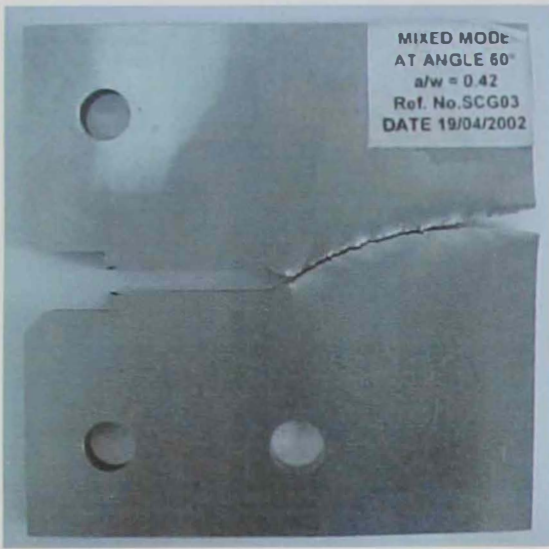


Figure 5.9 Variation of initiation load ( $P_i$ ) for  $a_0/w = 0.42$  and  $0.43$  against loading angle ( $\psi$ ).



(a)

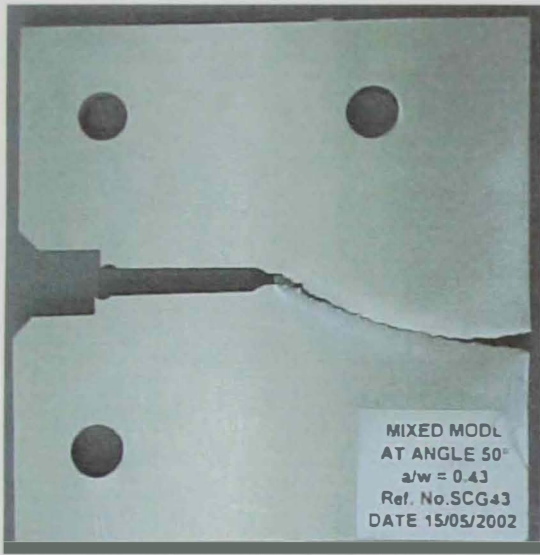


(b)



(c)

Figures 5.10 Sample photographs of fractured specimens for  $a_0/w = 0.42$ .  
(a)  $\psi = 60^\circ$ . (b)  $\psi = 65^\circ$ . (c)  $\psi = 75^\circ$ .



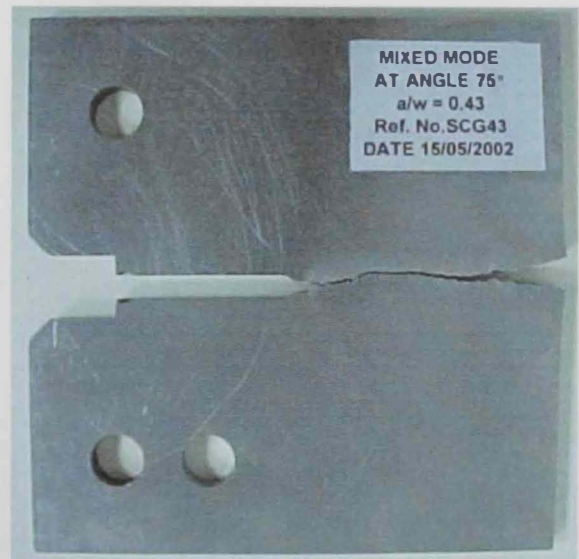
(a)



(b)



(c)



(d)

Figures 5.11 Sample photographs of fractured specimens for  $a_0/w = 0.43$ ;  
(a)  $\psi = 50^\circ$ . (b)  $\psi = 60^\circ$ . (c)  $\psi = 65^\circ$ . (d)  $\psi = 75^\circ$ .

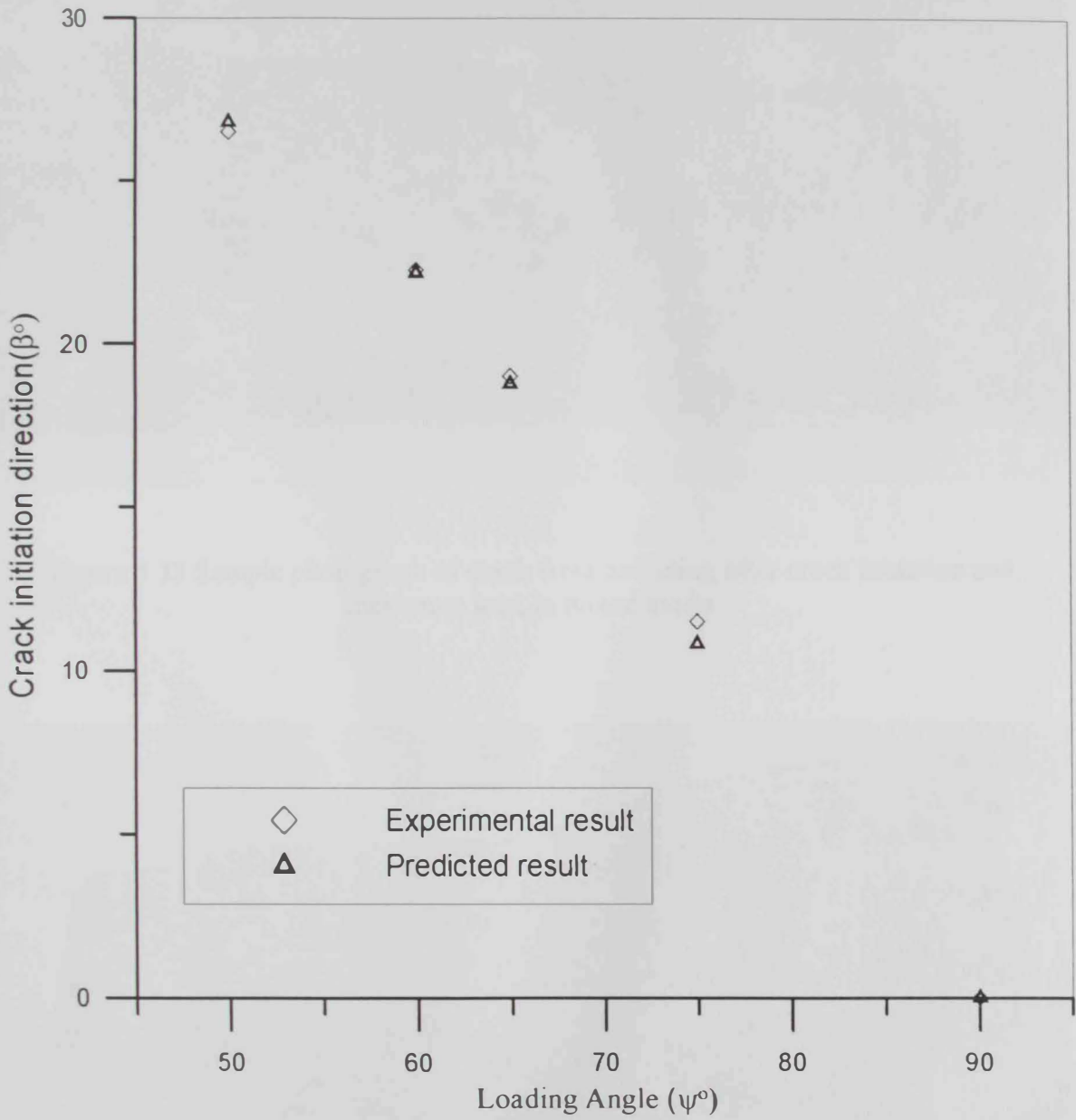


Figure 5.12 Comparison between experimental and predicted mixed mode crack initiation direction  $\theta^\circ$  and loading angle  $\psi^\circ$





Figure 5.13 Sample photograph of crack front tunneling after crack initiation and maximum load in mixed mode.

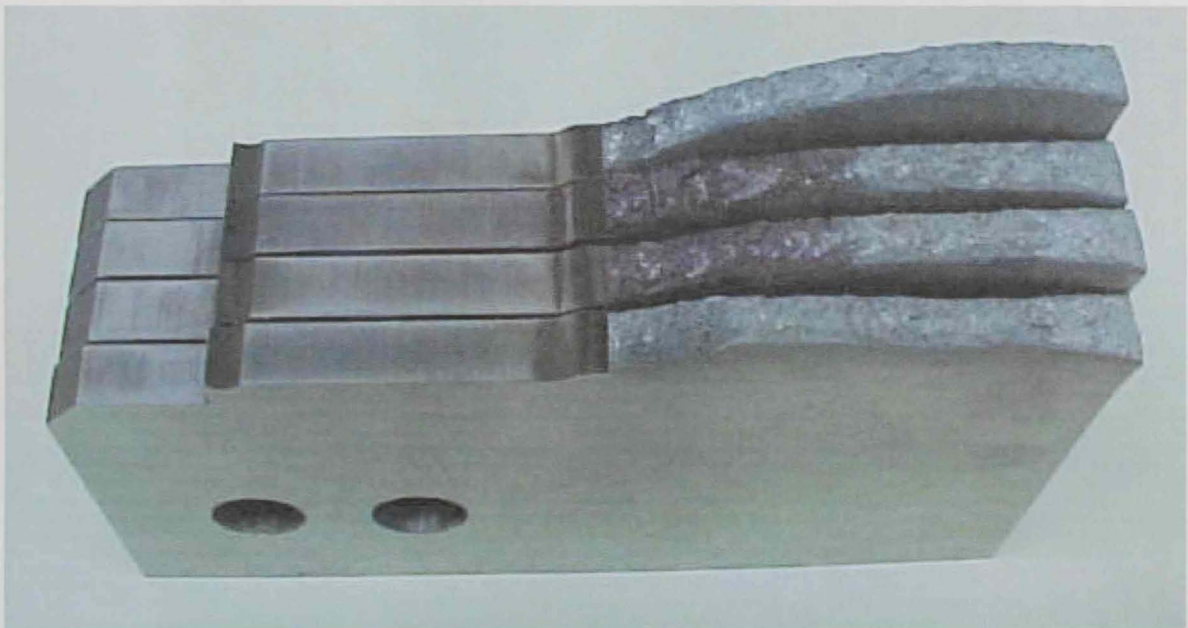


Figure 5.14 Sample photograph of the fracture surfaces in mixed mode specimen for different loading angles.

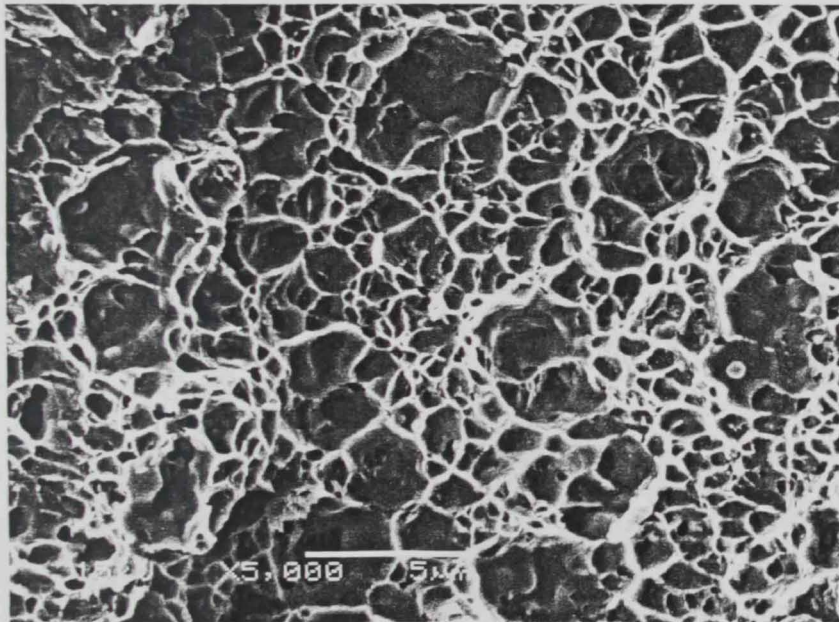
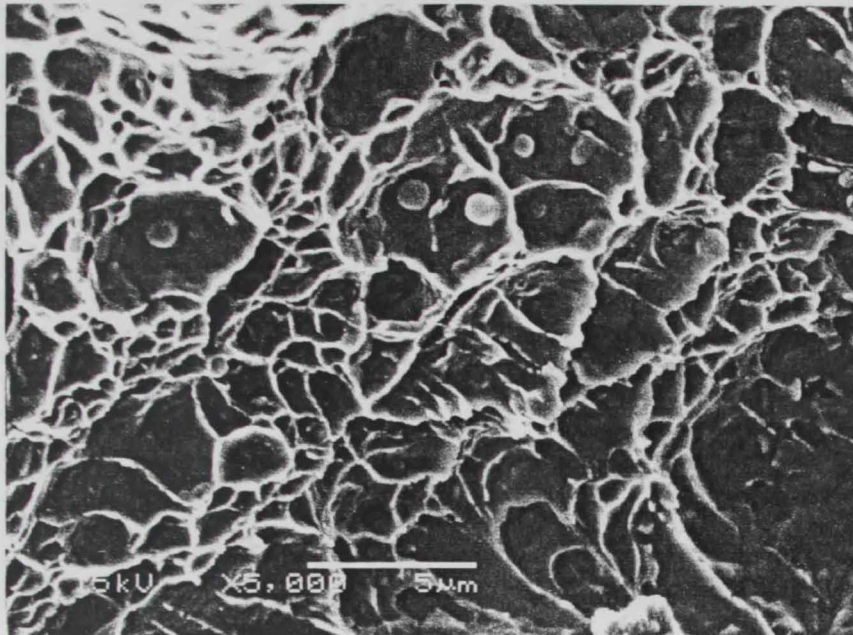


Figure 5.15 Scanning electron micrographs samples for mixed mode ( $a_0/w = 0.43$ ,  $\psi = 50^\circ$ ) stable crack growth region.

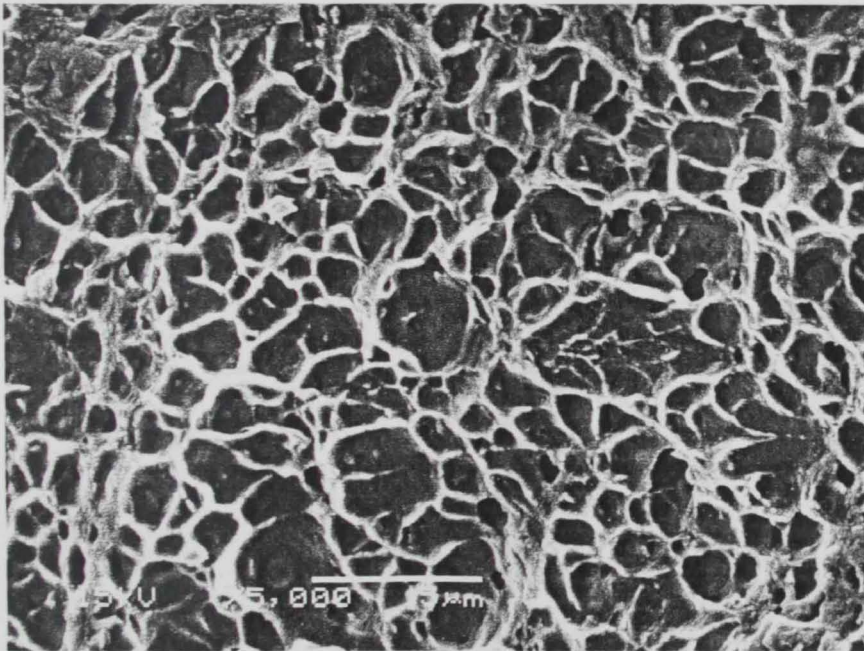
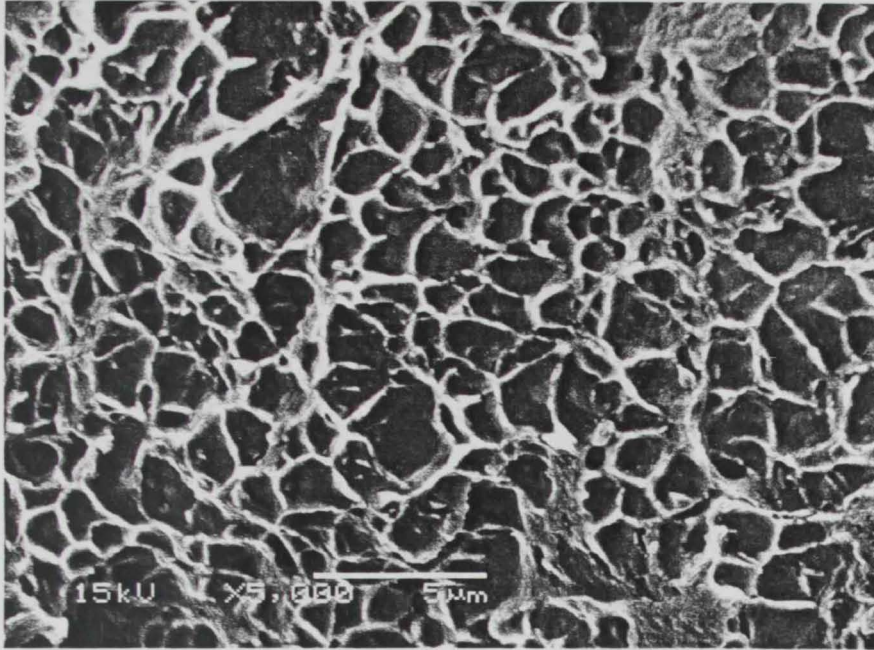
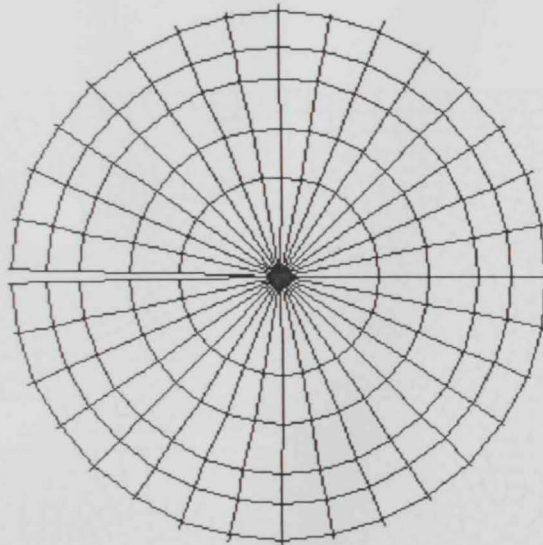
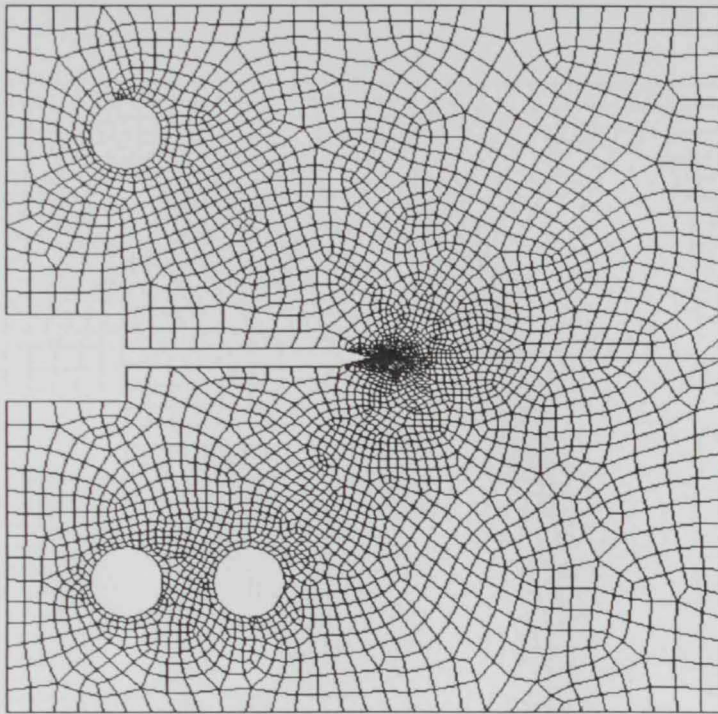
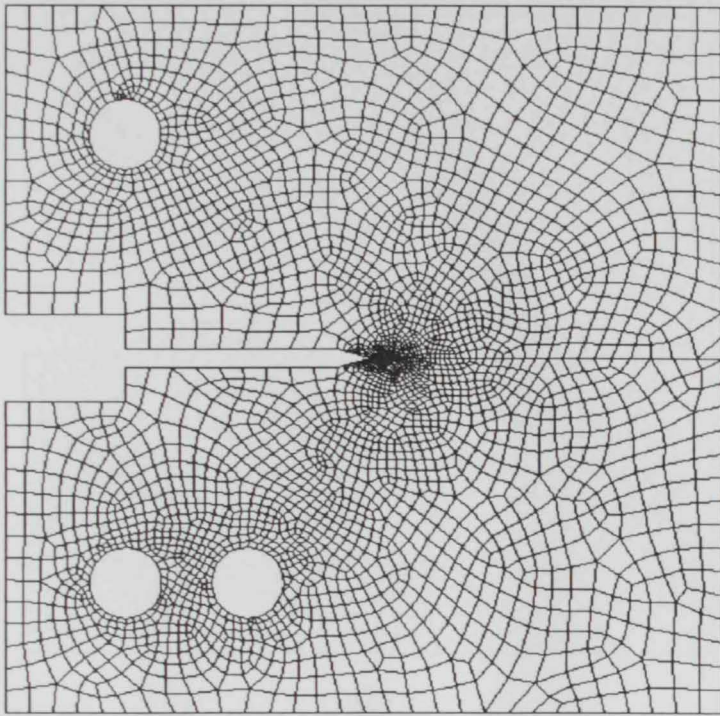


Figure 5.16 Scanning electron micrographs samples for mixed mode ( $a_0/w = 0.43$ ,  $\psi = 50^\circ$ ) unstable crack growth region.

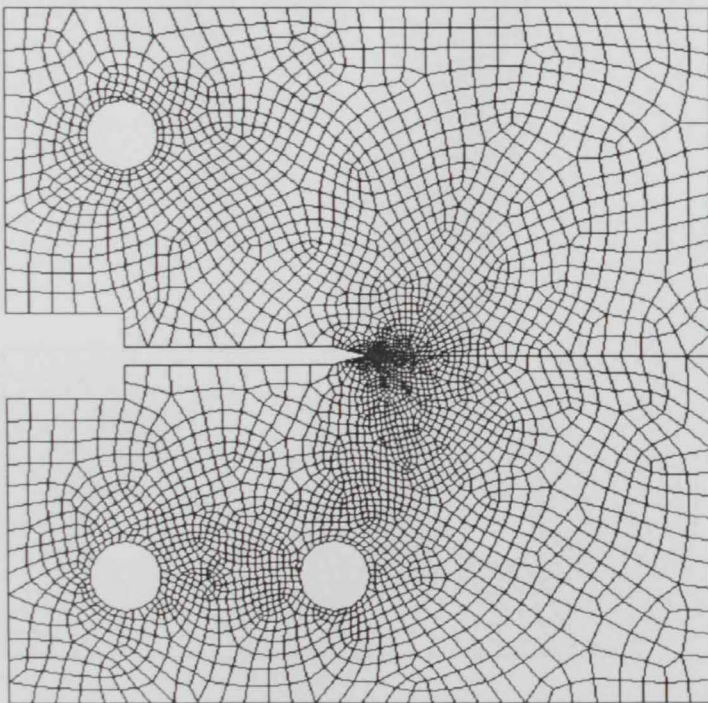


Details at the crack tip  
(a)

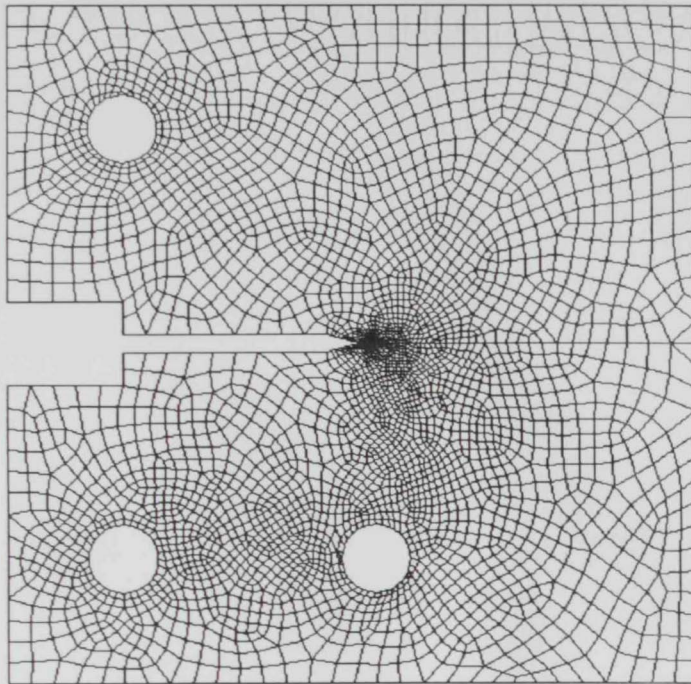
Figure 5.17 Discretisation for determining direction of initial stable crack extension;  
 number of element = 4365, number of nodes = 13467.  $a_0/w = 0.42$ ,  $\psi = 75^\circ$ ,  
 (b)  $a_0/w = 0.43$ ,  $\psi = 75^\circ$ . (c)  $a_0/w = 0.43$ ,  $\psi = 65^\circ$ . (d)  $a_0/w = 0.43$ ,  $\psi = 60^\circ$ ,  
 (e)  $a_0/w = 0.43$ ,  $\psi = 50^\circ$ .



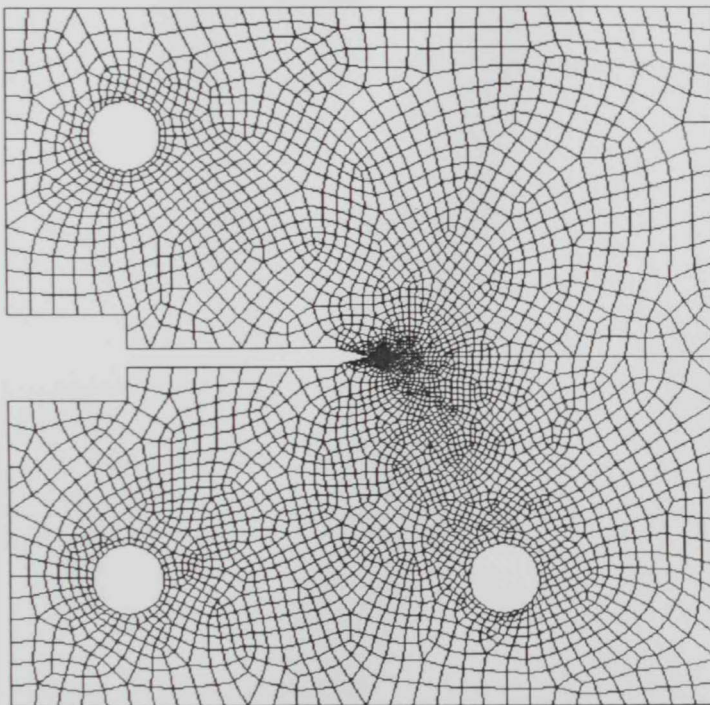
(b)



(c)



(d)



(e)

Figure 5.17 (Cont.)

# Chapter six

CHAPTER SIX: INTRODUCTION AND CONCLUSIONS

## 1. INTRODUCTION

The purpose of this chapter is to provide a comprehensive overview of the research findings presented in the preceding chapters. It aims to highlight the key contributions and implications of the study.

## 2. DISCUSSION

The experimental results indicate that the proposed method significantly outperforms existing approaches in terms of accuracy and efficiency.

Experimental results show that the proposed method achieves a higher accuracy rate compared to baseline methods across various test scenarios.

The results demonstrate that the proposed method is robust to noise and maintains high performance even in challenging environments.

Overall, the findings suggest that the proposed method is a promising solution for the problem at hand, offering improved performance and reliability.

The experimental setup and parameters used in this study are detailed in the following sections, providing a clear understanding of the methodology.

The results of the experiments are presented in the following tables and figures, illustrating the performance of the proposed method.

The proposed method shows superior performance in terms of both accuracy and computational efficiency, making it a viable option for practical applications.

The experimental results are consistent across multiple trials, indicating the reliability and reproducibility of the proposed method.

## CHAPTER 6

# DISCUSSION AND CONCLUSIONS

### 6.1. INTRODUCTION

This chapter is dedicated for the general discussion on results, suggestion of some directions for further investigations and summary of the main conclusions.

### 6.2. DISCUSSION

#### On The Experimental Studies

Experimental tests were performed in mode I and mixed mode (I and II). Different combinations of  $a_0/w$  ratios and loading angles  $\psi$  were used. In case of mode I  $\psi = 90^\circ$  stable crack growth (SCG) specimens of five different values of  $a_0/w$  ratios (0.41, 0.42, 0.43, 0.44 and 0.45) were tested. In case of mixed mode, stable crack growth specimens for four different loading angles values ( $75^\circ$ ,  $65^\circ$ ,  $60^\circ$  and  $50^\circ$ ) with two different values of  $a_0/w$  ratios (0.42 and 0.43) were tested. It was not possible to go in for load inclinations  $\psi$ , which result in a higher mode II contributions because of the limited capacity of the available MTS machine, the difficulty in introducing fatigue pre-crack to CT specimen due to the unavailability of such facility in the MTS machine and the limitations involved in the CT specimen to accommodate for more mode II contributions. As a consequence, the combination of  $\psi = 50^\circ$  with  $a_0/w = 0.43$  couldn't be tested. It is a good idea to study the stable crack growth (SCG) behavior of 4340 steel alloy through another specimen configuration, e.g. TPB, and CTS specimens. That facilitates



dominance of pure mode II. Stable crack growth through other materials and specimens configurations were reported by some investigators [e.g. 74-86].

The experimental observations on mode I and mixed mode show that there is a considerable blunting preceding the crack initiations. This blunting might contribute in the earlier non linearity in the load-load line displacement (L-LLD) curve. The crack becomes little sharper near the tip after extension. It may be worthwhile looking into how the initial spurt of extension can be located adequately on the L-LLD curves. The experimental observations show also that the blunting in mixed mode is more compared to mode I at onset of stable crack growth. That remarkable blunting was also observed by some workers [e.g. 83].

There was a considerable tunneling during the courses of the stable crack growth starting from initiation up to the full separation of the specimen passing through the instability point. The tunneling is more severe in the case of mixed mode and there are some evidences showing that the extent of tunneling increases as the crack proceed. The extent of the tunneling increases as the loading's angles reduces from mode I case ( $\psi = 90$ ). The magnitude of tunneling, as high as 13 mm, was observed for the mixed mode, around the maximum load.

In mixed mode the crack extends initially almost along a straight line. making an inclination angle with the initial crack. The inclination angle increases as the loading angle  $\psi^\circ$  decreases from  $90^\circ$  (mode I).

## On Finite Element Studies

The finite element results agree reasonably with the experimental results, in case of mixed mode, regarding the direction of initial crack extension. Due to constraints of time the elastic plastic finite element analysis couldn't be performed to characterize the whole stable crack growth and to predict the experimental results involving the load displacement diagrams, initiation and maximum loads, range of stable crack growth, and crack edge profile. This is an issue of great importance to be considered for further investigations. Since the load-displacement diagram are available and the crack extends along a straight path initially, it is significant to investigate whether these curves could be predicted employing the COA criterion and following the same procedure reported in references [74-81].

## 6.3. CONCLUSION

Some of the conclusions which can be made are as follows:-

- 1- Both the initiation and maximum loads increase as the loading angle  $\psi^\circ$  decreases from mode I case (i.e.,  $\psi = 90^\circ$ )
- 2- The ratio of maximum to initiation loads varies in the range of 2.0 to 2.2. For the whole range of loading angles tested.
- 3- Both the initiation and maximum loads decrease as  $a_0/w$  ratio increases in both modes I and mixed mode. The initial spurt of extension is generally moving in mixed mode than in the mode I.
- 4- There is a considerable blunting in both mode I and mixed mode before stable crack growth (SCG) initiation.

- 5- The amount of stable crack growth increases as  $a_0/w$  ratio decreases and loading angle  $\psi$  reduces from  $90^\circ$ . The range of stable crack growth is more in case of mode I.
- 6- There is a considerable tunneling in both mode I and mixed mode. The tunneling is generally more in the case of mixed mode. The extent of tunneling increases with crack extension.
- 7- The crack extends almost along a straight course initially in mixed mode loading. The angle of direction from the initial crack increases as the loading angle reduces from mode I case ( $\psi = 90^\circ$ ).
- 8- The directions of initial crack extension predicted through an elastic finite element analysis in conjunction with the maximum tangential principal stress (MTPS) criteria agree well with the experimental results.
- 9- The fracture surfaces show tension dominated dimpled fracture in mode I and mixed mode.
- 10- The spread of the plastic zone, at initiation, along the line of cracks extension is more than that in the transverse direction.

# Reference

## REFERENCE

1. Norman E. Dowling, 'Mechanical Behavior of Materials: Engineering Methods for deformation, Fracture, and Fatigue', Second Edition, Prentice Hall, Inc., Upper Saddle, New Jersey 07458, 1999.
2. T.L. Anderson, Fracture Mechanics: Fundamentals and Applications, Second Edition, CRS Press LLC, Boca Raton London, New York, Washington, D.C., 1995.
3. Westergaard H. M., 'on the stress distribution at the base of a stationary crack', Journal of applied Mechanics, vol., 24 pp109-114, 1959
4. Irwin G.R., Analysis of stresses and strains near the end of a crack traversing a plate, Journal of Applied Mechanics, vol. 24, pp.361 – 364, 1959.
5. Sneddon I. N., the distribution of stress in the neighborhood of a crack in an elastic solid. Proceedings, Royal Society of London, A-187, pp.229-260, 1946.
6. Williams M. L., 'Bearing pressures and cracks', Journal of Applied Mechanics, Vol.6 pp.49-53, 1939.
7. ASTM E399 standard test method for plane strain fracture toughness for metallic materials, ASTM E339-81, pp.592 – 622.
8. Broek, David, Elementary fracture mechanics, pp.122-127, 3<sup>rd</sup> edition, Noordhof, Groningen, 1984
9. Erdogan, F. and Sih, G. C., 'On crack extension in plates under plane loading and transverse shear', Trans. ASME, J. Basic Engg. Vol. 85, pp.519-527, 1963.

10. Maiti, S. K. and Smith, R. A., 'Theoretical and experimental studies on the extensions of cracks subjected to concentrated loading near their faces to compare the criteria for mixed mode brittle fracture', *J. Mech. Phys. Solids*, Vol. 31, pp. 389-403, 1983.
11. Wu, H. C., 'Dual fracture criterion for plane concrete', *Proc. ASME, J. Engg. Mech. Div.*, vol. 100, pp.1167-1181 1974.
12. Sih, G. C., 'A special theory of crack propagation', in 'Methods of Analysis and Solutions to Crack Problems' (ed. G. C. Sih) *Mechanics of fracture*, Vol. 1. Noordhoff Int. Pub. Leyden, pp. xxi-xiv, 1973.
13. Freund L. B., *Dynamics fracture mechanics*, Cambridge University press, New Yourk , New Yourk 10011, 1998.
14. Freund L. B. and Rosakis A. J. the structure of the near tip-field solution during transient elastodynamic crack growth. *Journal of the Mechanics and Physics of Solids*, Vol. 40, pp.699-719, 1992.
15. Irwin, G. R., 'Fracture' in 'Handbuch der Physik' Vol. VI, (ed. S. Flugge), Springer-Verlag, Berlin, pp.551-590, 1958.
16. Orwan, E., 'Energy criteria of fracture', *Welding J.*, Vol. 34, pp.1575-1605 (1955)
17. Irwin, G. R., Kies, J. A. and Smith, H. L., 'Fracture strength relative to onset and arrest of crack propagation', *proceedings of the American Society for Testing Materials*, 85, pp.640-657, 1958.
18. Dugdal, D. S., 'Yielding of steel sheets containing slits', *J. Mech. Phys. Solids*, Vol 8, pp.100-108, 1960.
19. Han, G. T. and Rosenfield, A. R., 'Local yielding and extension of a crack under plane stress' *Acta Metallurgica*, Vol. 13, pp.293-306, 1965.

20. Bilby, B. A. , Cottrell, A. H. and Swinden, K. H., 'The Spread of Plastic yield from a notch', Proceedings of the Royal Society, London, Vol. A272, pp.304-314 1963.
21. Goodier, J. N. and Field, F. A., 'Fracture of Solids' (ed. D. C. Drucker and J. J. Gilman), Wiley, New York, pp. 103-118, 1963
22. Kanninen, M. I., Mukherjee, A. K., Rosenfield, A. R. and Hahn, G. P., 'The speed of ductile crack propagation and the dynamics of flaw in metals', Mechanical Behavior of Materials under Dynamic Loads, (ed. U. S. Lindholm), Springer-Verlag, New York, pp.96-133, 1969.
23. Wells, A.A., 'Application of fracture mechanics at and beyond general yielding', Brit. Weld. J., Vol.8, pp563-570, 1963.
24. Burdekin, F. M. and Stone, D. E. W. 'The crack opening displacement approach to fracture mechanics in yielding materials', J. Strain Anal. , Vol. 1 pp. 145-163, 1966.
25. Turner, C. E., 'Yielding fracture mechanics', J. Strain Anal. Vol. 10, pp.207-216, 1975.
26. Rice, J.R., 'A path independent integral and the approximate analysis of strain concentration by notches and cracks', J. Appl. Mech., vol. 35pp.379-386, 1968.
27. Budiansky B., 'A reassessment of deformation theories of plasticity', Journal of Applied Mechanics, Vol.26, pp.259-264, 1959.
28. Hult, J. A. H. and McClintock, F.A., 'Elastic-plastic stress and strain distributions around sharp notches under repeated shear', Proc. 9<sup>th</sup> int. Congress for applied Mechanics, Vol. 8, University of Brussels.
29. Hutchinson, J. W., 'Singular behavior at the end of a tensile crack in hardening material', J. Mech. Phys. Solids, Vol. 16, pp.13-31, 1968.

30. Rice, J.R. and Rosengren, G.F., 'plane strain deformation near a crack tip in power law hardening material', *J. mech. Phys. Solids*, Vol. 16, pp. 1-12, 1968.
31. McMeeking, R. M., 'Finite deformation analysis of crack-tip opening in elastic-plastic material and implications for fracture, *J. Mech. Phys. Solids*, Vol.25, pp.357-381, 1977.
32. Sumpster, J. D. and Turner, C. E., 'Use of the J-integral in elastic – plastic Fracture studies by finite element method', *J. Mech. Engg. Sci.*, Vol.18, No.3, pp.97-112 1976.
33. McClintock, F. M., 'Plasticity aspects of fracture', in 'fracture An Advanced Treatise', (ed. H. Liebowitz), Vol.3, Academic Press, N. Y. , pp.47-225, 1971.
34. Rice, J.R. and Johnson, M. A., 'The role of large crack tip geometry changes in plane strain fracture, in *inelastic Behavior of Solids*', (eds. M. P. Kanninen et al.) McGraw Hill, N. Y., pp.641-672, 1970
35. Sih, C.F., de Lorenzi, H.G. and Andrews, W.R., 'Studies on crack initiation and stable crack growth ', *ASTM-STP668*, pp.65-120, 1979.
36. McMeeking, R. M and Parks, D. M., 'On criteria for J-Dominance of crack-tip fields in large-scale yielding' in 'Elastic-plastic Fracture', *ASTM STP 668*, pp. 175-194, 1979.
37. Hutchinson, J.w., ' A course on Nonlinear Fracture Mechanics', Dept. of Solid Mechanics, The Technical Univ. of Denmark, 1979
38. Shih, C. F. and German, M. D., 'Requirements for a one parameter Characterization of crack-tip fields by the HRR singularity', *Int. J. Fract*, Vol.17, pp.27-43, 1981.



39. Ower, D. M., Zhuang, S., Rosakis, A. J. and Ravichandran, G., 'Experimental determination of dynamic crack initiation and propagation fracture toughness in thin film aluminum sheets; International Journal of Fracture, Vol. 90, pp. 153-174, 1998.
40. Anderson, D. D., 'Experimental Investigation of Quasistatic and dynamic fracture properties of titanium alloy's, Ph.D. Thesis, California Institute of technology, Pasadena, California, 2002.
41. McClintock, F. A. and Irwin, G.R., 'Plasticity aspects of fracture mechanics', in 'Fracture Toughness Testing and its applications', ASTM STP 381, pp. 84-113, 1965.
42. Rice, J. R., 'Elastic-plastic models for stable crack growth' in Mechanics and Mechanism of Crack Growth, (ed. M. J. Center Publication, pp.14-39 (1975). Proc. Of Conf. at Cambridge, England April 1973.
43. Broberg, K. B., 'On stable crack growth', J. Mech. Phys. Solids, Vol.23, pp.215-237, 1975
44. Chitaley, A. D. and McClintock, F. A., 'Elastic-plastic mechanics of steady crack growth under anti-plane shear', J. Mech. Phys. Solids, Vol.19, pp.117-163, 1971.
45. McClintock, F.A., 'Local criteria for ductile fracture', Int. J. Fract. Mech., Vol.4, pp.101-130, 1968.
46. Cherepanov, G. P., 'Mechanics of Brittle Fracture', Gos. Izdat. , Moscow, p.271, 1974
47. Amazigo, J. C. and Hutchinson, J. W., 'Crack-tip fields in steady crack-growth with linear strain-hardening' J. Mech. Phys. Solids, Vol.25, pp.81-97, 1977.
48. Rice, J. R. and Sorensen, E. P., 'Continuing crack-tip deformation and fracture for plane-strain crack growth in elastic-plastic solid', J. Mech. Phys. Solids, Vol.26, pp.163-168, 1978.

49. Hutchinson, J. W., and Paris, P. C., 'The theory of stability analysis of J-controlled crack growth', in 'Elastic-plastic fracture', ASTM STP 668, pp.37-64, 1979
50. Paris, P.C., Tada, H., Zahoor, Z and Ernst, H. 'Instability of the tearing mode of elastic-plastic crack growth', ASTM STP 668, pp.5-36, 1979
51. Shih C.F., 'Relationships between the J-integral and the crack opening displacement for stationary and extending cracks', Vol.29, pp. 305-326, 1981.
52. Andrews, W. R. and Shih, C. F., 'Thickness and side-groove effects on J- and  $\delta$ -resistance curves for steel at 93 degree C, in 'Elastic-Plastic Fracture', ASTM STP 668, PP.426-450, 1979.
53. Ma Fashang, Sutton M. A., Deng x., 'Plane strain mixed mode crack-tip stress fields characterized by a triaxial parameter and plastic deformation extent based characteristic length', Journal of the Mechanics and physics of solids, vol. 49, pp.2921-2953, 2001.
54. Chen, J. Y., Huang, Y., and Hwang, K. L., 'Mode I and Mode II plane-stress near-tip fields for crack in materials with strain-gradient effect', Key Engineering Materials, vol.16. 154-149, pp.19-28, 1998.
55. Fleck, N. A. and Hutchinson, J. w., in Advances in applied Mechanics, J. W. Hutchinson and T. Y. Wu, eds., Academic Press, New York, vol.33, pp. 295-361, 1996.
56. Schiøtz J, Carlsson A E, Canel L M and Thomson R, 'Effect of crack blunting on subsequent propagation', Mater. Res. Soc. Symp. Proc. 409 95,1996.

57. Schiøtz J, Canel L M and Carlsson A E, 'Effects of crack tip geometry on dislocation emission and cleavage: a possible path to enhanced ductility', *Phys. Rev. B* 55 6211,1997.
58. Gumbsch P and Beltz G E, 'On the continuum versus atomistic descriptions of dislocation nucleation and cleavage in nickel Modeling Simulation', *Mater. Sci. Eng.* 3 597,1995
59. Gumbsch P, 'An atomistic study of brittle fracture: towards explicit failure criteria from atomistic modeling', *J. Mater. Res.* 10 2897,1996
60. Thomson R, 'Intrinsic ductility criterion for interfaces in solids', *Phys. Rev. B* 52 7124,1995
61. Lisa L Fisher and Glenn E Beltz, ' Continuum mechanics of crack blunting on the atomic scale: elastic solution', *Modeling Simul. Mater. Sci.Eng.*, Vol 5. pp.517-537, 1997
62. Lisa L Fisher and Glenn E. Beltz, 'The effect of crack blunting on the competition between dislocation nucleation and cleavage', *Journal of the Mechanics and physics of solids*, Vol.49, pp. 635-654, 2001
63. Mourad, A. -H. I., 'Experimental and finite element studies on various modes of two dimensional stable crack growth; PhD thesis, Mechanical Engineering Department, IIT, powai, Bombay, India
64. Begley, J. A., and Landes, J. D., 'The J-integral as a fracture criterion in fracture toughness', *ASTM; STP 514*, PP.1-20, 1972.
65. Green, G. and Knott, J. F., 'On effects of thickness on ductile crack growth in mild steel', *J. Mech. Phys. Solids*, Vol. 23, pp.167-183, 1975.

66. Andersson, H., 'A finite-element representation of stable crack growth', *J. Mech. Phys. Solids*, Vol. 21, pp.337-356, 1973.
67. Andersson, H., 'Finite-element treatment of a uniformly moving elastic-plastic crack-tip', *J. Mech. Phys. Solids*, Vol. 22, pp.285-308 (1974)
68. De Koning, A. J., 'A contribution to the analysis of quasistatic crack growth in sheet materials', in 'advances in Research on the strength and Fracture of Materials', Prof. ICF 4, 197, Waterloo, ( ed. D. M. R. Taplin), Pergamon Press, N. Y. Vol. 3A, pp.25-32, 1978.
69. Luxmoore, A., Light, M. F. and Evans., W. T., 'A comparison of energy release rates, the J-integral and crack tip displacements', *Int. J. Fract.*, Vol.13, pp.257-259, 1979.
70. Newman, Jr., J. C., 'An elastic -plastic finite element analysis of crack initiation, stable crack growth and instability', *ASTM-STP 883*, PP. 93-117, 1984.
71. kanninen, M. F. et al., 'Elastic-plastic fracture mechanics for two-dimensional stable crack growth and instability problems , *ASTM-STP 668*, pp. 121-150, 1979.
72. Wang, G. S., ' An EPFM analysis of crack initiation, stable growth and instability', *Engg. Fract. Mech.*, Vol. 50, No.2, pp.261-282, 1995.
73. Shan, G X., Kolednik, O. and Fischer, F. D., 'Anumerical investigation on the geometry depends of the crack growth resistance in CT specimens', *Int. J. Fract.* Vol.66, pp.173-187, 1994.
74. Maiti S. K. and Mahanty, D. K., 'Experimental and finite element studies on mode I and mixed mode (I and II) stable crack growth-II. Finite element analysis', *Eng. Fract. Mechs.*, Vol. 37, pp.1237-1250, 1990.

75. Maiti S . K., and A.-H. I. Mourad, 'Criterion for mixed mode stable crack growth-part I. Three point bend geometry', Engineering Fracture Mechanics Vol.52, pp. 321-347, 1995.
76. Maiti S. K. and Mourad A.-H. I., 'Criterion for mixed mode stable crack growth-part II. Compact tension geometry with and without stiffener', Engineering Fracture Mechanics Vol. .52, pp. 349-378, 1995.
77. Mourad A.-H. I. and Maiti S .K., 'Influence of state of stress on mixed mode stable crack growth through D16AT aluminum alloy', International Journal of Fracture, Vol. 72, pp. 241-258, 1995.
78. Mourad A. -H. I. and Maiti S .K., 'Mode I and mixed mode stable crack extensions through stiffened TPB specimens', Fatigue and Fracture of Engineering Materials and Structures, Vol. 18, pp. 648-652, 1995.
79. Mourad A.-H.- I. and Maiti S .K, Mode II stable crack growth, Fatigue and Fracture of Engineering Materials and Structures, Vol. 19, pp. 75-84, 1996.
80. Maiti S. K., Potdar Y. K. and Mourad A. -H. I. , Fracture of thin sheet under tension dominated loading. Proceedings of the 5<sup>th</sup> International Conference on sheet Metal (She. Met. 97), University of Ulster at Jordanstown, Northern Ireland, United Kingdom, pp. 157-156, 8-10 April 1997.
81. A. -H I. Mourad "Influence of stiffening on stable crack extensions through TPB specimen with offset edge crack", Scientific Bulletin, Faculty of Engineering, Ain Shams University, Vol. 35, pp. 339-358, No. 4, 2000.
82. Kolednik, O., 'On the physical meaning of the J-  $\Delta a$ - curves' Engineering Fracture Mechanics, Vol.38, pp.403-412, 1991.

83. Shan, G. X., Kolednik, O. and Fischer, F. D. ' Numerical investigations of stable crack growth in CT-specimens of SAE4340 steel', Computer Aided Assessment and control of localized Damage. Proceeding of the 3<sup>rd</sup> International conference on computer-Aided Assessment and control Localized Dange, Jun 21-23, Udine, Italy, pp.399, 1994
84. Ahmad, J., Barnes, C. R. and Kanninen, M. F., 'An elastoplastic finite-element investigation of crack initiation under mixed-mode static and dynamic loading', in 'Elastic-Plastic Fracture', ASTM STP 803, American Society for testing and Materials, Philadelphia, USA, pp. I-214-I-239, 1983.
85. Sakata, M., Aoki, S. and Kishimoto, K.: 'Mixed-mode elastic-plastic fracture of 2024-T351 aluminum alloy' in 'the Mechanism of fracture', Proc. Int. Conf. and Exposition on Ftigue, Corrosion Cracking, Fracture Mechanics and Failure Analysis', 2-6 December 1985, Salt Lake City, Otah, USA, (Ed. V. S. Goel), American Society for metals, pp.97-104, 1986.
86. Aoki, S., Kishimoto, K., Yoshide, T. and Sakata, M. 'A finite element study of the near crack tip deformation of a ductile material under mixed mode loading', J. Mech. Phys. Solids, Vol.35, pp.431-455, 1987.
87. Chow, C. L. and Wang, J. 'On crack initiation angle of mixed mode ductile fracture with continuum damage mechanics', Engg. Fract. Mech., Vol.32, pp.601-612, 1989.
88. Maccagno, T. M. and Knott. J. F. 'The mixed mode I/II fracture behavior of lightly tempered HY130 steel at room temperature', Engg. Fract. Mech., Vol. 41, No. 6, pp.805-820 (1992).

89. Hallback, N. and Nilsson, F. 'Mixed-mode I/II fracture behavior of an aluminum alloy', *J. Mech. Phys. Solids*, Vol.42, No.9, pp.1345-1374, 1994
90. Kamat, S. V. and Eswara Prasad, N. 'Comparison of fracture toughness of a 7XXX aluminum alloy under mode I, mode II and mode III loading', *Int. J. Fract.*, Vol. 63, pp. R-7-R-13 (1993).
91. Maccagno T. M. and Knott, J. F. 'The low temperature brittle fracture behavior of steel in mixed modes I and II', *Engg. Fract. Mech.*, Vol. 38, No.2/3, pp.111-128, 1991.
92. Ma, F., Deng, X., Sutton, M. A. and Newman Jr., J. C., 'A CTOD based mixed mode fracture criterion, Mixed Mode Crack Behavior ASTM STP 1359, PP. 86-110, 1999.
93. Sutton, M., A., Deng, X., Ma, F., Newman, J. C. Jr, James, M., 'Development and application of crack tip opening displacement – based mixed mode fracture criterion', *Int. J. Solids Struct.*, Vol. 37, pp.3591-3618, 2000.
94. Sutton, M. A., Boone, M. L., Ma, F., Heln, D., 'A combined modeling – experimental study of the crack opening displacement fracture criterion for characterization of stable crack growth under mixed mode I/II loading in thin sheet materials', *Engineering Fracture Mechanics*, Vol 66, pp.171-185, 2000.
95. Baker, A.: 'Three-dimensional constraint effects on stress intensity distributions in plate geometries with through-thickness cracks', *Fatigue Fract. Engg. Mater. Struct.*, Vol. 15, No. 11, pp. 1051-1069, 1992.
96. Davies, P. H., 'Predicting crack instability behaviour of burst tests from small specimens for irradiated Zr-2.5Nb pressure tubes', *ASTM Special Technical Publication*, Vol. 1321, 1997.

97. Susumu, M., 'Computer simulation of fast crack propagation and arrest in steel plate with temperature gradient based on local fracture stress criterion', ASTM Special Technical Publication, Vol. 1321, 1997.



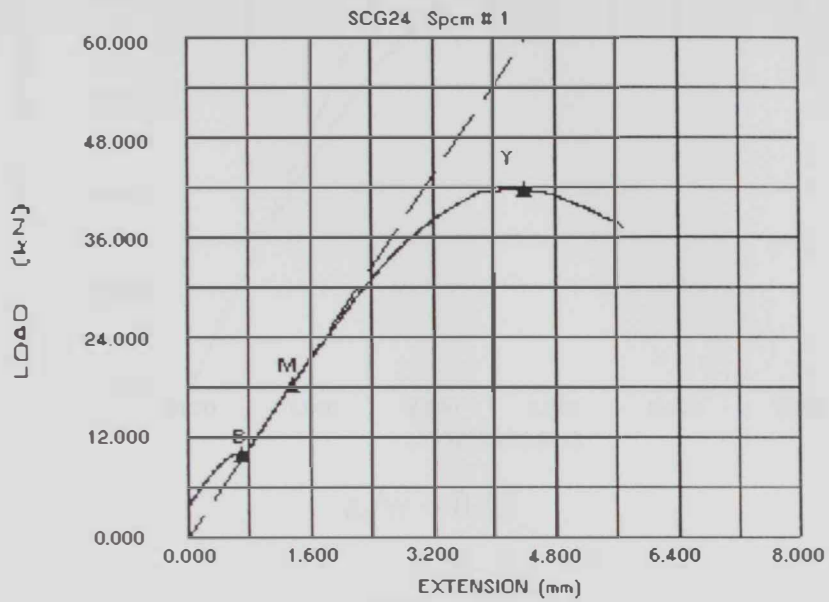
# Appendixes

## APPENDIXES

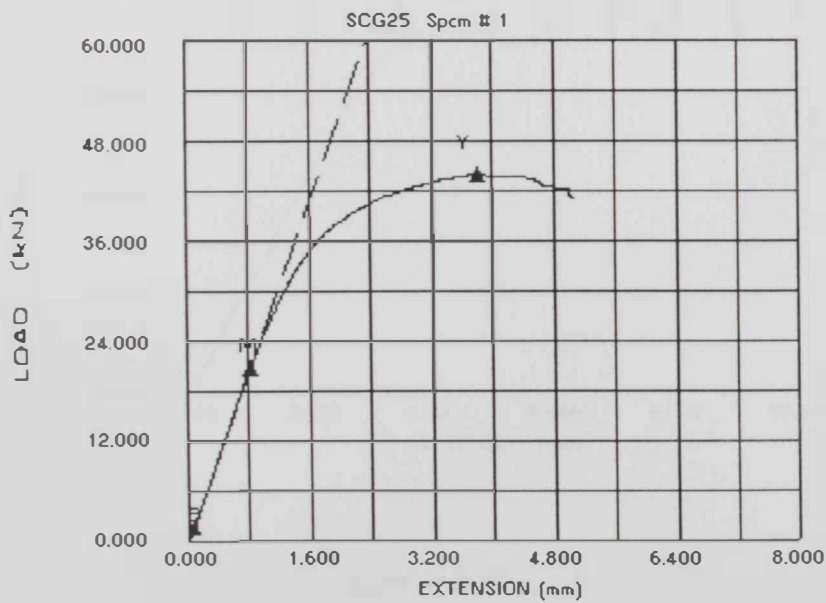
- 4A.** Samples of the load-over head displacement curves for mode I loading that obtained from the MTS machine
- 4B.** Finite Element Program used in Mode I Stable Crack Growth
- 5A.** Samples of the load-over head displacement curves for Mixed Mode loading that obtained from the MTS machine
- 5B.** Finite Element Program used in Mixed Mode Stable Crack Growth

## Appendix 4A

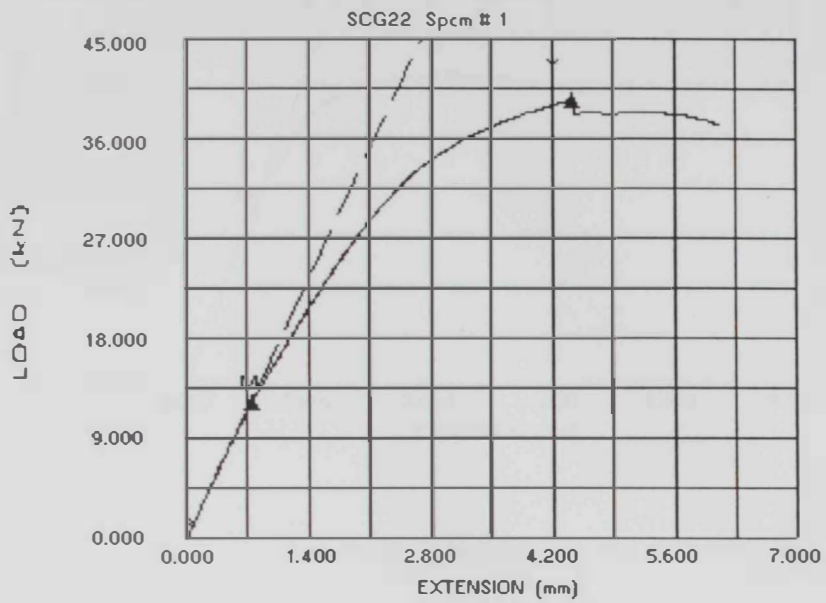
Samples of the load-over head displacement curves for mode I loading that obtained from the MTS machine



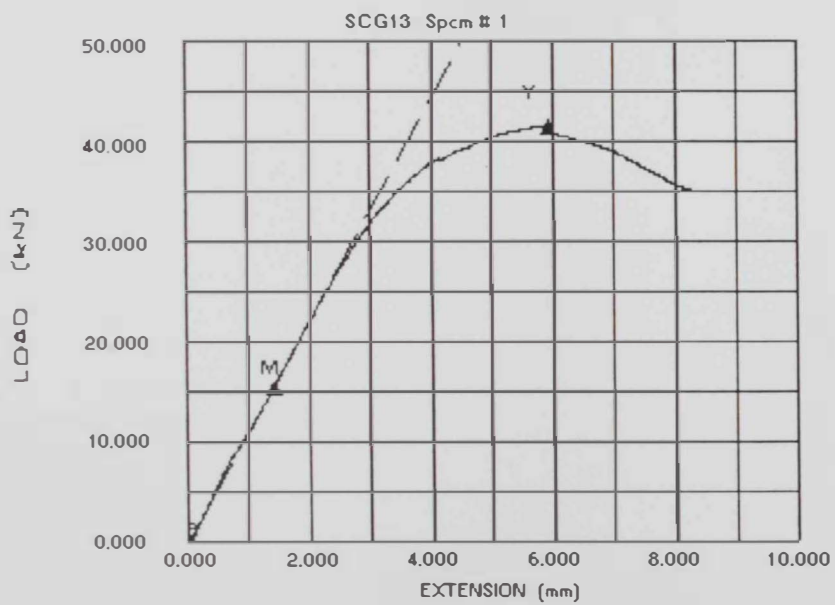
$$a_0/w = 0.41$$



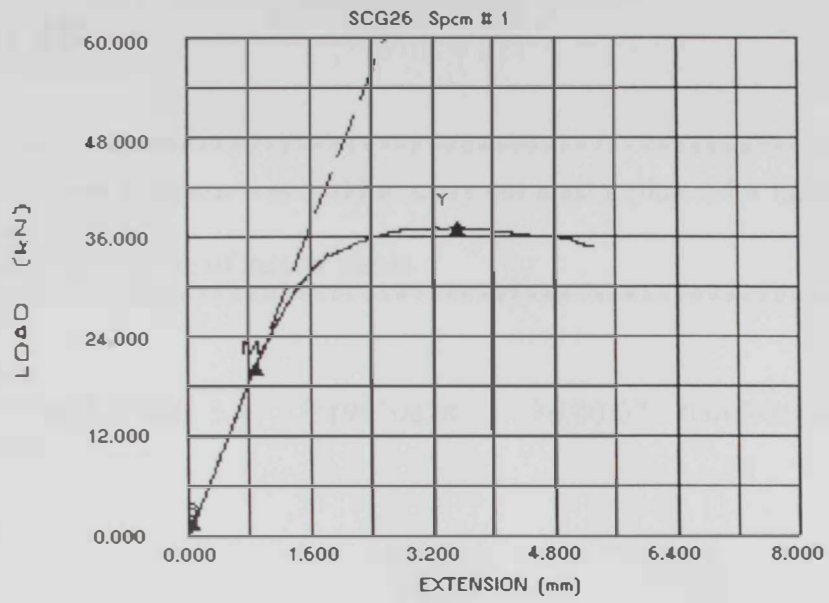
$$a_0/w = 0.42$$



$$a_0/w = 0.43$$



$$a_0/w = 0.43$$



$$a_0/w = 0.41$$

## Appendix 4B

```
*****
!* this finite element program was build to carry out elastic-plastic for mode I
!* Stable crack growth
!* Analysis for the purpose of master thesis.
*****

/GRA,POWER
/COM,ANSYS RELEASE 5.4 UP19970828      16:00:07  03/07/2002
/FILNAM,CMI
/PREP7
*AFUN,DEG
!*
!*
!* Variables
L=120      ! Length of specimen L
M=62      ! one half of the specimen M=L/2
a=41      ! Crack length
W=100     ! distance from load line to the end of specimen.
B=W-a
F=1.5
H=6
C=20
C2=2
C1=a-C2
Y=38
RAD=6
Thick=8
E = 200   ! Young modulus
Et= 10    ! Tangential modulus !!* all units in GPa
Nu= 0.3   ! poison ratio
Fy= 0 450 ! yield Strength
T=22     ! Force applied
!*
!*
!*
!* Define Keypoints
K,1,0,0,0
K,2,4,0,0
K,3,B,0,0
K,4,B,M,0
K,5,-a-c,M,0
K,6,-a-c,F+H,0
K,7,-a,F+H,0
```

```

K,8,-a,F,0
K,9,-C2-F/TAN(15),F,0
K,10,-c2,0,0
K,11,-C2-F/TAN(15),4,0
K,12,4,4,0
K,13,-a,Y,0
!*
LSTR, 1, 2
LSTR, 2, 3
LSTR, 3, 4
LSTR, 4, 5
LSTR, 5, 6
LSTR, 6, 7 !creat the lines which form the area of the modle
LSTR, 7, 8
LSTR, 8, 9
LSTR, 9, 10
LSTR, 10, 1
LSTR, 2, 12
LSTR, 12, 11
LSTR, 11, 9
!*
CIRCLE,13,RAD
!*
!*
!* Divide Top Arcs
LDIV,14, , ,3,0
LDIV,15, , ,3,0
!*
!*
FLST,2,10,4
FITEM,2,10
FITEM,2,1
FITEM,2,2
FITEM,2,3 ! Creat the area of the modle
FITEM,2,4
FITEM,2,5
FITEM,2,6
FITEM,2,7
FITEM,2,8
FITEM,2,9
AL,P51X
!*
AL,15,19,18,14,20,21,16,17 ! creat a loading hole
!*
AL,9,10,1,11,12,13 !* creat the area around the crack tip
!*

```

ASBA, 1, 2

ASBA,4,3,,KEEP

!\*  
!

!\* Define Element Data

ET,1,PLANE82

KEYOPT,1,3,3

KEYOPT,1,5,0

KEYOPT,1,6,0

R,1,Thick

!\*  
!

!

!\* Define the Material Properties

UIMP,1,EX, , ,E

UIMP,1,NUXY, , ,Nu

TB,BKIN,1,1, , ,

TBMODIF,2,1,Fy

TBMODIF,3,1,Et

!\*  
!

!

!\* Apply Boundary Conditions

DL,1, ,SYMM

DL,2, ,SYMM

DK,3, ,0, ,0,UX

!\*  
!

!

!\* Apply Loads

FK,14,FY,T/6

FK,15,FY,T/6

FK,18,FY,T/6

FK,19,FY,T/6

FK,20,FY,T/6

FK,21,FY,T/6

!\*  
!

!

LESIZE,1,0.2,,,,,,1

LESIZE,9,0.2,,,,,,1

LESIZE,10,0.2,,,,,,1

LESIZE,11,0.2,,,,,,1

LESIZE,12,0.2,,,,,,1

LESIZE,13,0.2,,,,,,1

!\*  
!

!

LESIZE,3,4,,,,,,1

LESIZE,4,4,,,,,,1

LESIZE,5,4,,,,,,1

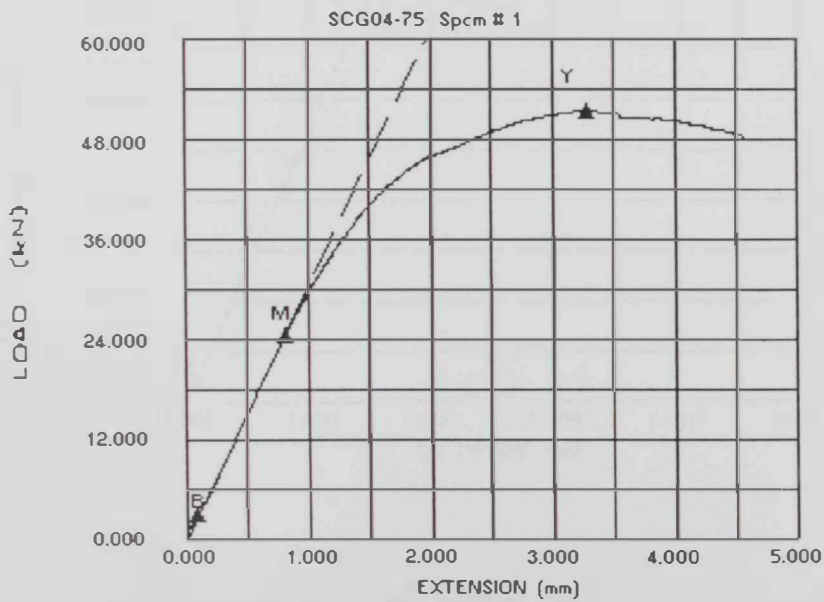
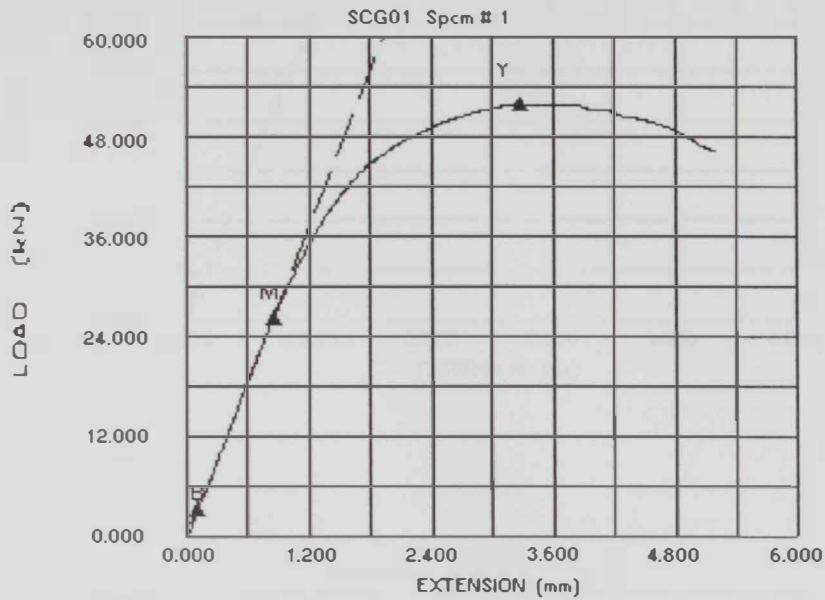
LESIZE,6,4,,,,,,1



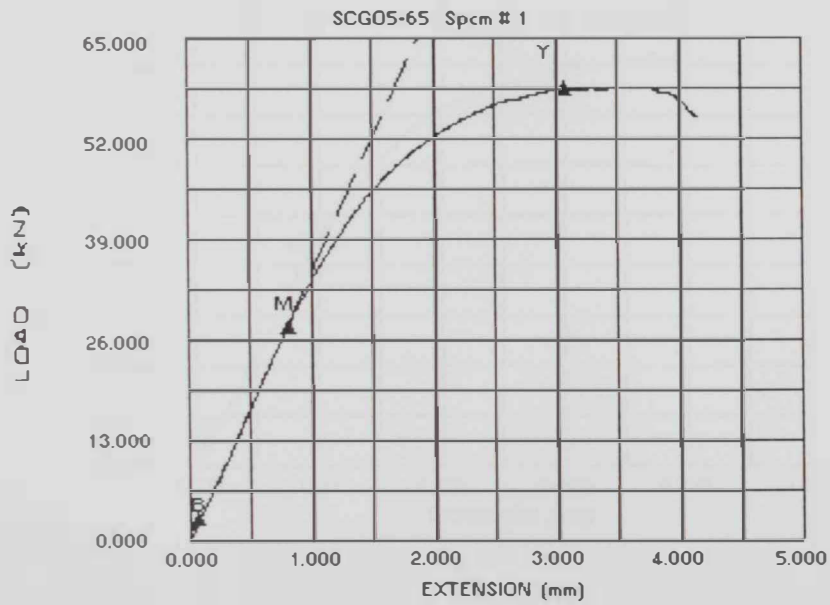
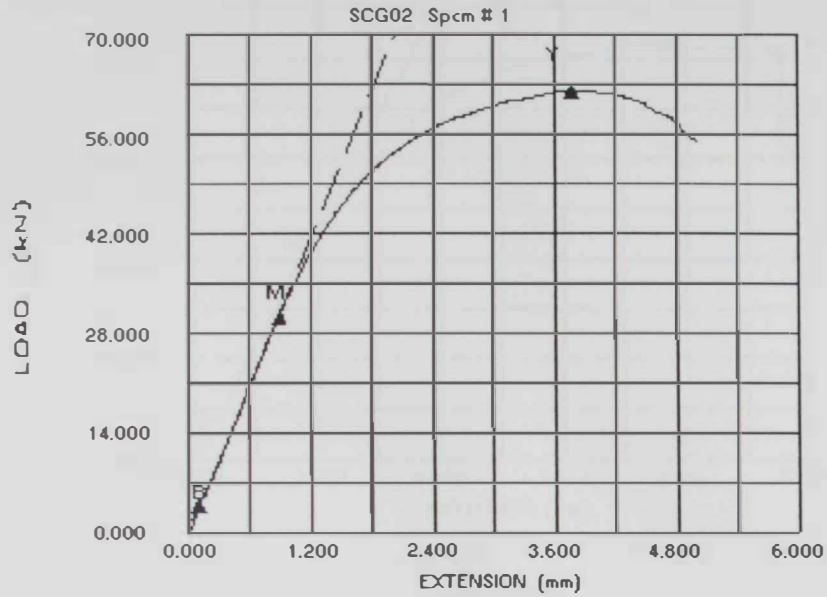
```
LESIZE,7,4,,,,,,,,1
!*
!*
LESIZE,14,2,,,1,,,1
LESIZE,15,2,,,1,,,1
LESIZE,16,2,,,1,,,1
LESIZE,17,2,,,1,,,1
LESIZE,18,2,,,1,,,1
LESIZE,19,2,,,1,,,1
LESIZE,20,2,,,1,,,1
LESIZE,21,2,,,1,,,1
!*
LESIZE,8,0.8, , ,.2, , , ,1
LESIZE,2,0.8, , ,5, , , ,1
!*
!*
!*
!*Meshing
/UI,MESH,OFF
MSHAPE,0,2D
MSHKEY,0
AMESH,1
AMESH,3
!*
!*
/SOLU
ANTYPE,0
NLGEOM,0
NROPT,FULL, ,OFF
NEQIT,10
DOFSEL,S, ,FX,FY
FCUM,REPL,1,
DOFSEL,ALL
!*
!* First load step (sub-step=0.05)
AUTOTS,1
TIME,1
DELTIM,0.05,0.01,0.10
OUTRES,ALL,ALL
KBC,0
SOLVE
!*
!*
SAVE
FINISH
```

## Appendix 5A

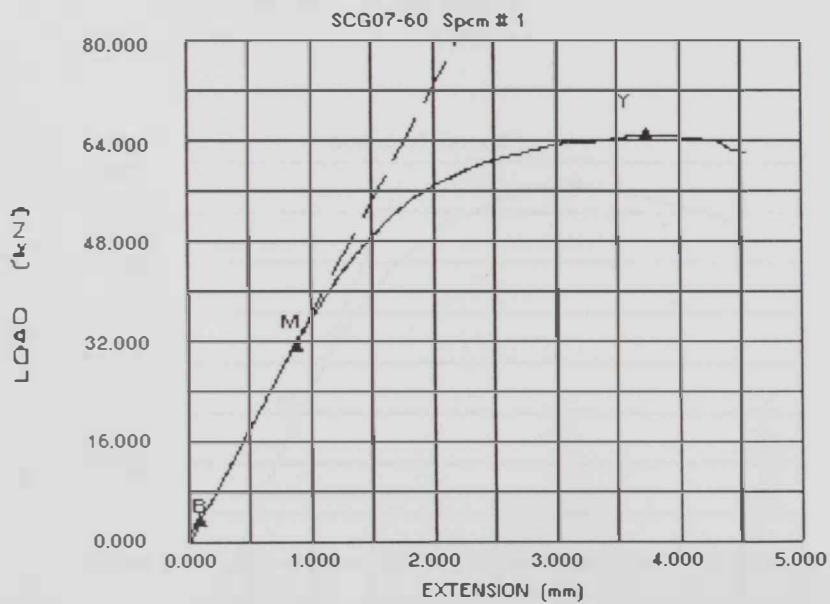
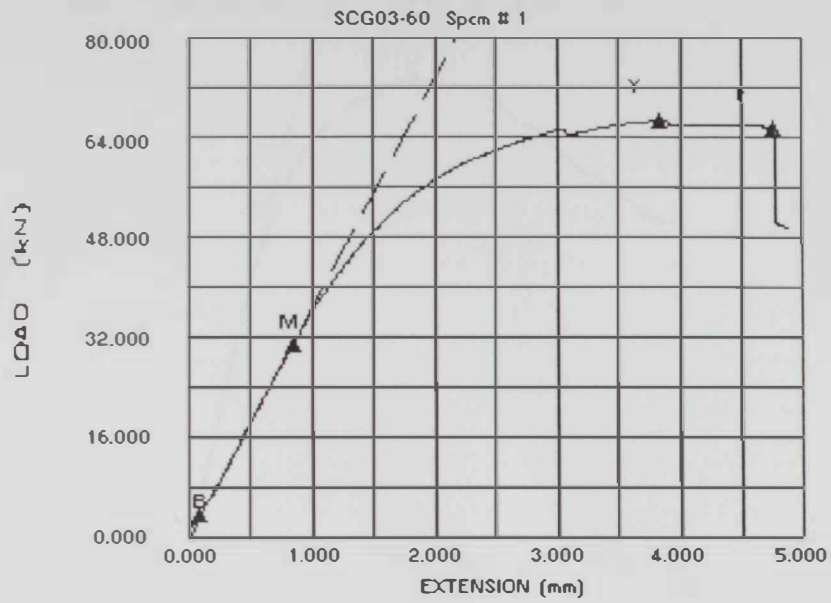
Samples of the load-over head displacement curves that obtained from the MTS machine



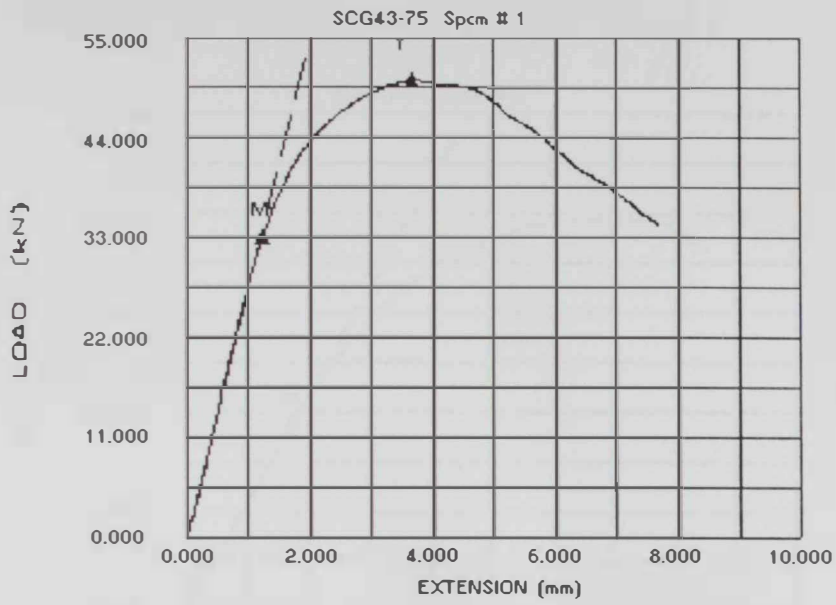
$$a_0/w = 0.42 \text{ and } \psi = 75^\circ$$



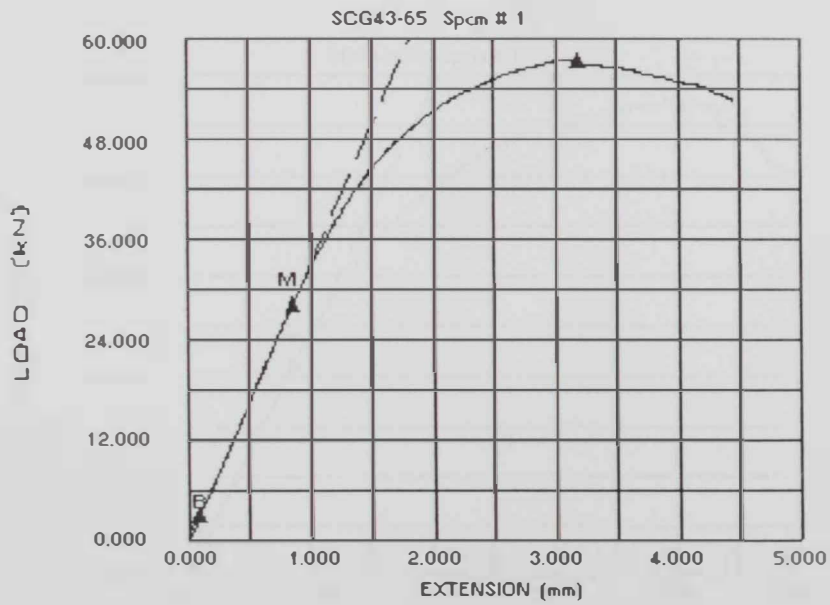
$$a_0/w = 0.42 \text{ and } \psi = 65^\circ$$



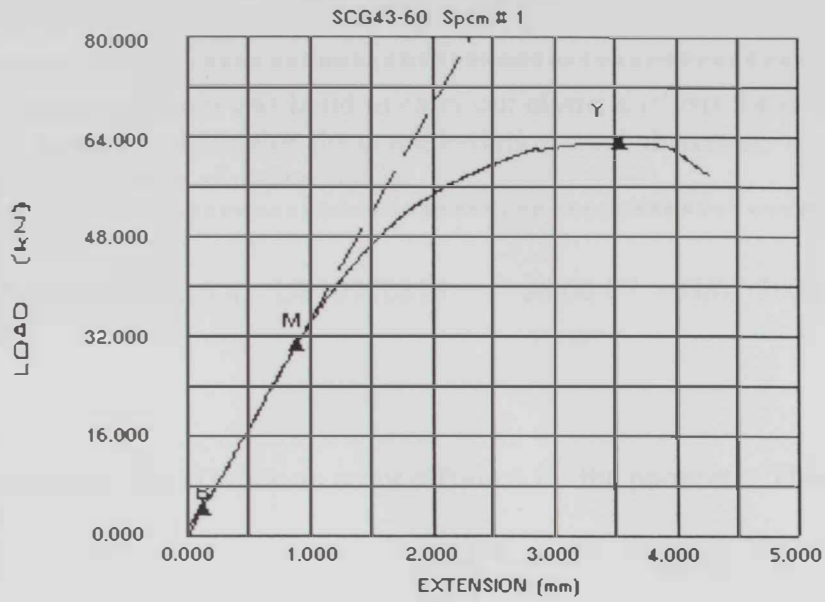
$$a_0/w = 0.42 \text{ and } \psi = 60^\circ$$



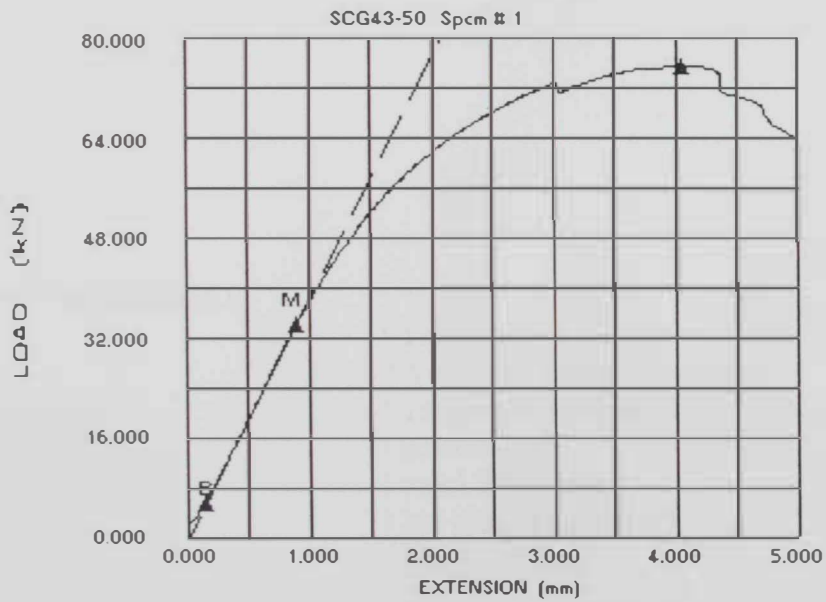
$$a_0/w = 0.43 \text{ and } \psi = 75$$



$$a_0/w = 0.43 \text{ and } \psi = 65$$



$$a_0/w = 0.43 \text{ and } \psi = 60$$



$$a_0/w = 0.42 \text{ and } \psi = 50$$

## Appendix 5B

```
*****  
!* this finite element program was build to carry out elastic analysis for mixed mode  
!* Stable crack growth to determine the crack initiation crack direction.  
!* Analysis for the purpose of master thesis.  
*****
```

```
/COM,ANSYS RELEASE 5.4 UP19970828 16:00:07 03/07/2002  
*AFUN,DEG  
BTOL,1e-9  
!*  
!* Variables  
*DIM,Theta,ARRAY,10 ! Define an array offside 4 for the parameter Theta  
Theta(1)=50  
Theta(2)=60  
Theta(3)=65  
Theta(4)=75  
L=120 ! Length of specimen L  
M=60 ! one half of the specimen M=L/2  
a=42 ! Crack length  
W=100 ! distance from load line to the end of specimen.  
B=W-a  
F=1.5  
H=6  
C=20  
C2=2  
C1=a-C2  
Y=38  
RAD=6  
!*  
!* MATERIAL PROPERTIES  
Thick=8 ! Thickness of material  
E=205 ! Young modulus  
Et=0 ! Tangential modulus !!* all units in GPa  
Nu=0.3 ! poison ratio  
!Fy=0.470 ! yield Strength  
Fy=1e10 ! No yielding (Elastic)  
T=0.001 ! Force applied  
!*  
!*  
*DO,1,1,4  
/FILNAM,CM1%Theta(i)%  
/PREP7  
!* Define the Material Properties
```

```

UIMP,1,EX,,E
UIMP,1,NUXY,,Nu
TB,BKIN,1,1,,
TBMODIF,2,1,Fy
TBMODIF,3,1,Et
!*
!* ELEMENT TYPE AND REAL CONSTANTS
ET,1,PLANE82                ! For Elasto-Plastic Analysis
KEYOPT,1,3,3
KEYOPT,1,5,0
KEYOPT,1,6,0
R,1,8,
!*
bc=2*Y/TAN(Theta(I))
!* Define Keypoints
K,1,0,0,0
K,2,B,0,0
K,3,B,M,0
K,4,-a-c,M,0
K,5,-a-c,F+H,0
K,6,-a,F+H,0
K,7,-a,F,0
K,8,-C2-F/TAN(15),F,0
K,9,-c2,.05,0
!*
!*
LSTR,1,2      ! Line L1
LSTR,2,3      ! Line L2
LSTR,3,4      ! Line L3
LSTR,4,5      ! Line L4
LSTR,5,6      ! Line L5
LSTR,6,7      ! Line L6
LSTR,7,8      ! Line L7
LSTR,8,9      ! Line L8
LSTR,9,1      ! Line L9
!*
!*
AL,1,2,3,4,5,6,7,8,9      ! Create Area A1 (Upper half of the Model)
CYL4,0,0,0.05,,1.5      ! Create Area A2 (Annulus Rad1=0.05mm, Rad2=1.5mm)
!*
ASBA,1,2          ! Subtract A2 from A1
!*
LSTR,15,10        ! Add lines for the annulus area
LSTR,18,19        ! Add lines for the annulus area
!*
AL,1,10,23,9,20,17      ! Create the annulus area

```



!\*  
ARSYM,Y,ALL, , , 0,0 ! Reflect the upper half of the model

!\*  
NUMMRG,ALL,0.0001,0.0001,,LOW

!\*  
CYL4,-a,Y,RAD ! Upper Circular Hole  
CYL4,-a,-Y,RAD ! Lower Left Circular Hole  
CYL4,-a+bc,-Y,RAD ! Lower Right Circular Hole

!\*  
!\*  
ASBA,4,7 ! Subtract Upper Hole  
ASBA,6,8 ! Subtract Lower Left Hole  
ASBA,4,9 ! Subtract Lower Right Hole

!\*  
KSCON,1,0.025,1,16,0,

!\*  
LESIZE,15,,,8,,,,1  
LESIZE,16,,,8,,,,1  
LESIZE,17,,,8,,,,1  
LESIZE,20,,,8,,,,1

!\*  
MSHAPE,0,2D  
MSHKEY,0

!\*  
AMESH,3 ! Mesh the small half circle  
AMESH,5 ! Mesh the small half circle

!\*  
LESIZE,10,,,8,,,,1  
LESIZE,12,,,8,,,,1  
LESIZE,13,,,8,,,,1  
LESIZE,23,,,8,,,,1

!\*  
LESIZE,1,,,28,20,,,,1  
LESIZE,9,,,28,20,,,,1  
LESIZE,14,,,28,20,,,,1

!\*  
LCCAT,17,20  
LCCAT,15,16  
LCCAT,10,23  
LCCAT,12,13

!\*  
MSHKEY,1

!\*  
AMESH,1 ! Mesh the big half circle  
AMESH,2 ! Mesh the big half circle

!\*

```

LESIZE,11,,8,,,,1
LESIZE,26,,8,,,,1
LESIZE,35,,8,,,,1
LESIZE,36,,8,,,,1
LESIZE,37,,8,,,,1
LESIZE,38,,8,,,,1
LESIZE,39,,8,,,,1
LESIZE,40,,8,,,,1
LESIZE,41,,8,,,,1
LESIZE,42,,8,,,,1
!*
LESIZE,22,,5,,,,1
LESIZE,34,,5,,,,1
LESIZE,8,,15,0.2,,,,1
LESIZE,33,,15,0.2,,,,1
LESIZE,21,,40,0.05,,,,1
!*
!* DIVIDE LINES 24 and 43 to allow for loaded keypoints
LDIV,24,(90-Theta(I))/90,,2,0
LDIV,43,(90-Theta(I))/90,,2,0
!*
LESIZE,24,,4,,,,1
LESIZE,48,,5,,,,1
LESIZE,43,,4,,,,1
LESIZE,49,,5,,,,1
!*
ESIZE,4,0
MSHKEY,0
!*
AMESH,6
AMESH,10
!*
!* BOUNDARY CONDITIONS
DK,25,,0,,0,ALL
DK,24,,0,,0,UY
!*
!* APPLY LOADS
KP1=KP(-a-RAD*COS(Theta(I)), Y+RAD*SIN(Theta(I)), 0)
KP2=KP(-a+bc+RAD*COS(Theta(I)), -Y-RAD*SIN(Theta(I)), 0)
FK,KP1,FX,-COS(Theta(I))
FK,KP1,FY,SIN(Theta(I))
FK,KP2,FX,COS(Theta(I))
FK,KP2,FY,-SIN(Theta(I))
!*
SAVE
FINISH

```

```
!*  
/SOLU  
SOLVE  
!*  
FINISH  
!*  
!* DELETE EVERYTHING  
/PREP7  
ACLEAR,ALL ! Delete all meshes  
ADELE,ALL, , ,1  
LDELE,ALL, , ,1  
KDELE,ALL  
FINISH  
*ENDDO  
FINISH
```



एन सी ई आर टी ई

एन सी ई आर टी ई

एन सी ई आर टी ई

एन सी ई आर टी ई

एन सी ई आर टी ई

एन सी ई आर टी ई

एन सी ई आर टी ई

एन सी ई आर टी ई

एन सी ई आर टी ई

एन सी ई आर टी ई

## دراسات على النمو المستقر للصدع

إن الهدف من هذا البحث هو تحري سلوك النمو المستقر لصدع (شرخ) خلال سبيكة فولاذية AISI 4340 وذلك بطريقة تجريبية . وفي هذا السياق أجريت سلسلة من اختبارات النمو المستقر للصدع خلال عينات الشد المدمجة بسمك ٨ ملليمتر تحت تأثير أحمال عمودية ومائلة على سطح الصدع وشبه ثابتة.

لقد استخدمت تقنية السلك القاطع باستخدام سلك نصف قطره ٠,٠٥ ملليمتر لإحداث مقدمة الشق (الصدع) . كما استخدمت خمس زوايا تحميل مختلفة ( $\psi$ ) بين محور التحميل وسطح الكسر وهي ٥٠ درجة و ٦٠ درجة و ٦٥ درجة و ٧٥ درجة و ٩٠ درجة (للتحميل المتعامد). وكذلك خمس نسب مختلفة من الطول الأصلي للصدع إلى عرض العينة ( $a_0/w$ ) ٠,٤١ و ٠,٤٢ و ٠,٤٣ و ٠,٤٤ و ٠,٤٥ . وكذلك تم استخدام تركيبات مختلفة من زوايا التحميل ونسب الطول الأصلي للكسر إلى عرض العينة ( $a_0/w$ ) .

تم الحصول على بيانات متعلقة باتجاه بدء امتداد الصدع الأولي وعلاقة الحمل مع الإزاحة على خط التحميل وأقل وأقصى حمل ومدى نمو الصدع المستقر وشكل مقدمة الصدع عبر سمك العينة وخصائص سطح الصدع وكذلك صور مجهرية لسطح الصدع بواسطة المجهر الإلكتروني الماسح. كان من الملاحظ أن مقدمة الصدع تصبح على شكل منحنى رغم أن المقدمة كانت مستقيمة في البداية وهذا واضح في كل مرحلة من مراحل نمو الصدع المستقر. في حالة التحميل المختلط ينمو الصدع في البداية على طول خط مستقيم يميل بزواوية تحدد اتجاه امتداد الصدع على الصدع الأصلي. زواوية التحميل ( $\psi$ ) ونسبة الطول الأصلي للكسر إلى عرض العينة ( $a_0/w$ ) يؤثران على سلوك نمو الكسر المستقر بشكل كبير.

تم تحديد اتجاه نمو الصدع المستقر الأولي بواسطة تحليل العنصر المحدود ولقد كان هناك اتفاق إلى حد كبير بين النتائج التجريبية والمتوقعة بواسطة التحليل العددي.





جامعة الإمارات العربية المتحدة

عمادة الدراسات العليا

برنامج علوم وهندسة المواد

## دراسات على النمو المستقر للصدع

اعداد

محمد بن جمعة بن حميد الغافري

رسالة مقدمة لعمادة الدراسات العليا

ضمن متطلبات الحصول على درجة الماجستير

في علوم وهندسة المواد

اشراف

البرفسور اسامة ابو زيد

قسم الهندسة الميكانيكية

جامعة الإمارات العربية المتحدة

د. عبدالحميد اسماعيل مراد

قسم الهندسة الميكانيكية

جامعة الإمارات العربية المتحدة